AD-A047 926 NORTHWESTERN UNIV EVANSTON ILL F/G 20/11
THERMOELASTIC PHENOMENA IN LUBRICATED SLIDING CONTACT.(U)
JAN 77 B N BANERJEE , R A BURTON N00014-75-C-0761
UNCLASSIFIED 5341-427 NL

1 OF 2
AD A047926

AD A047926

(12)

THERMOELASTIC PHENOMENA IN LUBRICATED SLIDING CONTACT

AD No. ____
DDC FILE COPY

DISTRIBUTION STATEMENT A
Approved for public release;
Distribution Unlimited

DDC
RECEIVED
DEC 21 1977
B

SECURITY CLASSIFICATION OF THIS PAGE (When Data Entered)

REPORT DOCUMENTATION PAGE

READ INSTRUCTIONS BEFORE COMPLETING FORM

1. REPORT NUMBER
2. GOVT ACCESSION NO.
3. RECIPIENT'S CATALOG NUMBER

4. TITLE (and Subtitle)

THERMOELASTIC PHENOMENA IN LUBRICATED SLIDING CONTACT.

5. TYPE OF REPORT & PERIOD COVERED

Sept[illegible] 1975 - Sept. 1976

6. PERFORMING ORG. REPORT NUMBER

5341-427

7. AUTHOR(s)

Barunendra N. Banerjee
Ralph A. Burton

8. CONTRACT OR GRANT NUMBER(s)

N00014-75-C-0761
Mod. P00001

9. PERFORMING ORGANIZATION NAME AND ADDRESS

Northwestern University
Evanston, IL 60201

10. PROGRAM ELEMENT, PROJECT, TASK AREA & WORK UNIT NUMBERS

NR 097-398/2-14-75 (473)

11. CONTROLLING OFFICE NAME AND ADDRESS

Procuring Contacting Officer
Office of Naval Research, Dept. of the Navy
Arlington, VA 22217

12. REPORT DATE

Jan[illegible] 1977

13. NUMBER OF PAGES

183

14. MONITORING AGENCY NAME & ADDRESS(if different from Controlling Office)

186p.

15. SECURITY CLASS. (of this report)

Unclassified

15a. DECLASSIFICATION/DOWNGRADING SCHEDULE

16. DISTRIBUTION STATEMENT (of this Report)

Reproduction in whole or in part is permitted for any purpose of the United States Government

DISTRIBUTION STATEMENT A
Approved for public release;
Distribution Unlimited

17. DISTRIBUTION STATEMENT (of the abstract entered in Block 20, if different from Report)

18. SUPPLEMENTARY NOTES

This report was presented as a Ph.D. dissertation to the Graduate School, Northwestern University, under the title "Thermoelastic Effects in the Parallel Sliding of Solid Surfaces Separated by a Viscous Liquid Film," by Barunendra N. Banerjee.

19. KEY WORDS (Continue on reverse side if necessary and identify by block number)

lubrication, thermoelastic, seals, hydrodynamic, tribology, instability, failure, deformation, heating (viscous)

20. ABSTRACT (Continue on reverse side if necessary and identify by block number)

Lubricated sliding motion is studied for thermoelastic effects, notably an instability that causes large thermoelastic deformation of a nominally flat surface. A configuration similar to a face seal is used, with one face consisting of a thermal conductor and the other of an insulator.

The roles of the pertinent parameters and material properties are

DD FORM 1 JAN 73 1473 EDITION OF 1 NOV 65 IS OBSOLETE
S/N 0102-014-6601

SECURITY CLASSIFICATION OF THIS PAGE (When Data Entered)

260 800

Block 20.

delineated. A simple equation is given for the threshold of thermoelastic instability when both faces are initially flat.

For the case of an initially wavy conducting face, the model for viscous heating envisages a full, coherent film on the one hand and, on the other, a broken film with zero heating in the cavitation zones. For both models, the continuous thermoelastic deformation of the conducting face, with changing sliding speed, is discussed and criteria for the onset of instability are presented.

Experiments are reported to corroborate the findings of the theoretical analyses.

ACCESSION for
NTIS White Section ✓
DDC Buff Section ☐
UNANNOUNCED ☐
JUSTIFICATION
PER FORM 50
BY
DISTRIBUTION/AVAILABILITY CODES
Dist. AVAIL. and/or SPECIAL
A

NOMENCLATURE

Unless otherwise mentioned in the text, the symbols have the following meanings:

a = a wave number, describes the time lag of propagation of a wave in the y-direction

a_1 = 'a' for the steadily moving, constant amplitude, wave

b = spatial exponent of growth of steadily moving temperature wave

c = wave velocity

C = specific heat

E = Young's modulus of elasticity

f = face load

F = non-dimensional f

$\bar{h}$ = mean thickness of lubricant film

h' = small surface perturbation

h_1, h_2 = amplitudes of sine and cosine components of h'

h_o = operating surface waviness

h = film shape

$\hat{h}$ = small change in $\bar{h}$

h_i = initial surface waviness

H = non-dimensional h

$\hat{H}$ = non-dimensional $\hat{h}$

H_i = non-dimensional h_i

K_M = thermal conductivity of metal

K_{oil} = thermal conductivity of lubricant

k_M = thermal diffusivity of metal $\left(\frac{K_M}{\rho C}\right)$

k_{oil} = thermal diffusivity of lubricant

ℓ = circumference of seal

L = width of seal face

p = pressure

p_o = zero-order pressure

p'' = pressure perturbation

p' = zero-average component of p''

$\hat{p}$ = constant component of p''

P_o = non-dimensional p_o

P'' = non-dimensional p''

P' = non-dimensional p'

$\hat{P}$ = non-dimensional $\hat{p}$

q = heating

Q = volume rate of flow

t = time

T = temperature perturbation

T_o = amplitude of T

u = velocity in x-direction; also non-dimensional sliding speed

u' = perturbation velocity in x-direction

U = sliding speed

v = surface displacement

w = velocity in z-direction

W = width factor for seal face $\left(\frac{L^2\kappa^2}{12}\right)$

x = distance along the edge of contact

X = non-dimensional x

y = distance normal to x

Y = non-dimensional h'

z = distance across the width of the face

α_M = coefficient of thermal expansion of metal

β = time-exponent of growth of T

δ = surface deflection

δ_{th} = thermal deformation

δ_E = elastic deformation

Δ_{th} = non-dimensional δ_{th}

Δ_E = non-dimensional δ_E

κ = wave number (2π/wavelength)

ϵ = non-dimensional h_o

λ = ($\kappa x + ay - \kappa ct$)

λ_1 = ($\kappa x - \kappa ct$)

μ = viscosity

ν = Poisson's ratio

Ψ = thermoelastic displacement potential

ρ = density

σ = normal stress

τ = shear stress

ξ = spatial exponent of growth of temperature wave in y-direction

χ = non-dimensional location of a load element

TABLE OF CONTENTS

	Page
NOMENCLATURE	iii
LIST OF ILLUSTRATIONS	viii
CHAPTER I - INTRODUCTION	1
CHAPTER II - INSTABILITY FOR INITIALLY FLAT SURFACES	13
2.1 Geometry and Procedure	13
2.2 Equations of Motion	17
2.3 Continuity Equation	19
2.4 Pressure Gradient	21
2.5 Non-steady, Moving, Temperature Perturbation	22
2.6 Temperature Distribution in Oil Film	26
2.7 The Energy Equation	28
2.8 Thermal Deflection	32
2.9 Elastic Deflection	35
2.10 The Narrow-Lip Seal	36
2.11 Instability Threshold of the Steadily Moving Perturbation	41
2.12 Instability of the Non-Moving Perturbation	49
2.13 Remarks	54
CHAPTER III - EXPERIMENTAL OBSERVATION OF THERMOELASTIC INSTABILITY	56
3.1 The Objective	56
3.2 The Experimental Set-up	58
3.3 The Measurement of Oil-Film Thickness	60
3.4 Procedure	61
3.5 Results and Observations	64
CHAPTER IV - INSTABILITY ANALYSIS FOR INITIALLY WAVY SURFACES	71
4.1 The Model	71
4.2 Heat Generation	76
4.3 Heat Conduction and Convection	77
4.4 Thermal Deformation	77
4.5 Hydrodynamic Pressure	78
4.6 Elastic Deformation	86

Page

4.7 Normalization of Variables. 88
4.8 Stability Analysis. 92
4.9 Notes on Various Parameters. 100

CHAPTER V - PREDICTION OF INSTABILITY FROM GIVEN INITIAL CONDITIONS FOR THE INITIALLY WAVY SURFACE. 110

5.1 Operating and Initial Conditions. 110
5.2 Determination of Initial Surface Profile, Load and Sliding Speed. 111
5.3 Results. 112
5.4 Remarks. 123

CHAPTER VI - EVOLUTION OF OPERATING CONDITIONS FROM GIVEN INITIAL CONDITIONS. 127

CHAPTER VII - CONCLUSIONS. 139

APPENDIX A - THE VALIDITY OF A PARABOLIC TEMPERATURE DISTRIBUTION. 142

APPENDIX B - EDGE DISPLACEMENT OF A SEMI-INFINITE PLATE UNDER NORMAL STRESS. 146

APPENDIX C - PHYSICAL PROPERTIES AND PARAMETERS. 150

APPENDIX D - PROGRAM FOR DETERMINING CRITICAL OPERATING CONDITIONS FOR THE INITIALLY WAVY SURFACE. . . . 151

APPENDIX E - THE FLEXIBLY MOUNTED, INITIALLY WAVY, SEAL FACE. 155

APPENDIX F - PROGRAM FOR COMPUTING FACE LOAD AND INITIAL FACE PROFILE CORRESPONDING TO GIVEN OPERATING CONDITIONS. 170

REFERENCES. 173

LIST OF ILLUSTRATIONS

Page

Figure 1 - Puck-on Washer Configuration. 3

Figure 2 - Three-Pin Model of Surface Contact. 4

Figure 3- Two Dimensional Model of Blade and Half-Space. . . 7

Figure 4 - Thin- Tube Geometry for Face Seal Analysis. . . . 8

Figure 5 - Photograph of Bronze Face with Burnt Tracks Illustrating the Movement of Hot Spots. 11

Figure 6 - Block Diagram for Analysis of Initially Flat Surfaces. 15

Figure 8 - Couette Flow, Definition Sketch. 18

Figure 9 - Pressure Flow, Definition Sketch. 20

Figure 10 - Shear Stresses and Pressure, Division of Composite Flow into Two Parts. 20

Figure 11 - Lag of Temperature Wave in Metal Body. 25

Figure 12 - Temperature Distribution in Oil Film. 27

Figure 13 - Axes of Coordinates for the Narrow-Face Seal. . . 38

Figure 14 - Maximum and Average Pressure in the Narrow-Face Seal 39

Figure 15 - Lines of Neutral Stability, Numerical Solution. . 43

Figure 16 - Lines of Neutral Stability, Families I and II. . . 46

Figure 17 - Lines of Neutral Stability, Families III and IV 47

Figure 18 - Domain of c and $\bar{h}$ in which U is Complex. 50

Figure 19 - Lines of Neutral Stability. 51

Figure 20 - Experimental Set-Up of Dow and Stockwell. . . . 57

Figure 21 - Experimental Set-Up Showing Probe Locations. . . 59

Figure 22 - Calibration Curve for Probe A. 62

Page

Figure 23 - Comparison of Experimental Data with Prediction of Chapter II. 65

Figure 24 - Oscillograms Showing Surface Profiles at Different Sliding Speeds. 66

Figure 25 - Oscillograms Showing Surface Profiles at Different Sliding Speeds. 68

Figure 26 - Photograph of Aluminum Face Showing Burnt Asperities. 69

Figure 27 - Definition Sketch for Operating Condition. 74

Figure 28 - Circumferential Pressure Distribution. 80

Figure 29 - Typical Location of Cavitation Pockets. 82

Figure 30 - Characteristics of Profiled Cast-Iron Seal Face. . 83

Figure 31 - Definition Sketch for Elastic Deformation Equation 87

Figure 32 - Non-Dimensional Coordinates for Operating Condition 89

Figure 33 - Block Diagram of Instability Analysis. 94

Figure 34 - Determination of Non-Dimensional Critical Speed for Operating Surface Waviness. 97

Figure 35 - Thresholds of Instability with Heating Based on Full Film and Cavitating Film. 98

Figure 36 - How Hydrodynamic Film Pressure Tends to Neutralize Relative Face Nutation. 99

Figure 37 - Illustration of Trigonometric Relationship for Arc cos. 106

Figure 38 - Non-Dimensional Critical Sliding Speeds for Non-Dimensional Loads. 113

Figure 39 - Critical Conditions Defined by Non-Dimensional Operating Surface Waviness, Sliding Speed and Load 114

Figure 40 - Chart Showing Operating Conditions and Threshold of Instability for Zero Heating in Cavitation Zones 115

Page

Figure 41 - Critical Sliding Speed for a Given Load and Initial Surface Waviness. 117

Figure 42 - Critical Mean Film-Thickness for a Given Load and Initial Surface Waviness. 118

Figure 43 - Critical Operating Surface Waviness for a Given Load and Initial Surface Waviness. 119

Figure 44 - Chart Showing Operating Conditions and Threshold of Instability with Heating Based on Full Continuous Film. 122

Figure 45 - Comparison Between Calculated Critical Speeds and Corresponding Empirical Equations. 124

Figure 46 - Heat Generation Based on Full Film and Cavitating Film. 126

Figure 47 - Definition Sketch for Calculation of Load. . . . 133

Figure 48 - Evolution of Mean Film-Thickness with Increasing Sliding Speed. 135

Figure 49 - Evolution of Operating Surface Waviness with Increasing Sliding Speed. 137

FigureE-1 - Definition Sketch for Analysis of the Flexibly Mounted Face. 156

FigureE-2 - Experimentally Measured Film-Thickness and Subsequent Theoretical Change by Perturbation until Surfaces Touch, for Flexible and Floating Mountings. 162

CHAPTER I

INTRODUCTION

In recent years, it has been recognized that high speed sliding contact is associated with macroscopic instabilities of interfacial pressure and temperature. Generally referred to as "thermoelastic instability", the phenomenon occurs through the interaction of frictional heating, heat transfer, interfacial pressure generation and wear. At certain operating conditions and for certain combinations of material properties, thermoelastic instability can cause nominally flat surfaces to deform locally so that the load acting on the interface is carried mainly by a number of patches or asperities. This implies high contact pressure at certain points, with surrounding regions of lower pressure and relative surface parting which, in turn, concentrates the frictional heating at these points. The resulting high temperature at these points causes them to expand rapidly, thereby aggravating the situation through a progressively worsening cycle of reduced "contact area", more concentrated heating, greater thermal expansion. The surface configuration, once disturbed, can, at least in theory, undergo runaway and catastrophic deformation, and hence the term "instability". In practice, of course, a damper is expected to be provided by the mechanism of wear and/or elastic suppression of the thermally induced growth. Wear, which in turn depends on interfacial pressure, can wear down a prospective asperity faster than it grows; normal pressure on the surface can elastically flatten or squash down an asperity at the moment of its conception.

Either of these circumstances represents a stabilizing feedback arrangement whereby any prospect of asperity formation is nipped in the bud. However, since both of these stabilizing mechanisms depend on the magnitude of interfacial pressure, it is conceivable that asperity formation may proceed to a certain point before the pressure is large enough to negate further thermal growth. In such a case, thermoelastic instability will still be said to occur, although a stable patch-like contact configuration will eventually evolve. Such patch-like contact, in fact, may be incompatible with many applications.

Thermoelastic instability can conceivably affect numerous practical applications involving differing geometrical configurations. It was experimentally observed by Sibley and Allen [1] while studying the friction and wear characteristics of unlubricated ceramics. Three stationary pucks were pressed against the face of a rotating washer, as shown in fig. (1). This configuration approximates that of disc brakes. For certain materials and sliding speeds, bright hot spots were observed to form and move in apparently periodic patterns. It was concluded, further, that higher friction coefficients (producing high frictional heating) and lower wear rates were conducive to more dramatic displays of hot spots.

Much the same conclusions were drawn by Barber [2] who analyzed the case of three pins pressed against a moving surface, as illustrated in fig. (2). Arguing that all contact problems consist of surfaces touching only at a number of points (as opposed to geometrically true surface contact), Barber went on to show that even slight disparities in the loads carried by the pins (as is almost inevitable in practice) leads to the highest frictional force at the end of the pin bearing the greatest

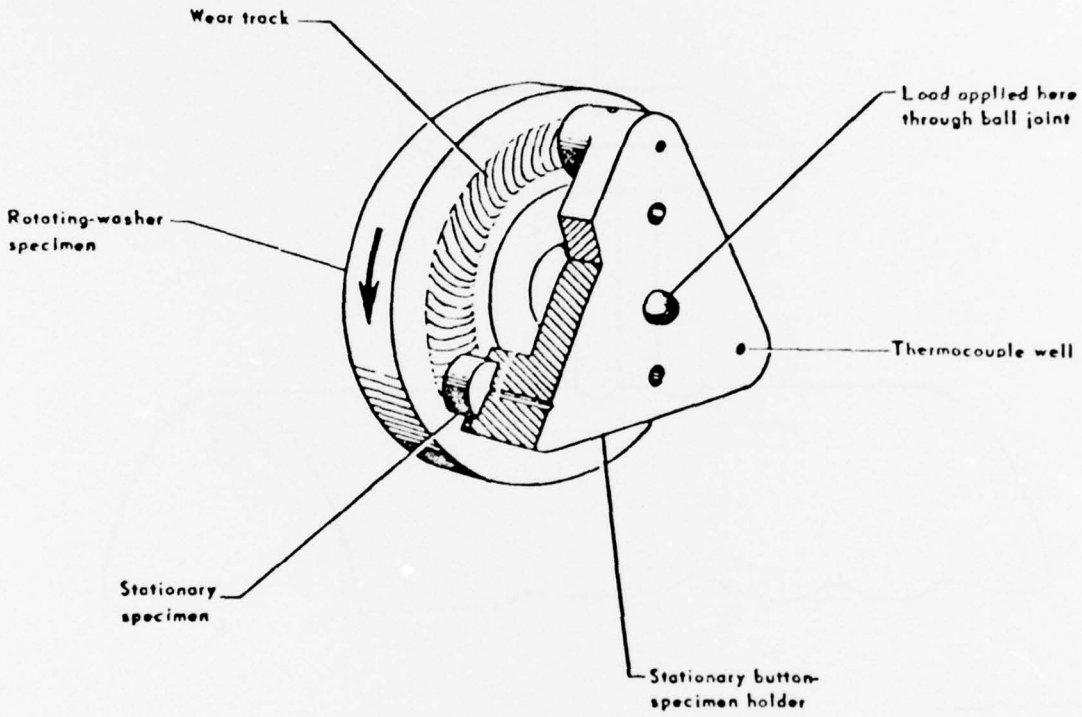

Figure 1. Puck-On-Washer Configuration (Sibley and Allen, ref. 1)

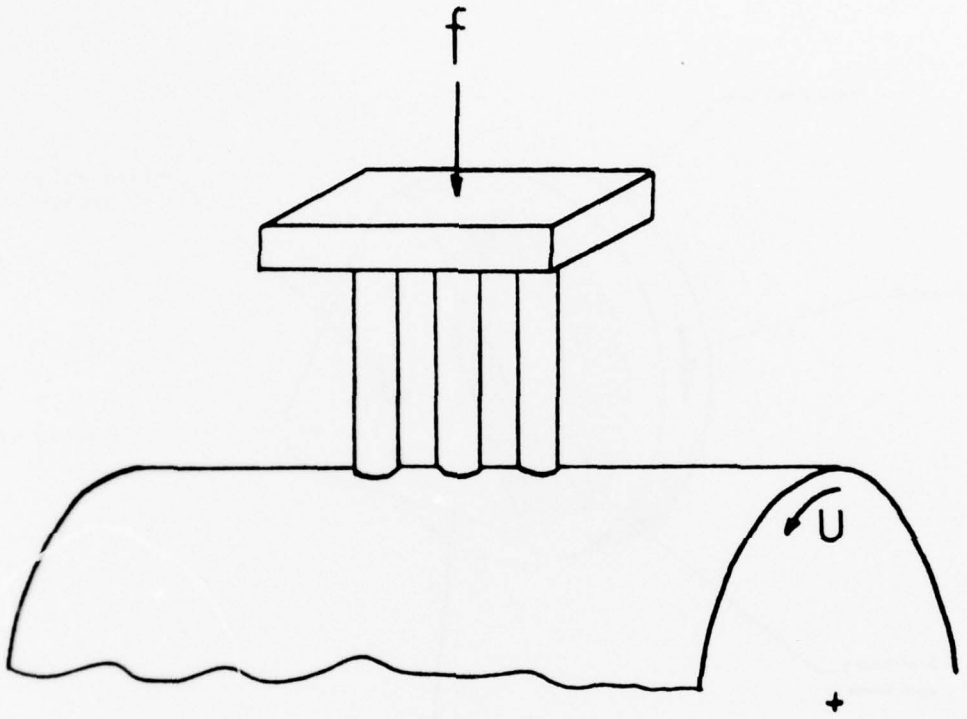

Figure 2. Three-Pin Model of Surface Contact

load. That pin, then, is heated the most, expands the most and carries an increasingly greater share of the total load. Eventually, this process can lead to all the load being carried by the single pin, with the other two lifting off the surface. If, however, the first pin acquires a share of the load for which its wear rate exceeds the rate of thermal expansion, it will begin to be worn down. A second pin will begin to carry more and more load while the first will cool off and lift from the moving surface. Eventually it will be the third pin's turn, and thus the load will continue to shift from one pin to another. If, on the other hand, the rate of wear is greater than that of thermal expansion from the very outset, all three pins will establish simultaneous contact and a stable situation will prevail. It is also possible to have a quasi-stable contact configuration consisting of a single pin in contact, with a rate of frictional heat generation identical to that of the heat lost through conduction, convection and radiation.

The above findings were reinforced by Dow [3], who analyzed a similar model with two pins. The pins were assumed to be so short that their temperatures were functions of time alone, not of space. For given material properties, the criterion for the onset of thermoelastic instability was determined to be a critical sliding speed. It was shown, further, that such a critical sliding speed is obtainable irrespective of whether wear is present or absent, and that, in both cases, subcritical speeds correspond to thermoelastically stable operation.

Although the pin model is realistic in that so-called surface contact actually consists of multi-point contact, it fails to account for the conduction of heat along the surface, from one point of contact to

another. This effect was considered by Dow and Burton [4], who analyzed the two dimensional model of a semi-infinite knife-edge or scraper in sliding contact with the surface of a semi-infinite half-space as illustrated in fig. (3). Wear was neglected, restricting the applicability of the analysis to boundary-lubricated systems such as the apex seals in a Wankel engine. Once again a critical sliding speed was determined, above which instability would set in. In a subsequent paper [5], the authors studied the role of wear on the same contact geometry and found that thermoelastic instability would occur beyond the critical sliding speed and that the resulting patches of contact would then either move along the surface or oscillate in stress intensity about fixed nodal points.

Mechanical seals constitute a class of widespread applications in which thermoelastic instability can be of crucial importance in that surface distortions can jeopardize the sealing effect. A substantial body of literature exists for thermoelastic instability in face seals, wherein the seal is represented as a pair of thin-walled, co-axial tubes meeting end to end, with tangential sliding at the interface (fig. 4). The role of wear has been reconfirmed by Heckmann and Burton [6] who have shown that, other variables being identical, the system with the lower rate of wear will have the lower critical sliding speed and that if the wear rate exceeds a certain critical value, instability will not occur at any finite speed. Burton et al [7] have established that when a good thermal conductor slides on its own kind, unrealistically large values of friction coefficient are required for the occurrence of thermoelastic instability; they have concluded that, for a pair of identical

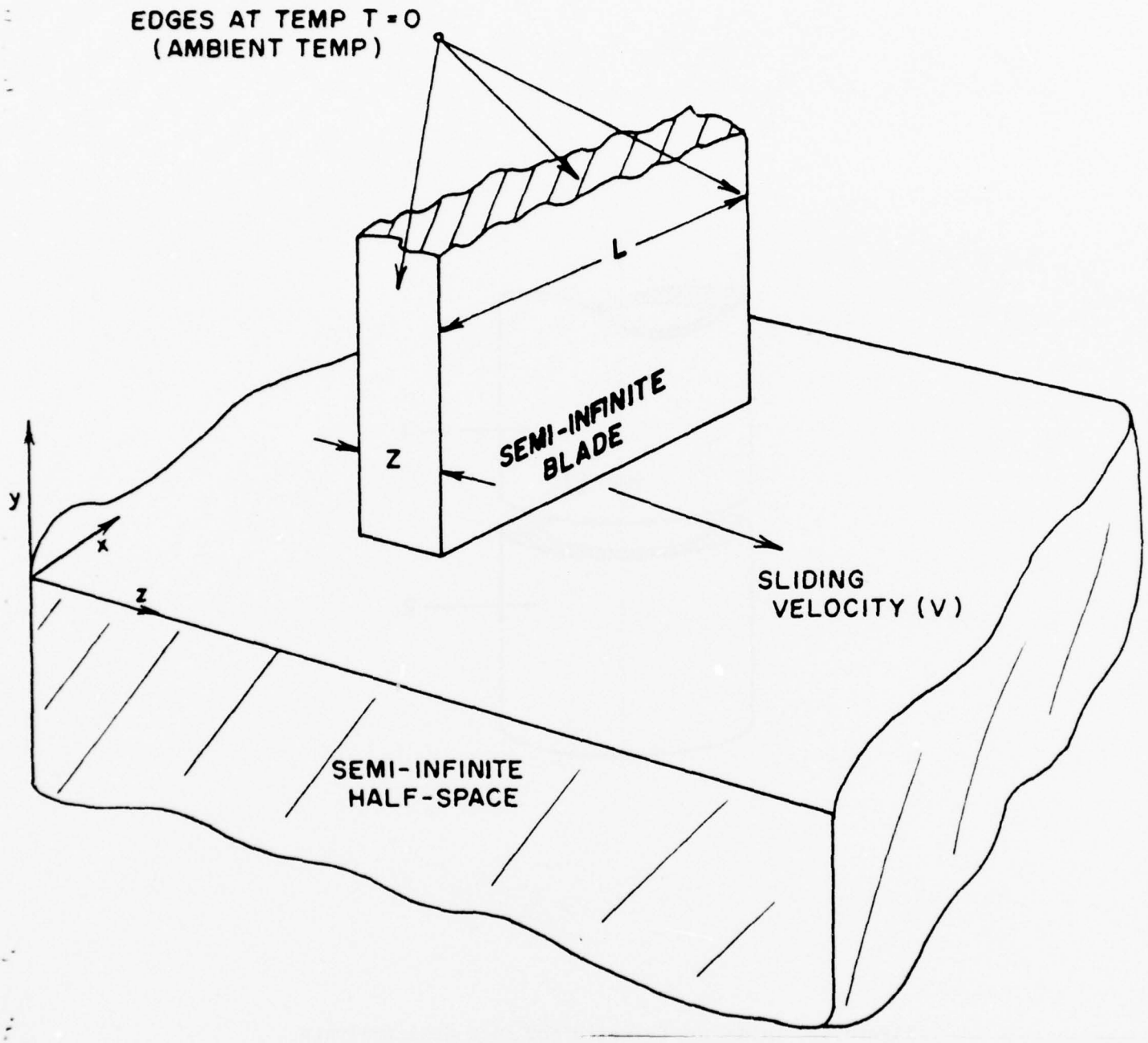

Figure 3. Two-Dimensional Model of Blade and Half-Space (Dow and Burton, ref. 4)

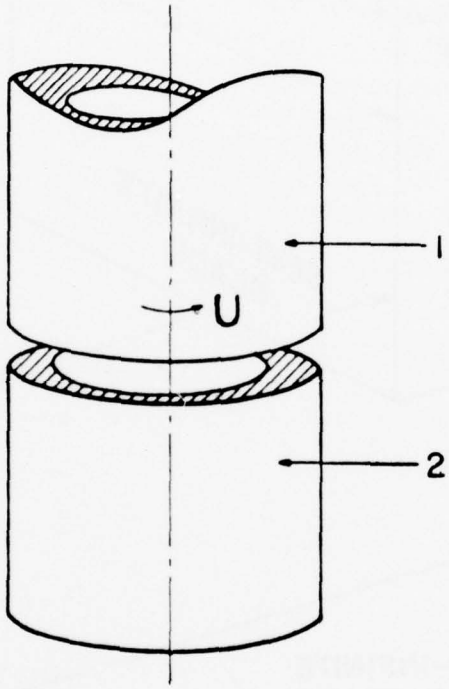

Figure 4. Thin-Tube Geometry for Face Seal Analysis

conducting materials, thermoelastic instability will not occur. A good thermal conductor sliding on a good insulator will experience such an instability the most readily. Burton [8] has elaborated on this aspect and pointed out that even when a pair of thermal conductors are used, thin deposits of oxides can render one surface a poor conductor relative to the other. A disturbance may then be relatively stationary on one surface, which will behave like a good conductor, while moving rapidly on the other, which will behave like a poor conductor. Such arguments have led to greater emphasis on conductor-insulator pairs in face seal studies.

In engineering practice, flat surfaces are never geometrically flat. Nevertheless, it has been shown that even perfectly flat surfaces will develop asperities [4]. In general, the roughness of a surface is composed of roughness components of numerous different wavelengths, and the largest wavelength is known to have the lowest critical speed [5]. In the case of the radial face seal, the largest possible wavelength is the circumference of the seal. It has also been shown that initially flat surfaces are deformed by thermoelastic instability so that contact occurs through a number of patches or hot spots which ultimately acquire a limiting configuration [9] in which the size of a patch is independent of load, but dependent on sliding speed. Burton and Nerlikar [10] have shown that the effect of increased load is heightened thermal effects leading to greater surface deformation and increased leakage. They have also demonstrated [11] that if initial surface curvature is taken into account and the load at the outset is assumed to be borne by a number of Hertzian contacts, increase of sliding speed monotonically

decreases the width of the contact patches. This effect has been shown to be quite dramatic if the Hertzian patches are assumed to overlap, implying full contact but non-uniform pressures. Kilaparti [12] has experimentally demonstrated thermoelastic instability by running a metal cup with a flat lip on a slab of glass. At high speeds, bright flashes or hot spots have been seen to form and slowly traverse the face. Photographs of the metal face taken after such runs (fig. 5) show dark tracks indicative of the path traversed by the hot spots.

There are numerous other applications where thermoelastic instability may be of consequence. In gas turbines [13], where very high speeds and temperatures prevail, severe problems can conceivably arise from occasional contact between blade tips and shrouds. In electrical machinery involving high current flows, frictional and electrical heating can significantly alter the contact at the brushes, thereby generating high resistance in the current flow paths and further exacerbating electrical heat generation. Such problems have in fact been reported and now await analysis.

All of the above work was concerned with dry friction. With wear assumed to be negligible, the results could be extended to include boundary lubricated cases. Left out was the large body of applications in which fluid films, liquid or gaseous, are maintained between the sliding surfaces. The present work seeks to fill that gap by asking whether thermoelastic instability can occur in the presence of a viscous lubricating film.

In view of the complexities involved, the study has been conducted in three phases. The first phase, simplified by an idealized model,

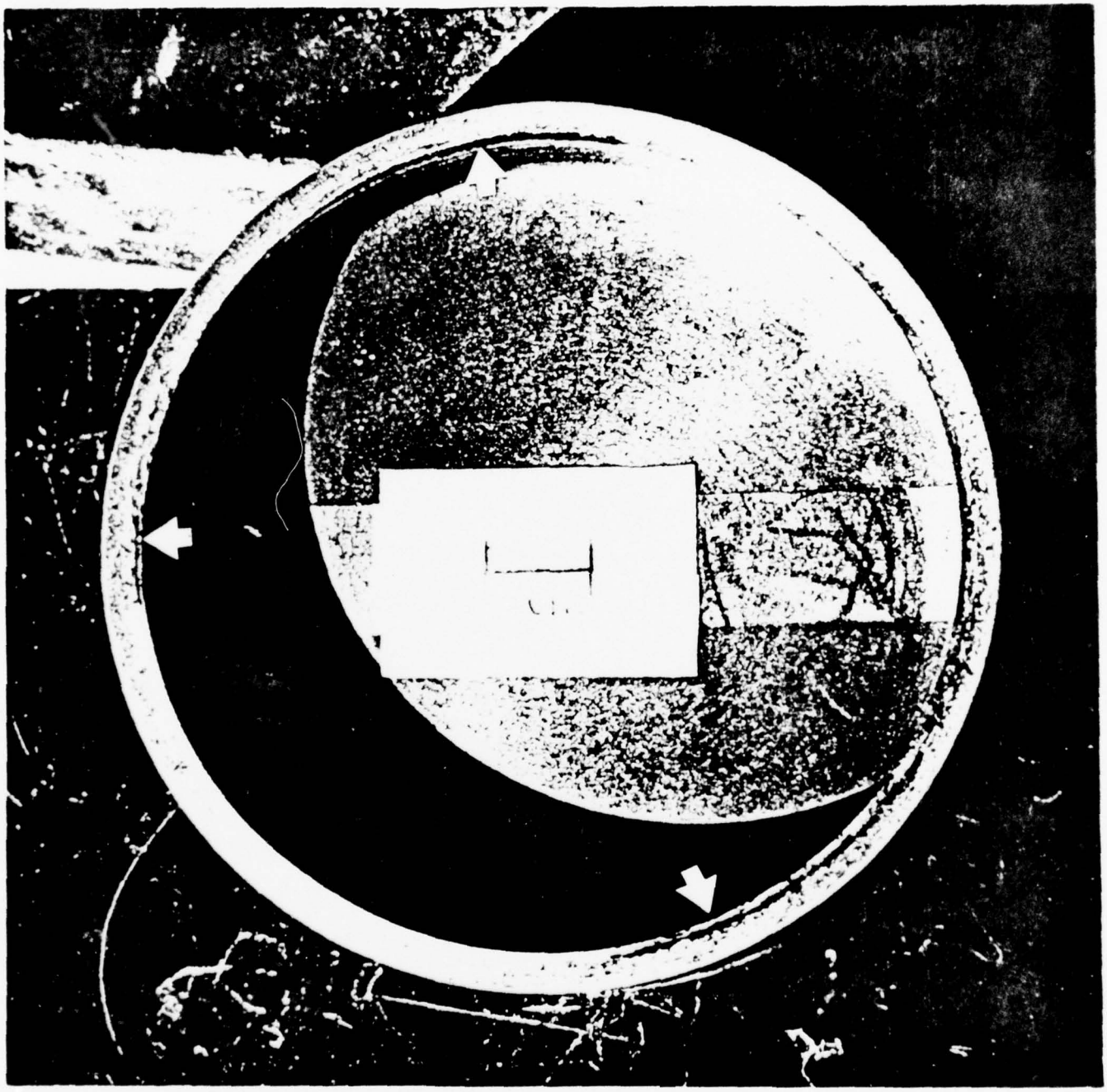

Figure 5. Photograph of Bronze Face With Burnt Tracks (Arrows) Illustrating the Movement of Hot Spots (Kilaparti, ref. 12)

deals with surfaces that are perfectly flat. No questions are asked as to whether such flat surfaces can exist in practice; instead, the question is posed as follows: "If, somehow, the surfaces are flat and separated by a film of liquid lubricant, is there a critical sliding speed above which thermoelastic instability will occur?" Such a critical speed is, in fact, obtained and seen to depend on the thickness of the film and material properties. Furthermore, it is seen that instability can occur only for a range of film thickness. The simplified model permits a fairly rigorous theoretical analysis.

The second phase consists of experiments run with the purpose of determining whether thermoelastic instability can be produced in the laboratory. Not only have they been observed and recorded, but also, much to the author's surprise, the measured critical speeds have been found to be embarrassingly close to those predicted by the idealized analysis of the first phase.

Finally, it is recognized that real surfaces are never geometrically flat. Even surfaces that are almost flat at the outset will, under thermoelastic effects, evolve through a succession of stable states into wavy surfaces as reported, for instance, by Taniguchi and Ettles [14]. Nonlinear effects make the analysis somewhat difficult. It is found, however, that in theory a number of operating conditions can be defined to represent neutrally stable thermoelastic states. In practice, such states will not be reached because they lie beyond the critical speed defined in the first phase, and this critical speed cannot be exceeded. This explains the close conformity between theoretically predicted and experimentally measured results, but not the exact mode by which the critical speed is actually attained.

CHAPTER II

INSTABILITY FOR INITIALLY FLAT SURFACES

2.1 Geometry and Procedure

Two circular, co-axial cylinders are pressed end to end and one is made to turn against the other (fig. 4). To simplify the analysis, the cylinders are replaced by two flat, co-planar blades that slide relative to each other along a straight, common edge or interface. This is not a great departure from the original configuration as long as the wall-thickness of the cylinders is small compared to the radius. This approximation will permit the use of the simpler cartesian coordinate system in applying such equations as the two-dimensional Fourier heat conduction equation.

During sliding, if the pressure is uniform along the interface, the temperature will gradually rise to a steady-state value determined by distant boundary conditions. If, however, a small disturbance perturbs the uniform pressure, prevailing conditions may cause this disturbance to grow, to be damped out, or to remain unchanged. If it remains unchanged, the system is in neutral stability. In that case, the effects triggered by the perturbation will together result in regenerating the original perturbation via some sort of a "closed-loop" phenomenon. Since the disturbance itself may be expressed as a Fourier series of waves along the common interface, the stability of the pressure (or temperature) distribution may be investigated in terms of the

stability of the component waves. In practice, such perturbations are often caused by small particles of debris in the interfacial space.

It has been pointed out that a like-on-like material pairing provides the best stability of operation, whereas a good thermal conductor sliding on a non-conductor has the greatest potential for instability. For this reason, the latter kind of material pairing is being studied. This also leads to considerable simplification of the analysis and a better chance of interpreting the relative influence of various material properties.

The problem is formulated as a linear one with linear heat transfer, thermal expansion and elastic displacement. The materials are assumed to obey Hooke's law and to have constant properties. The properties of the lubricant are also assumed constant to begin with and it is hoped that the results of the simplified analysis will provide valuable insight into the effects of variable properties. The problem is then dealt with as follows (see fig. 6):

1. It is assumed that the two surfaces are nominally flat at the outset and are separated by a lubricant film of a certain thickness $\bar{h}$.

2. A small perturbation is subsequently introduced in the form of a temperature wave which causes a small surface wave h' to develop on the conducting body. Since in the original cylinder configuration such a wave would have been continuous around the circumference, in the idealized flat-blade model the component harmonics of the wave must complete one or more full cycles between the "ends" of the plate.

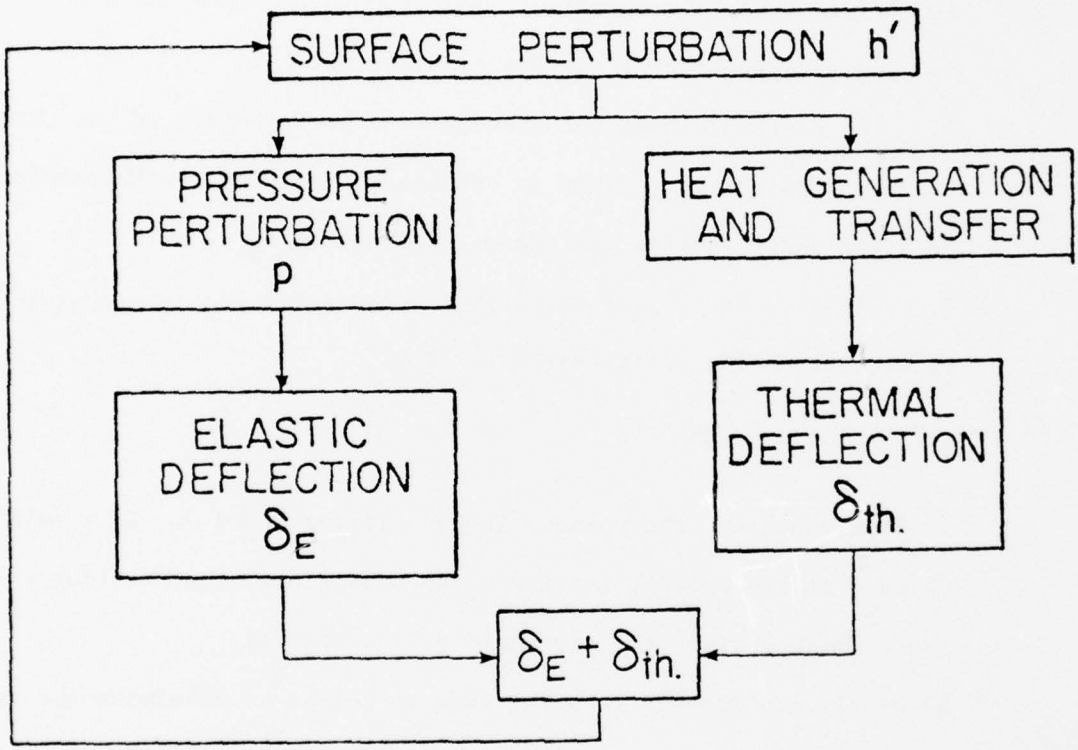

Figure 6. Block Diagram for Analysis of Initially Flat Surfaces

3. The surface wave h' alters the velocity distribution, the pressure distribution and the heat transfer in the oil film. The energy equation is used to functionally relate the temperature perturbation T with its effect h' (or vice versa, as far as the practical mechanism is concerned).

4. The resulting pressure disturbance is determined from the linearized Reynold's equation. This then determines the elastic (or pressure-generated) surface displacement δ_E.

5. The perturbed heat balance causes a perturbation in the thermoelastic displacement. This is obtained by solving the thermoelastic equation and is called the thermal deflection δ_{th}.

6. Finally, it is postulated that a neutrally stable situation does exist, for which, as explained earlier,

$$h' = \delta_{th} + \delta_E \quad .$$

In this equation, the unknown is the sliding speed U. If a solution exists, it represents, for the given conditions, the critical sliding speed which defines the threshold of instability.

Evidently, no attempt is being made to define or determine the entire time dependent behavior of any perturbation. The time-dependent problem is being confined to the special instance where the perturbation neither grows, nor decays with time. In other words, this analysis does not concern itself with such questions as to how the perturbation grows, if it grows, or how it decays if it decays. Rather, it intends to seek out the threshold at which such a system will become unstable. It is hoped that in this way a satisfactory design or operational criterion can be arrived at.

2.2 Equations of Motion

The upper plate consists of a good thermal conductor, the lower plate of a good insulator. At a certain instant, a surface displacement h' occurs on the top plate. This displacement represents a small perturbation, and has a wavelength that is large compared to $\bar{h}$, the film thickness, and $|h'|$ the amplitude of the perturbation.

The upper plate is moving steadily with a velocity U as shown in fig. (7), the lower plate being at rest.

For near-parallel, viscous, stream-line flow, the Navier-Stokes equations reduce to the two dimensional equation for creeping motion

$$\mu \frac{\partial^2 u}{\partial y^2} = \frac{dp}{dx}$$

assuming that the face is wide enough to permit the ignoring of "end-leakage" effects.

For constant μ,

$$u = \frac{1}{\mu} \frac{dp}{dx} \frac{y^2}{2} + Ay + B \qquad (2\text{-}1)$$

The velocity profile will change as shown in fig. (7). Moreover, the net velocity at any point may be thought of as the superimposition of a pure Couette flow on a flow between two plates in the presence of a pressure gradient. For the Couette flow, fig. (8),

$$u_2 = \frac{2y + \bar{h}}{2(\bar{h} + h')} U \qquad (2\text{-}2)$$

For the flow with pressure gradient, fig. (9), the following boundary conditions apply

(i) $y = -\frac{\bar{h}}{2}$, $u_1 = 0$

(ii) $y = \frac{\bar{h}}{2} + h'$, $u_1 = 0$

(iii) $y = \frac{h'}{2}$, $\frac{\partial u_1}{\partial y} = 0$

(iv) $y = \frac{h'}{2}$, $u_1 = u_c$

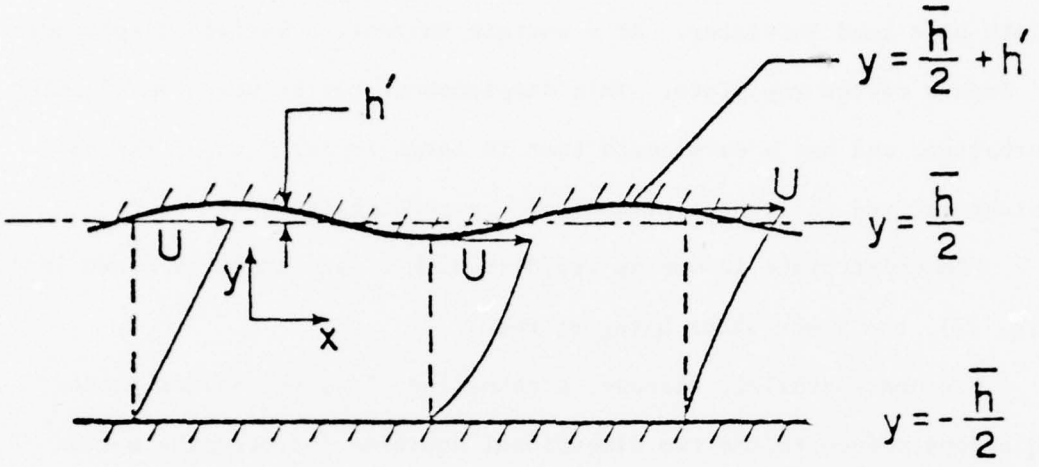

Figure 7. Coordinates System and Composite Velocity Profiles

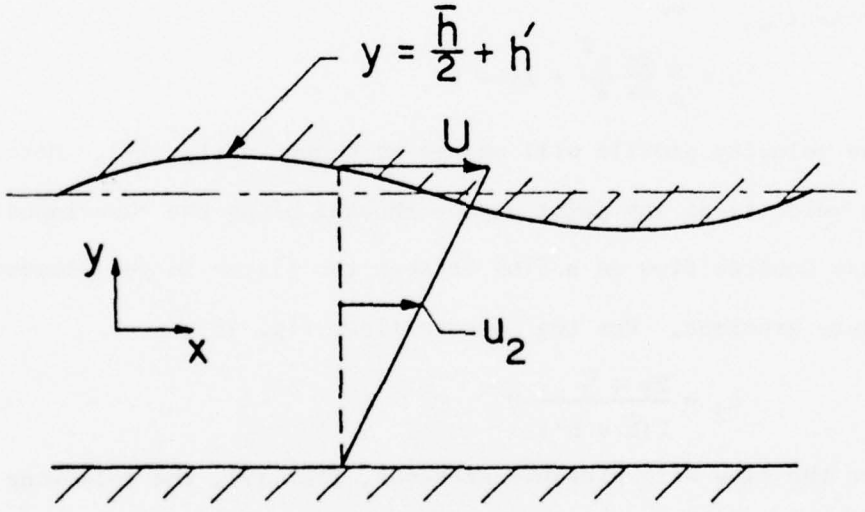

Figure 8. Couette Flow, Definition Sketch

Using the first of these, eq. (2-1) gives

$$A\,\frac{\bar{h}}{2} - B = \frac{1}{\mu}\,\frac{dp}{dx}\,\frac{\bar{h}^2}{8} \tag{2-3}$$

Boundary condition (ii) gives

$$A\left(\frac{\bar{h}}{2} + h'\right) + B = -\frac{1}{\mu}\,\frac{dp}{dx}\left(\frac{\bar{h}^2}{8} + \frac{\bar{h}h'}{2} + \frac{h'^2}{2}\right) \tag{2-4}$$

Adding together eqs. (2-3) and (2-4), one obtains

$$A = -\frac{h'}{2\mu}\,\frac{dp}{dx}$$

Eq. (2-3) then gives

$$B = -\frac{1}{\mu}\,\frac{dp}{dx}\,\bar{h}\left(\frac{h'}{4} + \frac{\bar{h}}{2}\right)$$

whence,

$$u_1 = \frac{1}{2\mu}\,\frac{dp}{dx}\left(y^2 - h'y - \frac{\bar{h}h'}{2} - \frac{\bar{h}^2}{8}\right)$$

Then, since the net velocity is given by

$$u = u_1 + u_2$$

one obtains

$$u = \frac{2y + h'}{2(\bar{h} + h')}\,U + \frac{1}{2\mu}\,\frac{dp}{dx}\left(y^2 - h'y - \frac{\bar{h}h'}{2} - \frac{\bar{h}^2}{4}\right) \tag{2-5}$$

in which dp/dx has yet to be determined.

2.3 Continuity Equation

Initially, prior to the occurrence of the surface displacement, Couette flow was in effect, for which the net flow is

$$Q_1 = \rho U\,\frac{\bar{h}}{2}$$

After the disturbance h' has occurred,

$$Q_2 = \rho U\,\frac{\bar{h} + h'}{2} + \rho u_c\,\frac{2}{3}\left(\bar{h} + h'\right) \quad \text{(refer to fig. (9))}$$

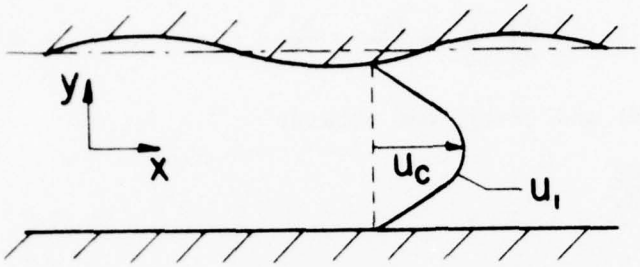

Figure 9. Pressure Flow, Definition Sketch

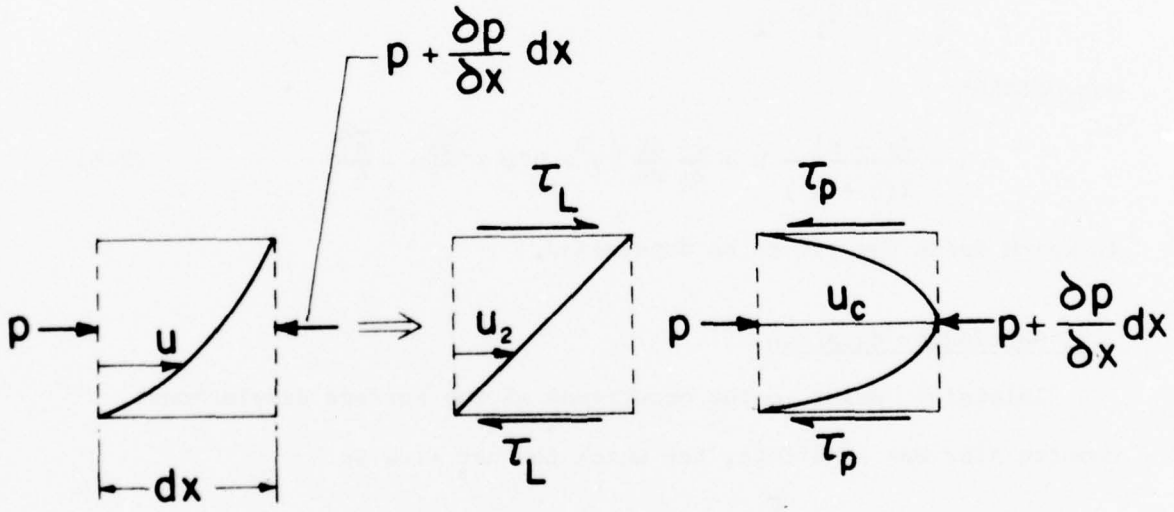

Figure 10. Shear Stresses and Pressure, Division of Composite Flow into Two Parts

For continuity of flow,

$$Q_1 = Q_2$$

whence

$$u_c = -\frac{3}{4}\frac{h'}{\bar{h} + h'} U \tag{2-6}$$

2.4 Pressure Gradient

In determining the pressure gradient dp/dx, the flow will again be broken up into two parts, one with a linear velocity profile, the other with a parabolic velocity profile, fig. (10). The shear stresses balance in the Couette flow part (subscript L denotes linear) of the composite flow. For the pressure flow, the condition for equilibrium is

$$2\tau_p \cdot dx = -\frac{\partial p}{\partial x}\left(\bar{h} + h'\right) dx \tag{2-7}$$

where

$$\tau_p = \mu\left(\frac{\partial u_1}{\partial y}\right)$$

or,

$$\tau_p = \mu \frac{2u_c}{\frac{\bar{h} + h'}{2}}$$

$\therefore$, from eq. (2-7),

$$\frac{dp}{dx} = -8\mu \frac{u_c}{\left(\bar{h} + h'\right)^2}$$

Noting that $h'/\bar{h} \ll 1$ and dropping terms containing squares of $h'/\bar{h}$, one obtains

$$\frac{dp}{dx} = -\frac{8\mu}{\bar{h}^2} u_c \left(1 - 2\frac{h'}{\bar{h}}\right) \tag{2-8}$$

Substituting for dp/dx from eq. (2-8) into eq. (2-5) gives u in terms of u_c. Use of eq. (2-6) then yields the velocity distribution in the flow. Dropping terms containing higher powers of $h'/\bar{h}$, one finds

$$u = \left\{ 3 \frac{h'}{\bar{h}^3} y^2 + \frac{y}{\bar{h}} \left(1 - \frac{h'}{\bar{h}} \right) + \frac{1}{2} - \frac{5}{4} \frac{h'}{\bar{h}} \right\} U \tag{2-9}$$

The perturbation velocity, then, is

$$u' = \left(\frac{3h'}{\bar{h}^3} y^2 - \frac{h'}{\bar{h}^2} y - \frac{5}{4} \frac{h'}{\bar{h}} \right) U \tag{2-10}$$

2.5 Non-steady, Moving, Temperature Perturbation

In the general case of a moving temperature wave whose amplitude is time-dependent, the temperature distribution in the metal may be of the form

$$T(x,y,t) = A\theta(t)Y(y)\sin(\kappa x + ay - \kappa ct)$$

and must satisfy the two-dimensional heat conduction equation,

$$\frac{\partial^2 T}{\partial x^2} + \frac{\partial^2 T}{\partial y^2} - \frac{1}{k_M} \frac{\partial T}{\partial t} = 0$$

Further, T will be required to satisfy the boundary condition that at the metal-oil interface

$$T \equiv T_s = T_o e^{\beta t} \sin(\kappa x - \kappa ct)$$

where T_o is a constant amplitude of the wave. It is easily seen that a temperature distribution T(x,y,t) that satisfies the above conditions is

$$T = T_o e^{\beta t} e^{-\xi y} \sin(\kappa x + ay - \kappa ct) \tag{2-11}$$

where

$$\xi = \frac{\kappa c}{2k_M a} \tag{2-12}$$

$$\beta = k_M(\xi^2 - \kappa^2 - a^2) \tag{2-13}$$

Equations (2-12) and (2-13), when solved for ξ and a in terms of β, give

$$\xi = \pm\left[\frac{1}{2}\left(\frac{\beta}{k_M} + \kappa^2\right) \pm \frac{1}{2}\sqrt{\left(\frac{\beta}{k_M} + \kappa^2\right)^2 + \frac{\kappa^2 c^2}{k_M^2}}\right]^{1/2} \tag{2-14}$$

and

$$a = \pm\left[-\frac{1}{2}\left(\frac{\beta}{k_M} + \kappa^2\right) \pm \frac{1}{2}\sqrt{\left(\frac{\beta}{k_M} + \kappa^2\right)^2 + \frac{\kappa^2 c^2}{k_M^2}}\right]^{1/2} \tag{2-15}$$

A few words are in order here on the nature of the parameters β, ξ, a and c. It is evident from eq. (2-11) that β represents the time-exponent of growth of the temperature perturbation T. The amplitude of this wave grows or diminishes accordingly as β is positive or negative and remains constant if $\beta = 0$.

The quantity ξ is the spatial exponent of growth of T in the "y" direction, i.e., into the body. It may be noted that in writing eq. (2-11), no explicit boundary condition was imposed, nor was a specific set of axes of co-ordinates defined. An implicit boundary condition is imposed by ξ on eq. (2-11). Since the perturbation T is dissipated as it travels into the body from its point of application, it is obvious that as $y \to \infty$, $T \to 0$. This requires that, in eq. (2-11), ξ must always be positive. In eq. (2-14), then, the outer minus sign must be ignored, as must the inner minus sign in order to ensure real values of ξ.

The quantity c is the traversal velocity of the temperature wave T. Equation (2-11) is written for a right-running wave; c may be either positive or negative to represent, respectively, a right-running or a left-running wave.

As the perturbation T penetrates the body in the "y" direction, its intensity is diminished. At the same time, however, at its surface of application (y=0, say), the original wave has moved a distance of 'c.t'. Thus at any plane $y > 0$, the corresponding perturbation $T|_{y>0}$ is not only smaller than T in amplitude, but also lags behind T in the direction of motion of the wave (fig. 11). The quantity a is a measure of this lag. Equation (2-12) indicates that c/a must have the same sign as ξ and since ξ must always be positive, c/a is always positive. Thus c and a must always have the same sign. Figure (11) is drawn directly from eq. (2-11). It is to be noted that since the lag is a result of the propagation of T, a non-moving wave (c=0) implies a=0.

Limiting Cases

One limiting case is that of c=0, viz. the non-moving wave. In this case, as is evident from eqs. (2-14) and (2-15),

$$\xi = \sqrt{\frac{\beta}{k_M} + \kappa^2}$$

and

$$a = 0$$

so that

$$T = T_o e^{\beta t} e^{-y\sqrt{\frac{\beta}{k_M} + \kappa^2}} \sin \kappa x$$

Another limiting case is that of β=0, viz, the case of the steadily moving, constant amplitude wave. In this case

$$b \equiv \xi = \left[\frac{1}{2}\kappa^2 + \frac{\kappa}{2}\sqrt{\kappa^2 + \frac{c^2}{k_M^2}}\right]^{1/2} \qquad (2\text{-}16)$$

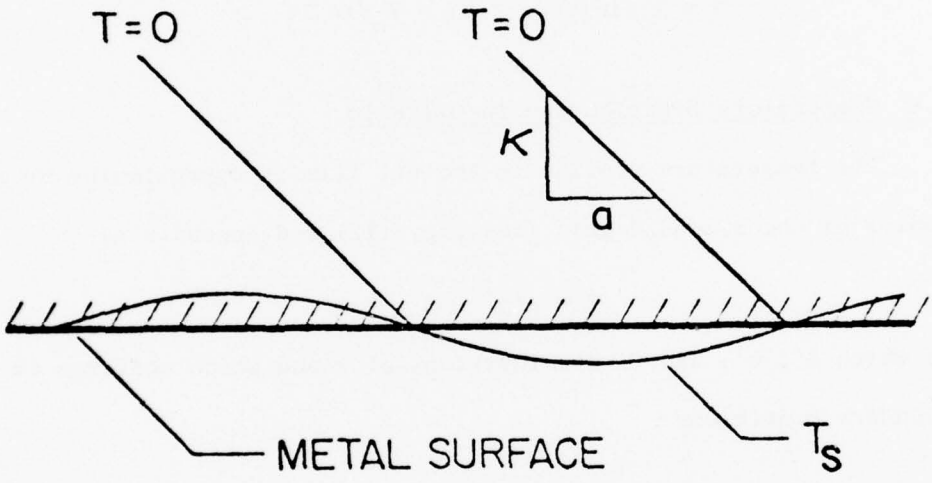

Figure 11. Lag of Temperature Wave in Metal Body

and

$$a_1 = a = \left[-\frac{1}{2}\kappa^2 + \frac{\kappa}{2}\sqrt{\kappa^2 + \frac{c^2}{k_M^2}} \right]^{1/2} \tag{2-17}$$

The temperature distribution is given by

$$T = T_o e^{-by} \sin(\kappa x + a_1 y - \kappa ct) \tag{2-18}$$

so that on the metal surface (y=0),

$$T = T_o \sin(\kappa x - \kappa ct) \equiv T_o \sin \lambda_1 \quad . \tag{2-19}$$

2.6 Temperature Distribution in Oil Film

The temperature profile in the oil film is approximated by a polynomial of the second degree (see fig. (12) and Appendix A):

$$T = A'y^2 + B'y + C' \tag{2-20}$$

in which A', B', and C' are functions of x and which conforms to the boundary conditions:

$$\text{at} \quad y = \frac{\bar{h}}{2} + h' \quad , \qquad T = T_o e^{\beta t} \sin \lambda_1 \tag{2-21}$$

$$\text{at} \quad y = \frac{\bar{h}}{2} + h' \quad , \qquad \frac{\partial T}{\partial y} = -\frac{K_M}{K_{oil}} T_o e^{\beta t} (\xi \sin \lambda_1 - a \cos \lambda_1) \tag{2-22}$$

$$\text{at} \quad y = -\frac{\bar{h}}{2} \quad , \qquad \frac{\partial T}{\partial y} = 0 \tag{2-23}$$

The first two boundary conditions derive from the fact that at the oil-metal interface the temperature is the same for the metal and the oil and the heat conducted in each medium is the same. Boundary condition (2-23) refers to the fact that the second body is a thermal insulator.

From eqs. (2-20) and (2-23), one obtains

$$B = A\bar{h}$$

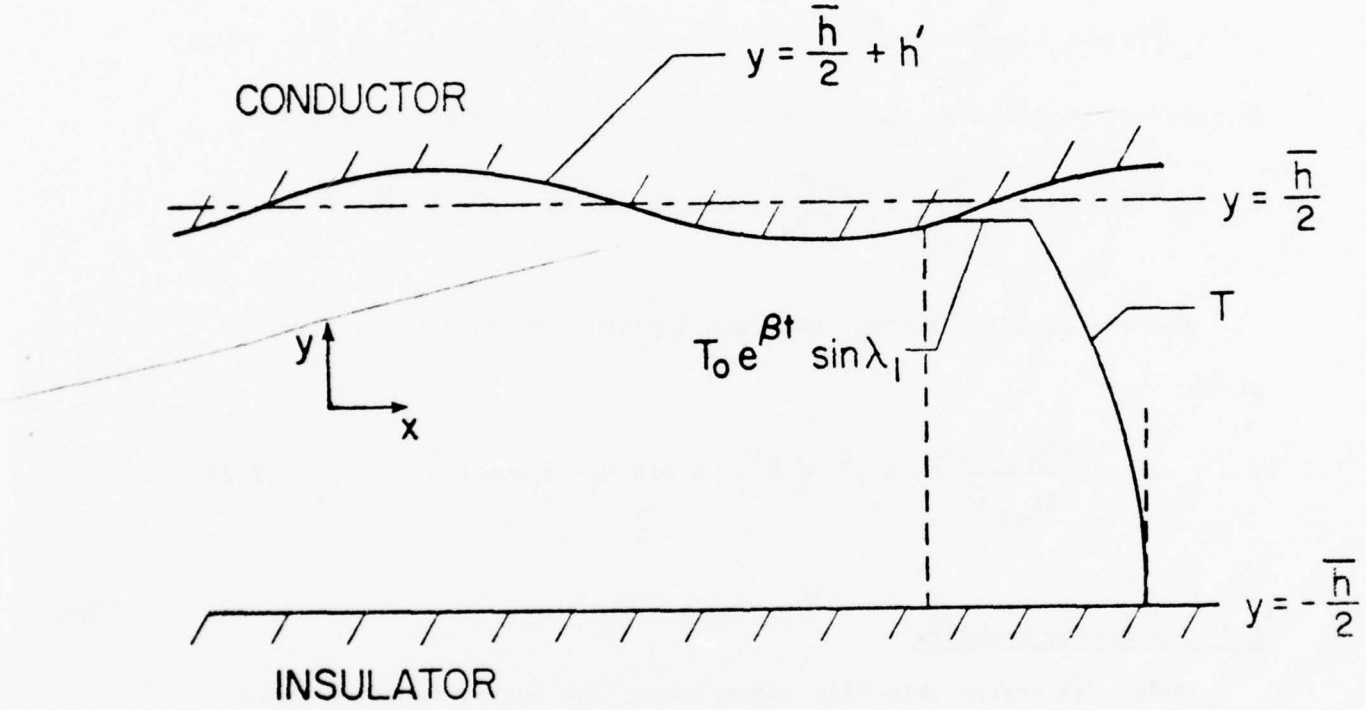

Figure 12. Temperature Distribution in Oil Film

From eqs. (2-20) and (2-22),

$$A = - \frac{K_M}{2K_{oil}} T_o e^{\beta t}\left(\xi \sin \lambda_1 - a \cos \lambda_1\right) \frac{1}{\bar{h}} \left(1 - \frac{h'}{\bar{h}}\right)$$

From eqs. (2-20) and (2-21),

$$C = T_o e^{\beta t} \sin \lambda_1 - B \left(\frac{3}{4} \bar{h}^2 + 2\bar{h}h'\right)$$

so that, finally, corrected to the first order of the perturbation,

$$T = T_o e^{\beta t} \sin \lambda_1 - \frac{K_M}{2K_{oil}} T_o e^{\beta t}\left(\xi \sin \lambda_1 - a \cos \lambda_1\right) \frac{1}{\bar{h}} \left(\bar{h}y + y^2 - \frac{3}{4} \bar{h}^2\right) \quad (2\text{-}24)$$

As before, two limiting cases may exist. For c=0, the non-moving wave,

$$T = T_o e^{\beta t} \sin \kappa x - \frac{K_M}{2K_{oil}\bar{h}} T_o e^{\beta t} \sqrt{\frac{\beta}{K_M} + \kappa^2} \sin \kappa x \left(\bar{h}y + y^2 - \frac{3}{4} \bar{h}^2\right) .$$

For the steadily moving, constant amplitude wave, β=0, eq. (2-24) gives

$$T = T_o \sin \lambda_1 - \frac{K_M T_o}{2K_{oil}\bar{h}} \left(\bar{h}y + y^2 - \frac{3}{4} \bar{h}^2\right) \left(b \sin \lambda_1 - a_1 \cos \lambda_1\right) \quad (2\text{-}25)$$

2.7 The Energy Equation

Under the stated thin-film assumptions, the energy equation takes the form

$$\int_{y_1}^{y_2} \left(\rho C u \frac{\partial T}{\partial x} + \rho C \frac{\partial T}{\partial t}\right) dy - \int_{y_1}^{y_2} K_{oil} \frac{\partial^2 T}{\partial y^2} dy = \int_{y_1}^{y_2} \mu \left(\frac{\partial u}{\partial y}\right)^2 dy \quad (2\text{-}26)$$

Here C is the specific heat of the oil. The first and second term on the left hand side are, respectively, the convective and local contributions to the increase of internal energy of the oil. The third term on the left is the negative of the heat conducted <u>into</u> the oil while the right hand term is the heat generated through friction.

Define

$$q_{cc} \equiv \int_{y_1}^{y_2} \rho\ C\ u\ \frac{\partial T}{\partial x}\ dy$$

$$q_{c\ell} \equiv \int_{y_1}^{y_2} \rho\ C\ \frac{\partial T}{\partial t}\ dy$$

$$q_k \equiv \int_{y_1}^{y_2} K_{oil}\ \frac{\partial^2 T}{\partial y^2}\ dy$$

$$q_g \equiv \int_{y_1}^{y_2} \mu \left(\frac{\partial u}{\partial y}\right)^2 dy$$

Using eqs. (2-24) and (2-9), one finds

$$q_{cc} = \frac{U\kappa T_o e^{\beta t}}{2k_{oil}} \left\{K_{oil}\bar{h} \cos \lambda_1 + \frac{1}{4} K_M \bar{h}^2 \left(a \sin \lambda_1 + \xi \cos \lambda_1\right)\right\} \qquad (2\text{-}27)$$

For the non-propagating wave, (c=0), eq. (2-27) reduces to

$$q_{cc} = \frac{U\kappa T_o e^{\beta t}}{2k_{oil}} \left\{K_{oil}\bar{h} \cos \kappa x + \frac{1}{4} K_M \bar{h}^2 \sqrt{\frac{\beta}{k_M} + \kappa^2} \cos \kappa x\right\} \qquad (2\text{-}28)$$

Returning to eq. (2-27), the steadily-moving, constant amplitude wave, (β=0), gives

$$q_{cc} = \frac{U\kappa T_o}{2k_{oil}} \left\{K_{oil}\bar{h} \cos \lambda_1 + \frac{1}{4} K_M \bar{h}^2 \left(a_1 \sin \lambda_1 + b \cos \lambda_1\right)\right\} \qquad (2\text{-}29)$$

Equation (2-24) yields

$$q_{c\ell} = \frac{T_o e^{\beta t}}{k_{oil}} \left\{\beta\ \bar{h}\ K_{oil} + \frac{1}{3} K_M \bar{h}^2 \left(\beta\xi - \kappa c a\right)\right\} \sin \lambda_1$$

$$- \frac{T_o e^{\beta t}}{k_{oil}} \left\{c\ \bar{h}\ K_{oil} + \frac{1}{3} K_M \bar{h}^2 \left(\beta a + \kappa c \xi\right)\right\} \cos \lambda_1 \qquad (2\text{-}30)$$

For the non-propagating wave (c=0), this becomes,

$$q_{c\ell} = \frac{T_o \beta e^{\beta t}}{k_{oil}} \left(\bar{h}\, K_{oil} + \frac{1}{3} K_M \bar{h}^2 \sqrt{\frac{\beta}{k_M} + \kappa^2} \right) \sin \kappa x \qquad (2\text{-}31)$$

The steadily moving, constant amplitude wave (β=0) gives, from eq. (2-30),

$$q_{c\ell} = \frac{T_o}{k_{oil}} \left\{ -\frac{1}{3} K_M \bar{h}^2 \kappa c a_1 \sin \lambda_1 - \left(\kappa c \bar{h}\, K_{oil} + \frac{1}{3} K_M \bar{h}^2 \kappa c b \right) \cos \lambda_1 \right\}$$

or

$$q_{c\ell} = - \frac{T_o c \kappa}{k_{oil}} \left\{ \frac{1}{3} K_M \bar{h}^2 a_1 \sin \lambda_1 + \left(\bar{h}\, K_{oil} + \frac{1}{3} K_M \bar{h}^2 b \right) \cos \lambda_1 \right\} \qquad (2\text{-}32)$$

The frictional dissipation is obtained from eq. (2-9) for the velocity distribution:

$$q_g = - \mu \frac{U^2}{\bar{h}} h'$$

Nothing has been said yet about h' other than that it is a small surface deformation that corresponds with the temperature perturbation T. Obviously, h' and T cannot both be arbitrarily chosen, as one is a function of the other. In this case an arbitrary T has been chosen and h' will follow from it. At this stage, however, it is appropriate to define the form h' will take, it being known that it must take some wave form.

Let $h' \equiv h_1 \sin \lambda_1 + h_2 \cos \lambda_1$ where h_1 and h_2 are unknowns to be subsequently determined.

Then,

$$q_g = - \mu \frac{U^2}{\bar{h}} \left(h_1 \sin \lambda_1 + h_2 \cos \lambda_1 \right) \qquad (2\text{-}33)$$

The above, derived from the velocity distribution alone, is dependent on the nature of the temperature perturbation only through h_1 and h_2.

Thus the basic form, given by eq. (2-33), is true for all cases. The heat conducted <u>into</u> the oil, q_k, is derived from eq. (2-24) and found to be

$$q_k = - K_M T_o e^{\beta t} \left[\xi \sin \lambda_1 - a \cos \lambda_1 \right] \tag{2-34}$$

For c=0, the above becomes

$$q_k = - K_M T_o e^{\beta t} \sqrt{\frac{\beta}{k_M} + \kappa^2} \sin \kappa x$$

For β=0, eq. (2-34) gives

$$q_k = - K_M T_o \left[b \sin \lambda_1 - a_1 \cos \lambda_1 \right] \tag{2-35}$$

In all of the above equations, constant fluid properties have been assumed. If q_{cc}, $q_{c\ell}$, q_k, and q_g are substituted for in eq. (2-26), the sine and cosine terms on the left-hand side must be equal, respectively, to those on the right-hand side. Thus, using eqs. (2-26), (2-27), (2-30), (2-33) and (2-34), one obtains:

$$h_1 = - \frac{\bar{h}^3 T_o e^{\beta t}}{\mu U^2 k_{oil}} \left[\frac{1}{8} U\kappa K_M \bar{h} a + \beta \left(K_{oil} + \frac{1}{3} K_M \bar{h} \xi \right) - \frac{1}{3} K_M \bar{h} \kappa c a \right]$$

$$- \frac{\bar{h}^2}{\mu U^2} K_M \xi T_o e^{\beta t} \tag{2-36}$$

and

$$h_2 = - \frac{\bar{h}^3 T_o e^{\beta t}}{\mu U^2 k_{oil}} \left[\frac{U\kappa}{2} \left(K_{oil} + \frac{1}{4} K_M \bar{h} \xi \right) - \kappa c \left(K_{oil} + \frac{1}{3} K_M \bar{h} \xi \right) \right.$$

$$\left. - \frac{1}{3} K_M \bar{h} \beta a \right] + \frac{\bar{h}^2}{\mu U^2} K_M T_o e^{\beta t} a \tag{2-37}$$

For c=0, i.e., for a non-moving wave, the above two equations become:

$$h_1 = -\frac{\bar{h}^3 T_o e^{\beta t}}{\mu U^2 k_{oil}}\left[\beta\left(K_{oil} + \frac{1}{3} K_M \bar{h}\sqrt{\frac{\beta}{k_M} + \kappa^2}\right)\right] - \frac{\bar{h}^2}{\mu U^2} K_M T_o e^{\beta t}\sqrt{\frac{\beta}{k_M} + \kappa^2} \qquad (2\text{-}38)$$

and

$$h_2 = -\frac{\bar{h}^3 T_o e^{\beta t}}{\mu U^2 k_{oil}}\left[\frac{U\kappa}{2}\left(K_{oil} + \frac{1}{4} K_M \bar{h}\sqrt{\frac{\beta}{k_M} + \kappa^2}\right)\right] \qquad (2\text{-}39)$$

The corresponding relations for the steadily moving, constant amplitude wave (β=0) are

$$h_1 = -\frac{\bar{h}^3 T_o}{\mu U^2 k_{oil}}\left[\frac{1}{8} U\kappa K_M \bar{h} a_1 - \frac{1}{3} K_M \bar{h} \kappa c a_1\right] - \frac{\bar{h}^2}{\mu U^2} K_M T_o b$$

or

$$h_1 = -\frac{\bar{h}^2 T_o K_M}{\mu U^2}\left[\frac{\kappa \bar{h}^2 a_1}{k_{oil}}\left(\frac{1}{8} U - \frac{1}{3} c\right) + b\right] \qquad (2\text{-}40)$$

and

$$h_2 = -\frac{\bar{h}^2 T_o}{\mu U^2}\left[\left\{\frac{U\kappa\bar{h}}{2k_{oil}}\left(K_{oil} + \frac{1}{4} K_M \bar{h} b\right) - \frac{\bar{h}}{k_{oil}} \kappa c\left(K_{oil} + \frac{1}{3} K_M \bar{h} b\right)\right\} - K_M a_1\right] \qquad (2\text{-}41)$$

2.8 Thermal Deflection

Under the action of the temperature wave (**eq.** (2-11)) generated in the metal, its surface undergoes a thermal deflection which may be determined by solving the thermoelastic equation:

$$\frac{\partial^2 \psi}{\partial x^2} + \frac{\partial^2 \psi}{\partial y^2} = (1 + \nu)\alpha_M T \qquad (2\text{-}42)$$

where T is given by eq. (2-11) and y is measured into the metal from its surface.

Equation (2-42) has the homogeneous solution

$$\Psi_H = e^{\beta t} e^{-\kappa y}\left(C \cos \lambda_1 + D \sin \lambda_1\right)$$

and a particular solution

$$\Psi_p = P\, e^{\beta t} e^{-\xi y} \cos \lambda + Q\, e^{\beta t} e^{-\xi y} \sin \lambda$$

where C, D, P and Q are constants. In order for Ψ_p to satisfy eq. (2-42), one must have

$$P = \frac{\kappa c}{\beta} Q$$

and

$$P = \frac{(1 + \nu)\alpha_M T_o k_M \kappa c}{\kappa^2 c^2 + \beta^2} \tag{2-43}$$

$$Q = \frac{(1 + \nu)\alpha_M T_o k_M \beta}{\kappa^2 c^2 + \beta^2} \tag{2-44}$$

Then

$$\Psi = \Psi_H + \Psi_p \tag{2-45}$$

whence

$$\begin{aligned} v = \left.\frac{\partial \Psi}{\partial y}\right|_{y=0} &= -\kappa e^{\beta t}\left(C \cos \lambda_1 + D \sin \lambda_1\right) \\ &\quad - \xi e^{\beta t}\left(P \cos \lambda_1 + Q \sin \lambda_1\right) \\ &\quad + a e^{\beta t}\left(Q \cos \lambda_1 - P \sin \lambda_1\right) \end{aligned}$$

Here "v" is the normal displacement of the surface. If this displacement is suppressed, a thermoelastic normal stress σ_y and zero shear stress will appear at the boundary. Putting v=0 in the above equation, the sums of the coefficients of the sine and cosine terms must each be zero. This leads to

$$C = \frac{1}{\kappa} (a Q - \xi P) \tag{2-46}$$

and

$$D = - \frac{1}{\kappa} (\xi Q + aP) \tag{2-47}$$

Thus

$$\Psi = e^{\beta t} e^{-\kappa y} \left(C \cos \lambda_1 + D \sin \lambda_1 \right) + e^{\beta t} e^{-\xi y} (P \cos \lambda + Q \sin \lambda) \tag{2-48}$$

in which C, D, P and Q are given by eqs. (2-46), (2-47), (2-43) and (2-44) respectively.

The thermal stress corresponding to the displacement potential Ψ in eq. (2-48) can now be derived from Hooke's Law:

$$\sigma_y = \frac{E}{1-\nu^2} \left[\frac{\partial^2 \Psi}{\partial y^2} + \nu \frac{\partial^2 \Psi}{\partial x^2} - (1 + \nu) \alpha_M T \right]$$

The surface stress is given by

$$\sigma_s = \sigma_y \Big|_{y=0}$$

and a corresponding imaginary pressure p_1 can be defined such that

$$p_1 \equiv - \sigma_s$$

which holds the surface flat, but stressed. In order to determine the thermally induced deflection, under zero σ_s, p_1 must be relieved by the superimposition of another imaginary pressure p_2 such that

$$p_1 + p_2 = 0$$

The surface can then be thought of as being stress-free and subjected to the fullest deflection. Dow [3] has shown that p_2 gives a deflection:

$$\delta_{th} = \frac{2p_2}{E\kappa} = - \frac{2p_1}{E\kappa} \qquad \text{(see Appendix B, eq. (B-5))}$$

Carrying out the above steps, one obtains

$$\delta_{th} = \frac{2\kappa\,\alpha_M T_o e^{\beta t}}{\kappa^2 c^2 + \beta^2}\left[\left\{\beta k_M\left(1 - \frac{\varepsilon}{\kappa}\right) - k_M ca\right\}\sin\lambda_1 + \left\{\kappa c k_M\left(1 - \frac{\varepsilon}{\kappa}\right) + \frac{a k_M \beta}{\kappa}\right\}\cos\lambda_1\right] \tag{2-49}$$

This gives, for the case of the non-propagating wave (c=0),

$$\delta_{th} = \frac{2\alpha_M k_M T_o e^{\beta t}}{\beta}\left(\kappa - \sqrt{\frac{\beta}{k_M} + \kappa^2}\right)\sin\kappa x \tag{2-50}$$

If the temperature wave is moving steadily with a constant amplitude (β=0), eq. (2-49) gives

$$\delta_{th} = \frac{2\alpha_M k_M T_o}{\kappa c}\left\{-a_1\sin\lambda_1 + (\kappa - b)\cos\lambda_1\right\} \tag{2-51}$$

2.9 Elastic Deflection

Reynold's equation of hydrodynamic lubrication gives

$$\frac{\partial}{\partial x}\left(h^3\frac{\partial p}{\partial x}\right) = 6\mu\, U\frac{\partial h}{\partial x} \tag{2-52}$$

in which

$$h = \bar{h} + h'$$

and, since

$$\frac{h'}{\bar{h}} \ll 1,$$

$$h^3 = \bar{h}^3\left(1 + 3\frac{h'}{\bar{h}}\right)$$

in which $\bar{h}$ is constant. Then, integrating Reynold's equation twice and dropping the constants of integration, one has

$$p = \frac{6\mu U}{\kappa\bar{h}^3}\left(h_2\sin\lambda_1 - h_1\cos\lambda_1\right) \tag{2-53}$$

The constants of integration are dropped because of the need for p to be single-valued around the circumference, and because a pure constant, added to p, will merely represent a uniform pressure that produces no surface curvature. It has been shown that (eq. (B-5))

$$\delta_E = \frac{2p}{E\kappa} \tag{2-54}$$

Equations (2-53) and (2-54) then give the elastic displacement

$$\delta_E = \frac{12\mu U}{E\kappa h^3}\left(h_2 \sin \lambda_1 - h_1 \cos \lambda_1\right) \tag{2-55}$$

2.10 The Narrow-Lip Seal

In the preceding pages, no account has been taken of the width of the seal face (lip), although pressure and velocity have been assumed constant across the lip. The preceding analysis, therefore, applies to seals with lips that are wide enough to permit the ignoring of "end leakage." As with "long" and "short" bearings, we can here treat the "narrow-lip seal" as a separate class of face-type seals. Indeed, in the class of seals studied here, narrow lips are of the greater likelihood.

The simplified Navier-Stokes equations are

$$\mu \frac{\partial^2 u}{\partial y^2} = \frac{\partial p}{\partial x}$$

$$\mu \frac{\partial^2 w}{\partial y^2} = \frac{\partial p}{\partial z} \tag{2-56}$$

and the continuity equation is

$$\frac{\partial u}{\partial x} + \frac{\partial w}{\partial z} = 0 \tag{2-57}$$

With the present co-ordinate system, fig. (13), the boundary conditions are

$$y = -\frac{\bar{h}}{2} \quad : \quad u = 0 \ , \qquad w = 0$$

$$y = \frac{\bar{h}}{2} + h' \ : \quad u = U \ , \qquad w = 0$$

$$z = 0 \qquad : \quad \frac{\partial p}{\partial z} = 0 \ , \qquad p = p_{max.}$$

$$z = \pm \frac{L}{2} \quad : \quad p = 0$$

The above equations may be solved first for u and w and then for p, to obtain

$$u = \frac{1}{2\mu} \frac{\partial p}{\partial x} \left(y^2 - \frac{\bar{h}^2}{4} \right) + U \left(1 - \frac{h'}{\bar{h}} \right) \left(\frac{y}{\bar{h}} + \frac{1}{2} \right)$$

$$w = \frac{1}{2\mu} \frac{\partial p}{\partial z} \left(y^2 - \frac{\bar{h}^2}{4} \right)$$

$$p = \frac{3\mu U}{\bar{h}^3} \frac{dh'}{dx} \left(z^2 - \frac{L^2}{4} \right) \qquad (2\text{-}58)$$

where it has been assumed that

$$\frac{\partial p}{\partial x} \ll \frac{\partial p}{\partial z}$$

and where second and higher order terms have been dropped.

Along the center line (z=0), the pressure is maximum,

$$p_{max.} = - \frac{3\mu U L^2}{4\bar{h}^3} \frac{dh'}{dx} \qquad (2\text{-}59)$$

while the average pressure is (fig. 14)

$$\bar{p} = \frac{2}{3} p_{max.} = - \frac{\mu U L^2}{2\bar{h}^3} \frac{dh'}{dx}$$

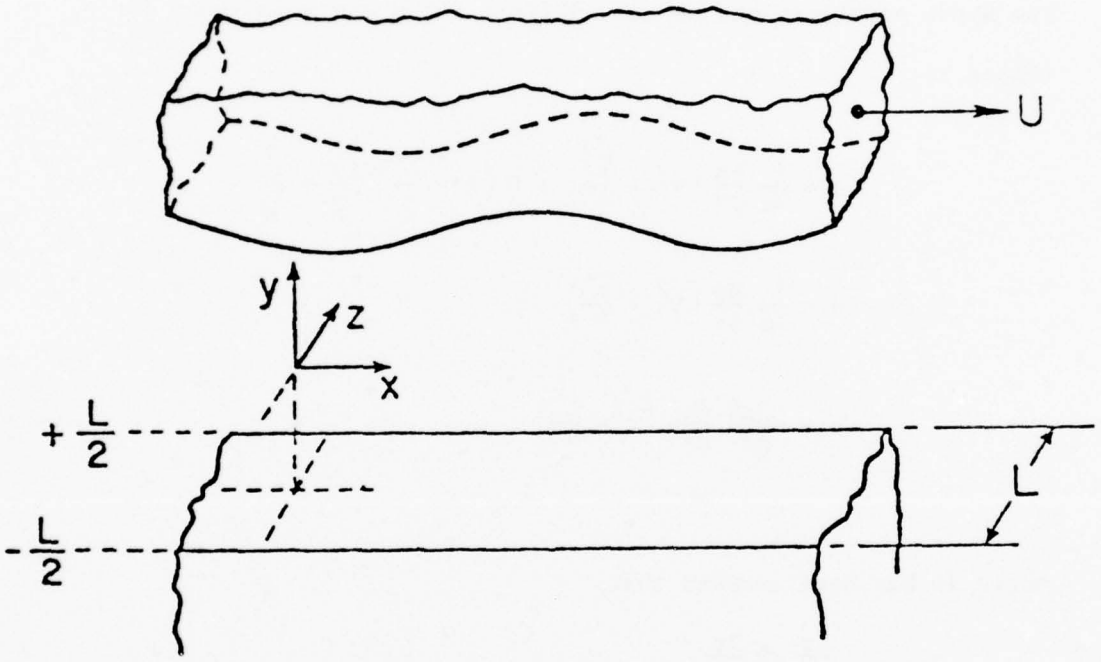

Figure 13. Axes of Coordinates for the Narrow-Face Seal

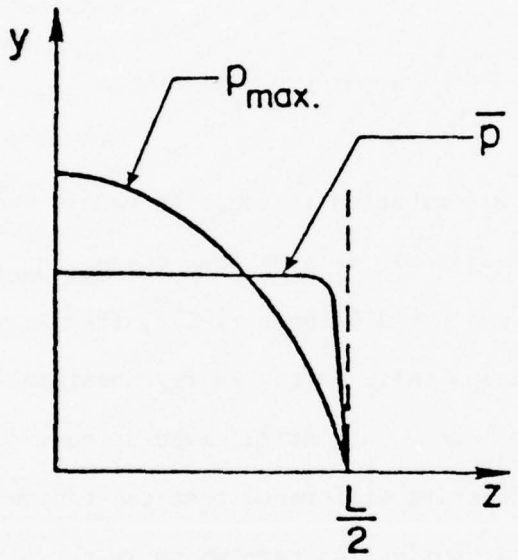

Figure 14. Maximum and Average Pressure in the Narrow-Face Seal

In the following, $\bar{p}$ is treated as the working pressure. The elastic deflection is then given by

$$\delta_E = \frac{2\bar{p}}{E\kappa}$$

whence

$$\delta_E = -\frac{\mu U L^2}{E\kappa\,\bar{h}^3}\,\frac{dh'}{dx}$$

If $h' = h_1 \sin\lambda_1 + h_2 \cos\lambda_1$,

$$\delta_E = -\frac{\mu U L^2}{E\,\bar{h}^3}\left(h_1\cos\lambda_1 - h_2\sin\lambda_1\right) \qquad (2\text{-}60)$$

The temperature distribution is found to remain unchanged and is still given by eq. (2-24). It is seen that q_k, q_g, q_{cc}, and $q_{c\ell}$ all remain as before and are given by eqs. (2-33), (2-32), (2-27) and (2-29) respectively. This means that, in the energy equation, all terms remain the same and h_1 and h_2 are still given by eqs. (2-35) and (2-36).

Thus the only effective difference that the narrow-lip consideration makes is in the elastic deflection term which is now $L^2\kappa^2/12$ times the value given by eq. (2-55). This is a non-dimensional multiplier which may be introduced in eq. (2-55) to denote the departure of the configuration from the wide-lip one. Let us call this factor W. Then

$$\delta_E = \frac{12\mu W}{E\kappa^2\bar{h}^3}\,U(h_2\sin\lambda_1 - h_1\cos\lambda_1) \qquad (2\text{-}61)$$

Here, for a narrow-face seal, W will have the appropriate value. The wide-lip seal is a limiting case of the narrow-lip one and is represented by W = 1.

2.11 Instability Threshold of the Steadily Moving Perturbation

In the absence of adequate understanding of the phenomena that occur in face-type seals, no prediction can be made as to whether a perturbation will necessarily be moving or stationary. This is why the temperature perturbation (eq.(2-11)) has been defined to include both possibilities. However, since the intention of this study is to determine the conditions under which the perturbation will neither grow nor decay, we shall require that $\beta=0$. Therefore we shall look at two distinct cases, one in which the perturbation is non-propagating ($c=0$) and another in which it is moving ($c\neq 0$). Although in the preceding pages these two cases have been referred to as limiting cases, they are, in fact, the only cases one needs to investigate.

As has been explained in section (2.1), the threshold of instability is determined by that combination of conditions for which

$$h' = \delta_{th} + \delta_E$$

Remembering that

$$h' \equiv h_1 \sin \lambda_1 + h_2 \cos \lambda_1$$

and using eqs. (2-51) and (2-61), one has

$$h_1 \sin \lambda_1 + h_2 \cos \lambda_1 = \frac{2\alpha_M k_M T_o}{\kappa c} \left\{ -a_1 \sin \lambda_1 + (\kappa - b) \cos \lambda_1 \right\}$$

$$+ \frac{12\mu W}{E\kappa^2 h^3} U \left(h_2 \sin \lambda_1 - h_1 \cos \lambda_1 \right)$$

This equation can be broken up into two equations in the two orthogonal sine and cosine components as follows:

$$h_1 = - \frac{2\alpha_M k_M T_o}{\kappa c} a_1 + \frac{12\mu W}{E\kappa^2 h^3} U h_2 \qquad (2\text{-}62)$$

and

$$h_2 = \frac{2\alpha_M k_M T_o}{\kappa c}(\kappa - b) - \frac{12\mu W}{E\kappa^2 \bar{h}^3} U h_1 \qquad (2\text{-}63)$$

h_1 and h_2 are given by eqs. (2-40) and (2-41) respectively. Substituting for h_1 and h_2, one obtains, from eq. (2-63),

$$U^2\left(\frac{2\alpha_M k_M}{\kappa}\frac{\kappa - b}{c} + \frac{3}{2}\frac{K_M W \bar{h}}{E\kappa\, k_{oil}} a_1\right) + U\left\{\frac{\bar{h}^3\kappa}{2\mu\, k_{oil}}\left(K_{oil} + \frac{1}{4} K_M \bar{h} b\right)\right.$$

$$\left. - \frac{4K_M W \bar{h}}{E\kappa\, k_{oil}} a_1 c + \frac{12 K_M W}{E\kappa^2 \bar{h}} b\right\} - \frac{\bar{h}^3\kappa}{\mu\, k_{oil}}\left(K_{oil} + \frac{1}{3} K_M \bar{h} b\right) c$$

$$- \frac{K_M \bar{h}^2}{\mu} a_1 = 0 \qquad (2\text{-}64)$$

Similarly, eq. (2-62) gives

$$U^2\left\{\frac{2\alpha_M k_M}{\kappa}\frac{a_1}{c} + \frac{6W}{E\kappa\, k_{oil}}\left(K_{oil} + \frac{1}{4} K_M \bar{h} b\right)\right\} + U\left\{- \frac{12W}{E\kappa\, k_{oil}}\left(K_{oil} + \frac{1}{3} K_M \bar{h} b\right) c\right.$$

$$\left. - \frac{12 K_M W}{E\kappa^2 \bar{h}} a_1 - \frac{K_M \bar{h}^4 \kappa}{8\mu\, k_{oil}} a_1\right\} + \frac{K_M \bar{h}^4 \kappa}{3\mu\, k_{oil}} a_1 c - \frac{\bar{h}^2 K_M}{\mu} b = 0 \qquad (2\text{-}65)$$

Equations (2-64) and (2-65) represent two algebraic equations in U and c. Owing to the complicated nature of these equations, it is not feasible to solve them simultaneously. However, each can be solved for a series of values of c, both positive and negative, to provide corresponding values of U. A simultaneous solution is represented by that value of c for which both equations give the same U. These solutions are carried out in the computer and graphed in fig.(15) in which the chain-dotted lines indicate the area of practical interest and $W = 10^{-4}$, which, for a seal diameter of 2 inches, corresponds to a seal lip width of 0.014 inch. The materials are aluminum sliding on glass, with $\kappa = 1.0$ in.$^{-1}$ for one complete wave. Each of the solutions is discussed separately.

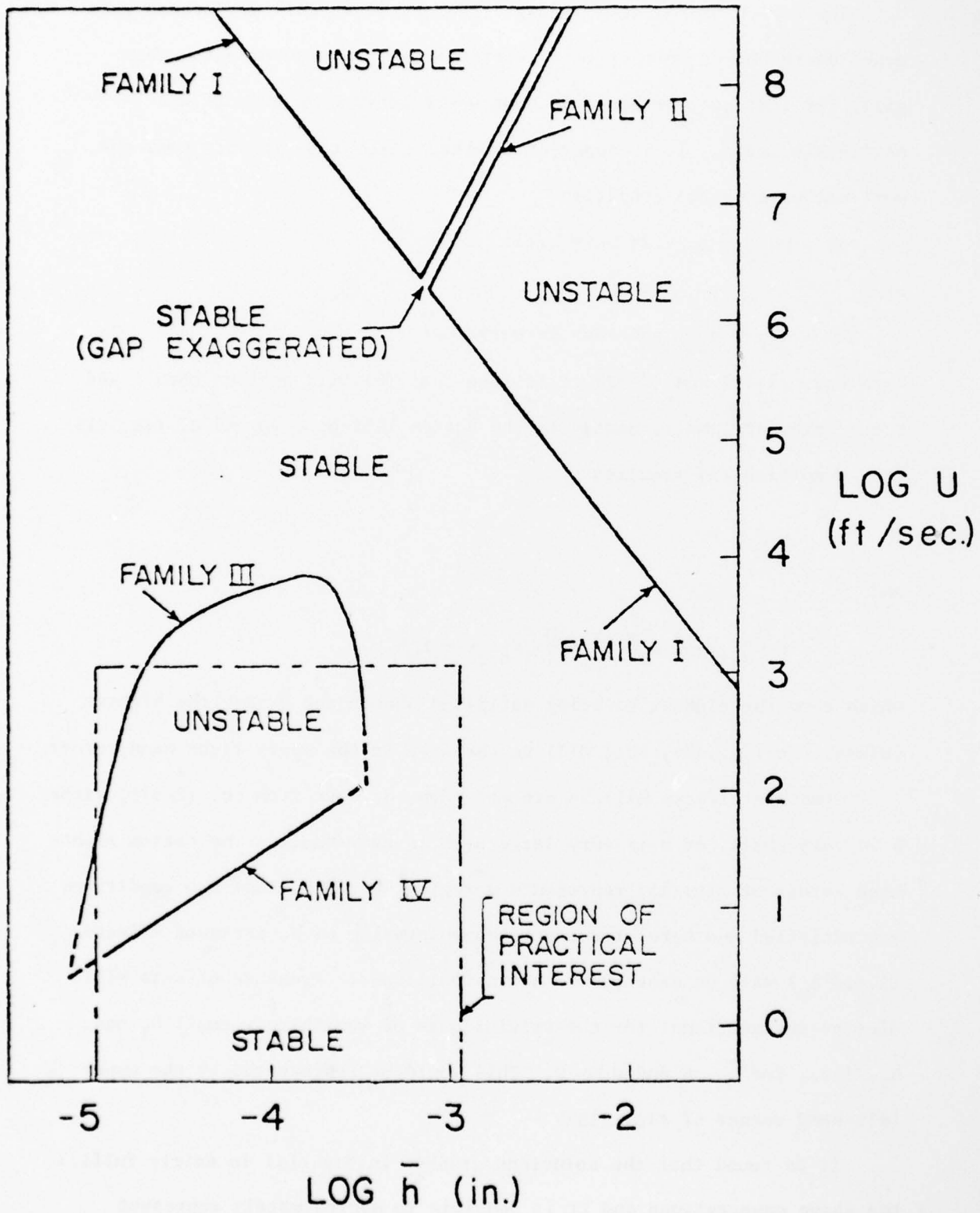

Figure 15. Lines of Neutral Stability, Numerical Solution ($W = 10^{-4}$)

The region represented by fig. (15) may be broadly subdivided into zones where one or more of certain effects may be predominant. There will, for instance, be one such zone where convection effects are negligibly small. It is apparent from eq. (2-26) that in this zone one must either have the condition

a) $\left(q_{c\ell} + q_{cc}\right)$ is very small

or

b) $q_{c\ell} = q_{cc}$ and each is very small

From eqs. (2-29) and (2-32) it is seen that (b) will be true when c and $\bar{h}$ are both very small, namely in the bottom left-hand corner of fig. (15).

Condition (a) requires

$$c \approx \frac{3}{8} U$$

and

$$c\left(K_{oil} + \frac{1}{3} K_M \bar{h} b\right) \approx \frac{U}{2}\left(K_{oil} + \frac{1}{4} K_M \bar{h} b\right)$$

which come the closest to being satisfied when $\bar{h}$ and U have the highest values. In fig.(15), this will be the area in the upper right hand corner.

Pressure effects will be minimal when, as seen from eq. (2-61), either W is very small, or $\bar{h}$ is very large or U is very small. The bottom right-hand corner of fig.(15) represents a region where the last two conditions are satisfied and here, for any reasonable value of W, pressure effects (i.e., δ_E) will be expected to be insignificant. Pressure effects will also be insignificant for the trivial case of vanishingly small h_1 and h_2, i.e., for $\bar{h} \sim 0$ and $U \gg 0$. This would be represented by the upper left-hand corner of fig. (15).

It is found that the solutions graphed in fig.(15) do fairly fulfill the above expectations and it is possible to approximately represent

each family of solutions by simple algebraic relations involving the critical sliding speed $U_{crit.}$, the corresponding wave speed $c_{crit.}$ and $\bar{h}$, as follows :

Family I (fig. 16)

$$U_{crit.} = \left(\frac{64\ K_M k_{oil}}{K_{oil}\ \kappa}\right) \frac{1}{\bar{h}^2} \tag{2-66}$$

$$\frac{U_{crit.}}{c_{crit.}} = \frac{8}{3} \tag{2-67}$$

(Pressure effects are negligible)

Family II (fig. 16)

$$U_{crit.} = \frac{E\ \kappa^2}{12\mu\ W}\ \bar{h}^3 \tag{2-68}$$

$$\frac{U_{crit.}}{c_{crit.}} = \frac{8}{3}$$

(Convection effects are insignificant)

Family III (subdivided into parts, fig. 17)

a) $$U_{crit.} = \frac{E^3 \kappa^4 \alpha_M}{864\ W^3 K_M \mu^2}\ \bar{h}^7 \tag{2-69}$$

$$\frac{U_{crit.}}{c_{crit.}} = \frac{6\ K_M W}{E\ \alpha_M k_M \kappa}\ \frac{1}{\bar{h}} \tag{2-70}$$

(Convection effects are negligible)

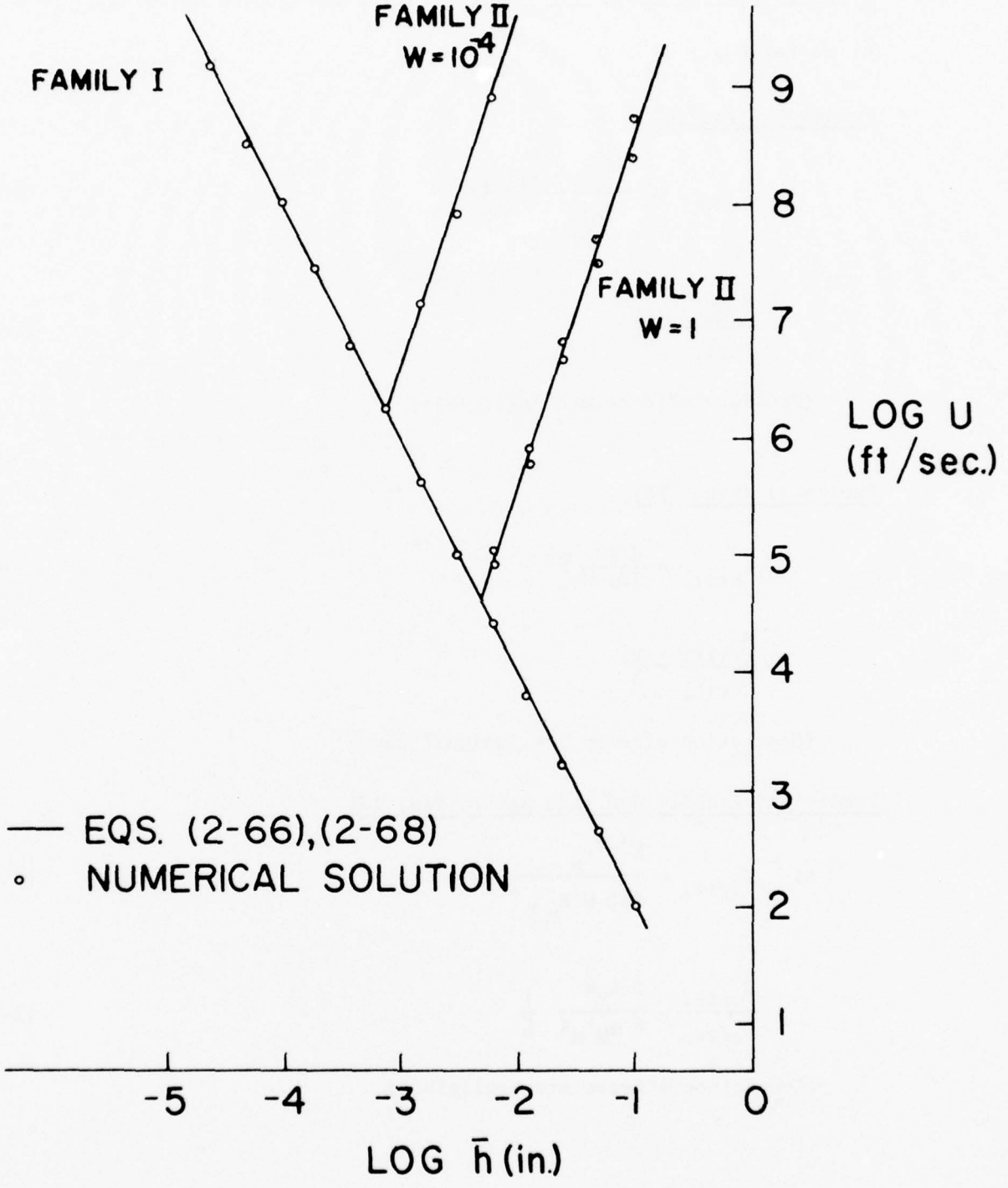

Figure 16. Lines of Neutral Stability, Families I and II

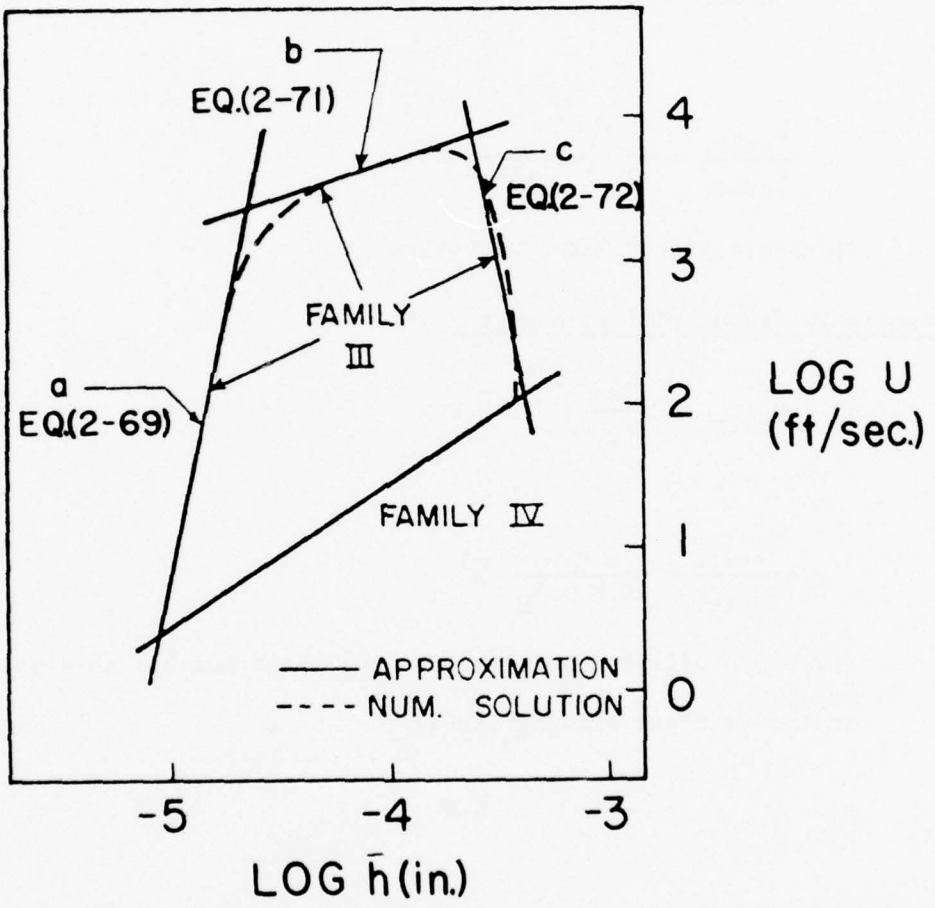

Figure 17. Lines of Neutral Stability, Families III and IV ($W = 10^{-4}$)

b) $$U_{crit.} = \left(\frac{2\,E\,k_{oil}\,\kappa}{3\,W\,\mu}\,\bar{h}\right)^{1/2} \qquad (2\text{-}71)$$

$$\frac{U_{crit.}}{c_{crit.}} = \frac{6\,K_M W}{E\,\alpha_M k_M \kappa}\,\frac{1}{\bar{h}}$$

(Both convection and pressure effects are significant)

c) $$U_{crit.} = \frac{8\mu\,\alpha_M k_{oil}^3}{K_M \kappa^5}\,\frac{1}{\bar{h}^8} \qquad (2\text{-}72)$$

$$\frac{U_{crit.}}{c_{crit.}} = \frac{K_M \kappa^2}{16\mu\,k_{oil}\alpha_M k_M}\,\bar{h}^4 \qquad (2\text{-}73)$$

(Pressure effects are unimportant)

Family IV (subdivided into parts)

a) $$U_{crit.} = \left(\frac{K_M}{\alpha_M \mu}\right)^{1/2}\,\bar{h}\,\kappa \qquad (2\text{-}74)$$

$$\frac{U_{crit.}}{c_{crit.}} = \frac{E\,\kappa}{16\,W\,\mu\,k_M}\,\bar{h}^3 \qquad (2\text{-}75)$$

(Pressure affects the critical wave speed but has no significant effect on the critical sliding speed)

b) $$U_{crit.} = \left(\frac{K_M}{\alpha_M \mu}\right)^{1/2}\,\bar{h}\,\kappa$$

$$\frac{U_{crit.}}{c_{crit.}} = \frac{3\,K_M k_{oil}}{2\,k_M K_{oil}}\,\frac{1}{\bar{h}\,\kappa} \qquad (2\text{-}76)$$

(Convection affects the critical wave speed but has no significant effect on the critical sliding speed)

Only families III and IV fall within the region of practical interest and enclose an area where instability prevails. Interestingly, they also enclose a region where U, as determined by eq. (2-64), is complex. Inside this complex region the actual system cannot support the values of c supplied in the computer calculations to determine U. Figure (18) shows the egg-shaped region containing the values of c and $\bar{h}$ for which U becomes complex. The peripheral points are the solutions representing, on this plane, families III and IV.

Figure (19) shows all the families of solutions in terms of $\frac{U}{c}$ and $(\bar{h}\kappa)$. The box-shaped region is the one referred to in the preceding paragraph. Using the algebraic expressions given by eqs. (2-66) through (2-76), it is possible to broadly define this region. Families I and II coalesce into the horizontal line below the box.

2.12 Instability of the Non-moving Perturbation

In the conclusion to the last section, it was noted that for very small wave velocities and negligible convection and elastic effects, a threshold of instability does exist (Family IV, fig. 15). To determine on which side of this line stable conditions prevail, one may check for values of the exponent β close to and on either side of this threshold.

In the energy equation (eq. 2-26) , q_g and q_k remain unchanged, while q_{cc} and $q_{c\ell}$, being small by comparison, drop out. Equation (2-39) becomes

$$h_2 = 0$$

while eq. (2-38) becomes

$$h_1 = -\frac{\bar{h}^2}{\mu U^2} K_M T_o e^{\beta} \sqrt{\frac{\beta}{k_M} + \kappa^2} \qquad (2\text{-}77)$$

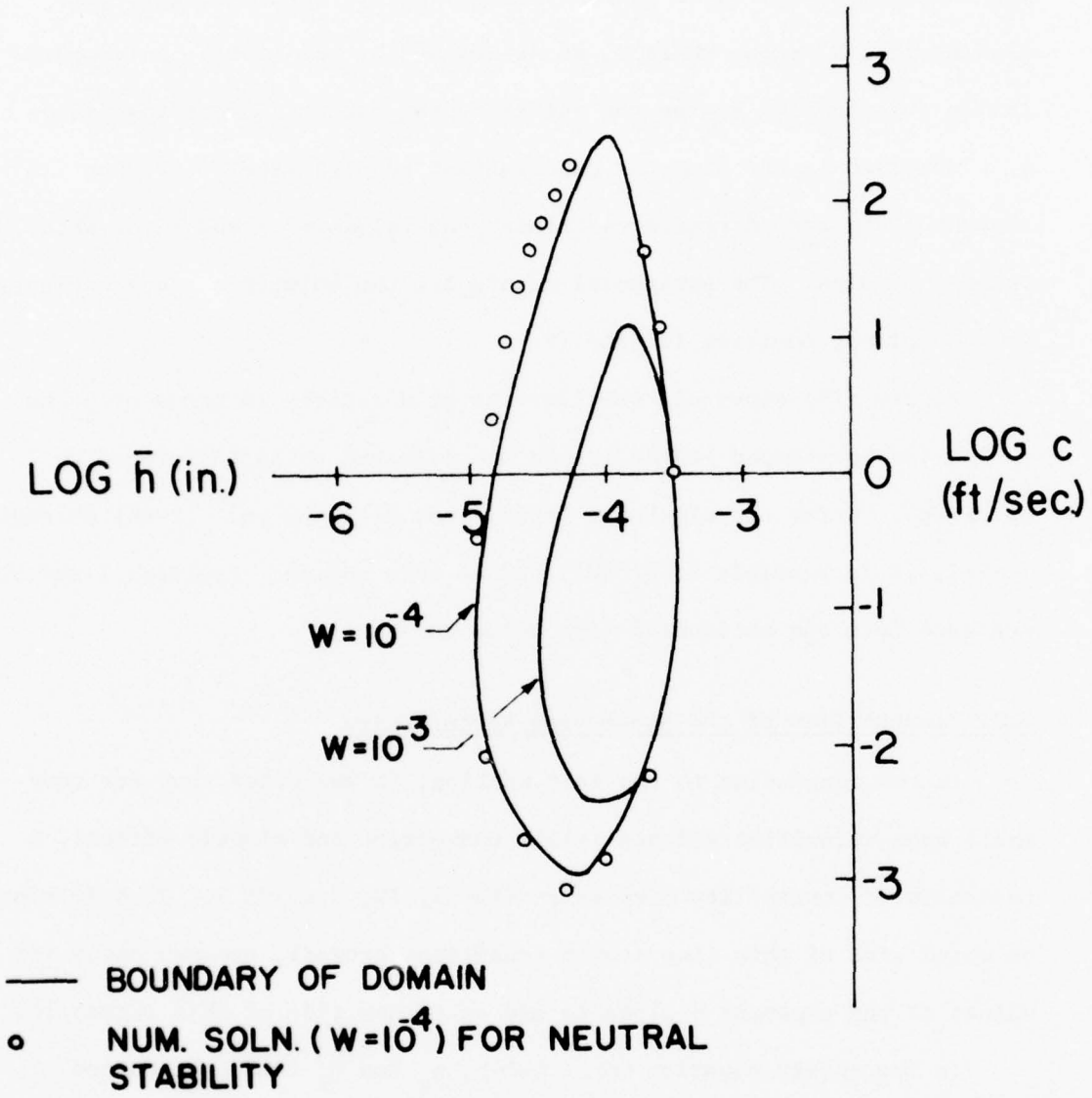

Figure 18. Domain of c and $\bar{h}$ in Which U is Complex

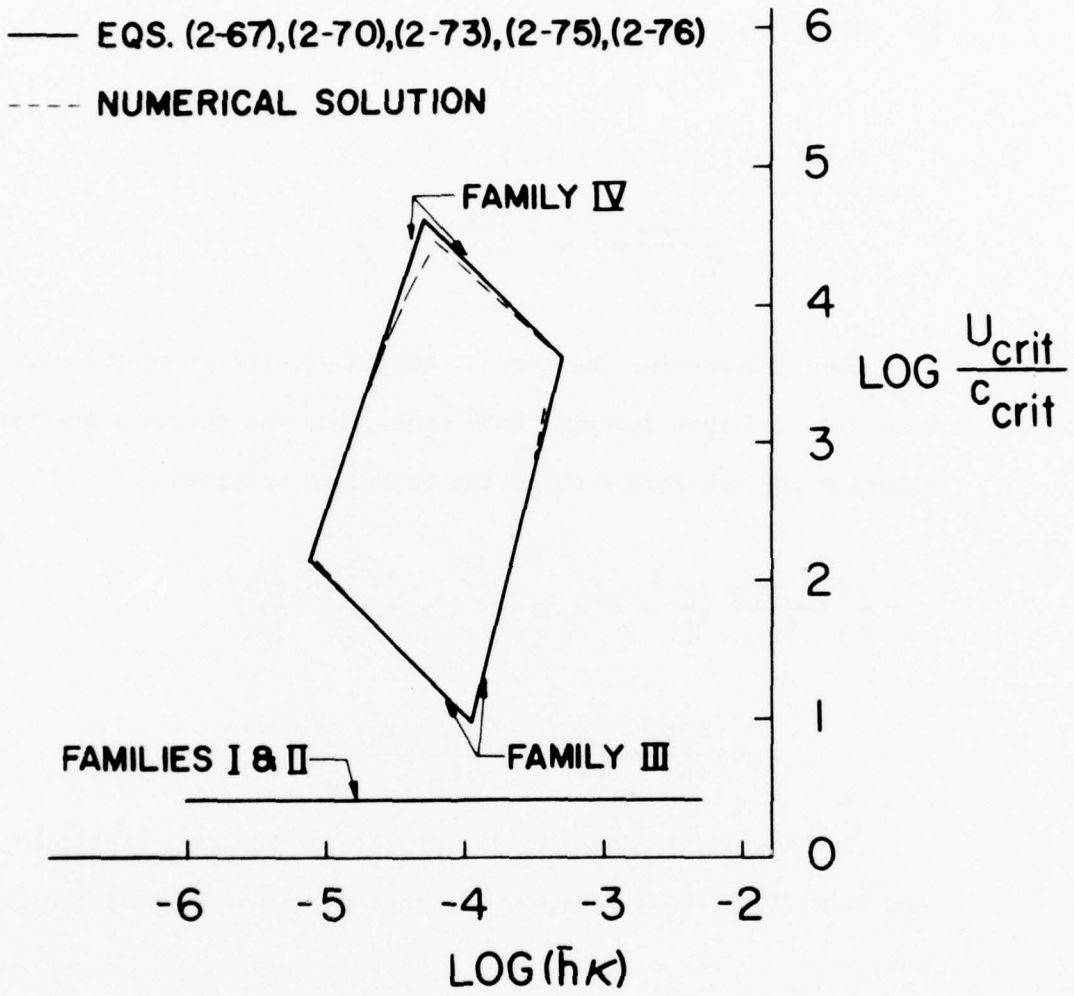

Figure 19. Lines of Neutral Stability ($W = 10^{-4}$)

The surface wave h' now becomes

$$h' = h_1 \sin \kappa x$$

and, since elastic effects are small compared to the thermal effects, the threshold condition is given by

$$h' = \delta_{th}. \tag{2-78}$$

Using eqs. (2-50), (2-77) and (2-78), one obtains

$$-\frac{\kappa}{\beta\sqrt{\frac{\beta}{k_M}+\kappa^2}} + \frac{1}{\beta} = \frac{K_M}{2\mu\,\alpha_M k_M}\,\frac{\bar{h}^2}{U^2} \tag{2-79}$$

Upon transposing the second term in eq. (2-79) to the right hand side and then squaring both sides, one can obtain a quadratic equation for non-zero β which can be solved to yield

$$\beta = \frac{1}{2}\left[\frac{4\mu\,\alpha_M k_M}{K_M}\left(\frac{U}{\bar{h}}\right)^2 - \kappa^2 k_M \pm \left\{\left(\kappa^2 k_M - \frac{4\mu\,\alpha_M k_M}{K_M}\frac{U^2}{\bar{h}^2}\right)^2 - 16\left(\frac{\mu\,\alpha_M k_M}{K_M}\frac{U^2}{\bar{h}^2}\right)^2 - \frac{\kappa^2 k_M^2 \mu\,\alpha_M}{K_M}\frac{U^2}{\bar{h}^2}\right\}^{1/2}\right] \tag{2-80}$$

The $\pm$ was introduced by the process of squaring mentioned above and it will be shown subsequently that the minus sign is the correct one.

As the threshold of instability is of principal interest here, one may seek the condition that gives $\beta=0$. In eq. (2-79), the limit of the left-hand side for $\beta \to 0$ is

$$\lim_{\beta \to 0} \frac{\kappa - \sqrt{\frac{\beta}{k_M}+\kappa^2}}{\beta\sqrt{\frac{\beta}{k_M}+\kappa^2}} = -\frac{1}{2k_M\kappa^2}$$

Introducing this in eq. (2-79), one obtains

$$\left(\frac{U}{\bar{h}}\right)^* = \kappa \sqrt{\frac{K_M}{\mu \alpha_M}} \tag{2-81}$$

where the superscript * refers to the point where $\beta=0$, i.e., the threshold of instability. It should be noted that eq. (2-81) is identical with eq. (2-74) for $U_{crit.}$.

A look at eq. (2-80) reveals that β will be non-zero if the plus sign is chosen. Moreover, if $(U/\bar{h})$ from eq. (2-81) is substituted into eq. (2-80), β becomes zero only when the negative sign is chosen. Therefore in eq. (2-80) the minus sign in the $\pm$ is the correct one.

β may be expressed in terms of $U/\bar{h}$. Let

$$V \equiv \frac{U}{\bar{h}}$$

and

$$V^* \equiv \left(\frac{U}{\bar{h}}\right)^*$$

Then eq. (2-80) can be shown to give

$$2\beta = -\kappa^2 k_M \left[1 - 4\left(\frac{V}{V^*}\right)^2\right] - \kappa^2 k_M \sqrt{1 + 8\left(\frac{V}{V^*}\right)^2} \tag{2-82}$$

The expression under the radical sign in eq. (2-82) may be expanded to the desired degree of approximation depending on the size of V/V^*; V^*, of course, is constant for a given geometry and given material properties. Knowing the sliding speed would then enable one to determine β readily from eq. (2-82). The critical or threshold condition is represented by

$$\frac{V}{V^*} = 1$$

which also corresponds to $\beta=0$. For $V/V^* \ll 1$, eq. (2-82) gives

$$\beta = - \kappa^2 k_M \tag{2-83}$$

In fig.(15), Family IV represents $V/V^* = 1$. On either side of this line, one may write

$$\frac{V}{V^*} = 1 + \epsilon$$

where ϵ may be positive (above the line) or negative (below the line). Equation (2-82) can then be written as

$$\beta = - \frac{\kappa^2 k_M}{2} \left[1 - 4(1 + \epsilon)^2 + \left\{ 1 + 8(1 + \epsilon)^2 \right\}^{1/2} \right]$$

For $|\epsilon| \ll 1$,

$$\beta = - \frac{\kappa^2 k_M}{2} \left[- \frac{16}{3} \epsilon \right]$$

If $\epsilon > 0$, $\beta > 0$. If $\epsilon < 0$, $\beta < 0$. Below the line representing Family IV in fig.(15), the system is stable. Above the line, instability prevails.

2.13 Remarks

In the lubricated face-type seal, a perturbation represented by a steadily moving wave may become unstable within a reasonable operating range. The sliding speed corresponding to neutral stability (Family IV, fig. 15) is given by

$$U_{crit.} = \left(\frac{K_M}{\alpha_M \mu} \right)^{1/2} \bar{h} \kappa \tag{2-84}$$

The wave velocity is very small and so are pressure and convection effects. Instability occurs when $U > U_{crit.}$ and is caused by viscous heating and heat conduction into the metal. The disturbances with the largest wave-lengths (smallest κ) become unstable first.

The threshold condition given by eq. (2-84) exists only for a range of film-thickness $\bar{h}$, which can be determined by using eqs. (2-70), (2-75), (2-73) and (2-76). The lower boundary of this range is given by

$$\bar{h} = \left[\frac{96\ K_M\ \mu W^2}{E^2 \alpha_M \kappa^2}\right]^{1/4}$$

and the upper boundary by

$$\bar{h} = \left[\frac{24\mu\ \alpha_M k_{oil}^2}{K_{oil} \kappa^3}\right]^{1/5}$$

Blok [15] has demonstrated a different mechanism for thermal instability of liquid films in which viscosity varies with temperature. The onset of such an instability is determined by a parameter r_s which expresses the heat flux through the slower (or stationary) wall as a fraction of the total heat flux across the film, and a dimensionless parameter N defined as

$$N \equiv \left(-\frac{d\mu}{dT}\right)_s \frac{U^2}{K_{oil}}$$

If the stationary surface is a thermal insulator, $r_s = 0$. It is shown that, for $r_s = 0$, the temperature dependence of viscosity does not affect the shear stress or heat flux in the film for $N < 0.4$. Furthermore, the critical value of N corresponding to $r_s = 0$ is 2.

In the present study, μ has been assumed constant across the film, for which a corresponding $(-d\mu/dT)$ can be obtained from a chart [16]. For the threshold condition represented by Family IV (fig. 15), it is seen that N varies between 0.016 and 0.26. This seems to justify the constant-viscosity formulation of the present study. It is also worthy of note that the present values of N do not approach the critical.

CHAPTER III

EXPERIMENTAL OBSERVATION OF THERMOELASTIC INSTABILITY

3.1 The Objective

Experiments were performed in the laboratory to verify the occurrence of thermoelastic instability in hydrodynamically lubricated face seals. The prediction of Chapter II was based on an analysis of initially flat surfaces, and while idealized theories often provide enlightening insight to complex practical problems, the proof of the validity of such idealizations lies in practical demonstration. No plans were made, nor any hopes entertained, for the precise quantitative corroboration of the predicted critical speeds. The intention was to confirm, through repeatable experiments, that the phemonenon predicted in theory was existent in practice.

Moving hot spots, believed to be caused by thermoelastic instability, had been observed and filmed by Sibley and Allen [1] and Kilaparti [12]. Dow [3] had briefly reported experimentally measured temperature non-uniformities, clearly originating from thermoelastic instability, in the two-pin model. In a very recent paper, Dow and Stockwell [17] have described experiments with the two-dimensional scraper model. The specimens used included commercial apex seals used in Wankel engines. The edge of a scraper was pressed against a rotating drum (fig. 20). Interfacial temperatures were measured by means of embedded thermocouples as well as by an infrared heat sensor, pointed at the interface and sweeping back and forth along it. The interfacial clearance was

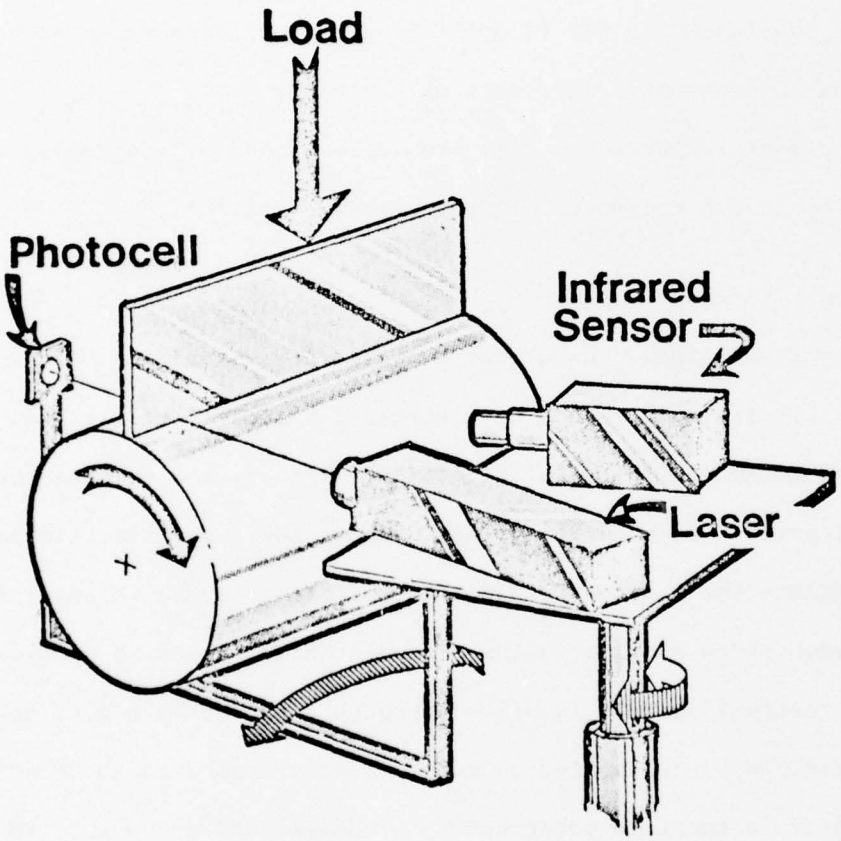

Figure 20. Experimental Set-Up of Dow and Stockwell (Ref. 17)

measured by a coupled laser-photocell combination that also swept along the interface and monitored the amount of light passing through. The experiments clearly demonstrated that, above a certain speed, temperature and clearance non-uniformities of large magnitudes occur and move along the interface. Some of these observations were made with the interface lubricated by SAE 10 oil fed by a wick (presumably boundary rather than hydrodynamic lubrication).

The present experiments [18] provide evidence of thermoelastic instability in the regime of hydrodynamic lubrication.

3.2 The Experimental Set-up

The rotating face consists of a cylindrical metal cup with a flat, thin lip. It is rigidly held on a vertical spindle (see fig. 21) having freedom of motion in the axial direction. The stationary face consists of a flat pyrex disc held in gimbals. Thus, the mean film thickness can change and the stationary face can tilt in response to any initial misalignment or to changes in the circumferential pressure profile.

The vertical spindle is driven through a pulley by a d.c. motor whose speed can be controlled to vary smoothly from 0 to above 4000 r.p.m. The spindle, in turn, is connected by a rubber band and pulley to a small generator whose voltage output is calibrated to measure the spindle turning speed.

The oil is held in a shallow pool on the glass. Placed in two holes in the glass, and rigidly affixed to it, are two eddy-current proximity probes. The first of these, probe A, reads the distance between its tip and the metal face; as the cup turns through one revolution, the entire circumferential profile of the film thickness is

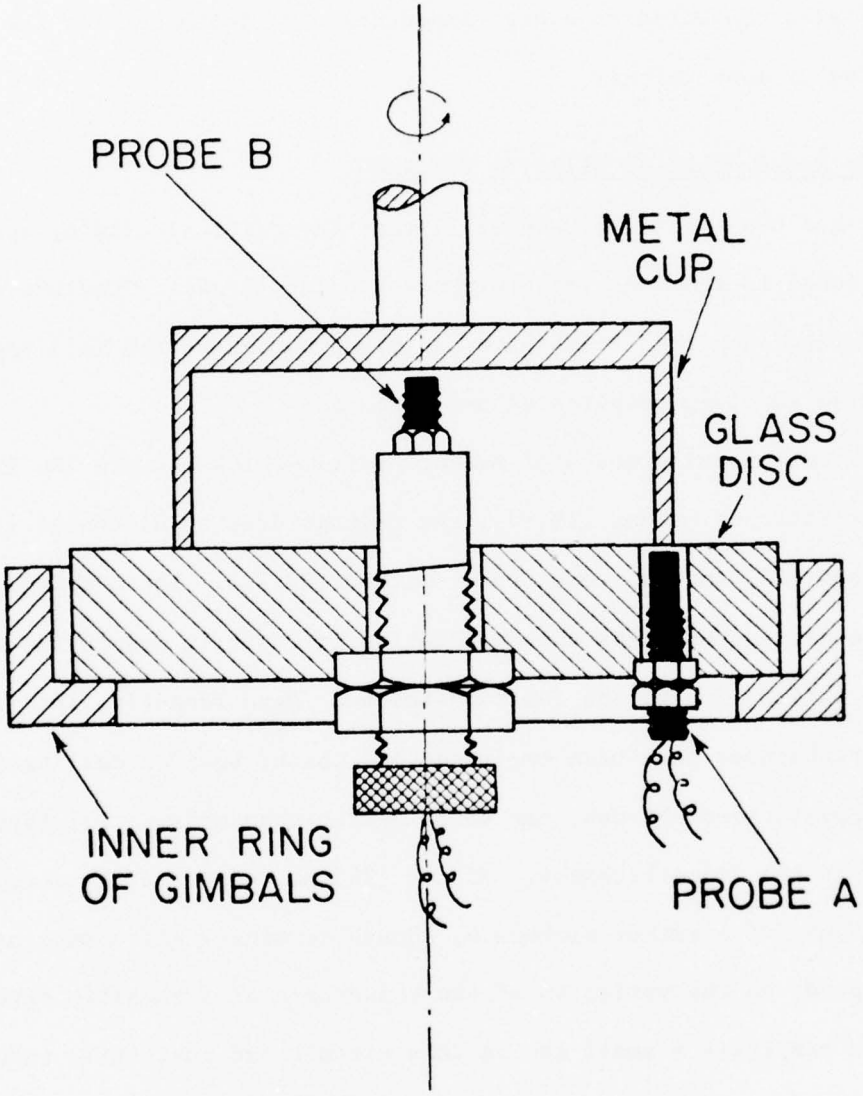

Figure 21. Experimental Set-Up Showing Probe Locations

recorded. The second probe (probe B) is located on the axis of the cup and measures vibrations or bouncing of the cup as a whole. Both probes are connected to a dual-beam oscilloscope to display cyclic patterns; each is also connected to a high-impedance d.c. voltmeter for the recording of mean values.

3.3 The Measurement of Oil-film Thickness

It has been shown in Chapter II that the critical sliding speed is proportional to the mean film-thickness, $\bar{h}$ (eq. 2-84). Previous attempts at measuring such thin films have had mixed successes and in a few cases have involved complicated arrangements.

The most popular means of measuring film-thickness are the electrical resistance method [19,20], the voltage drop or discharge voltage method [21] and the capacitance method [22,23]. These techniques have the serious drawback that cavitation in the film upsets the most careful calibration of the instrumentation. More recently, interferometric techniques have been employed [14] which, besides calling for very sophisticated set-ups, can do no better than measure relative changes in the film-thickness. Winney [24] has reported the development and use of a rather elaborate, though seemingly effective, probe that depends on the variation of the reluctance of a magnetic circuit. The film comprises a small gap in this circuit and cavitation induces little error because oil and air are non-ferromagnetic and have comparable permeabilities.

In the present instance, the use of the eddy-current probes presents a major difficulty. Viscous heating in the oil causes thermal expansion of the probes themselves (particularly probe A) and thus not

only alters the pre-set gap, but also shifts the calibration curve for the probe. However, the calibration constant, and hence the dynamic response of the probe to the passing metal surface, is not affected. A technique has been devised to circumvent the problem of zero-drift. An initial running-in period, at low speed, is allowed until the d.c. voltmeter reading for probe A stabilizes. Thereafter, the speed is gradually increased in steps and time is allowed at each step for stabilization of the d.c. voltmeter reading (indicating mean film-thickness) for probe A. Simultaneously, at a few of these steps, after the d.c. voltage stabilizes, the rotation of the cup is suddenly arrested, causing it to drop and rest on the glass. Voltages (d.c.) before and after this stoppage are noted and simultaneous photographs of the oscilloscope traces are taken. To this voltage drop is added the mean of the fluctuating (a.c.) component as indicated by the oscillogram for probe A before stoppage, to obtain $\bar{h}$. The calibration constant for probe A is 0.0024 in./volt and the digital voltmeter reads millivolts, thus providing a resolution of approximately 2.4 μin.

3.4 Procedure

In order to approximate the idealized conditions of Chapter II as far as practicable, the glass and the metal are ground and polished to a mirror finish.

Each probe, connected to its own 18-volt power supply and high-impedance voltmeter, is calibrated with respect to the metal surface it measures. Figure (22) shows such a calibration curve for a probe with a tip of 1/8 in. diameter; it also shows a probable initial setting when mounted on the test apparatus. The two probes, A and B, are found

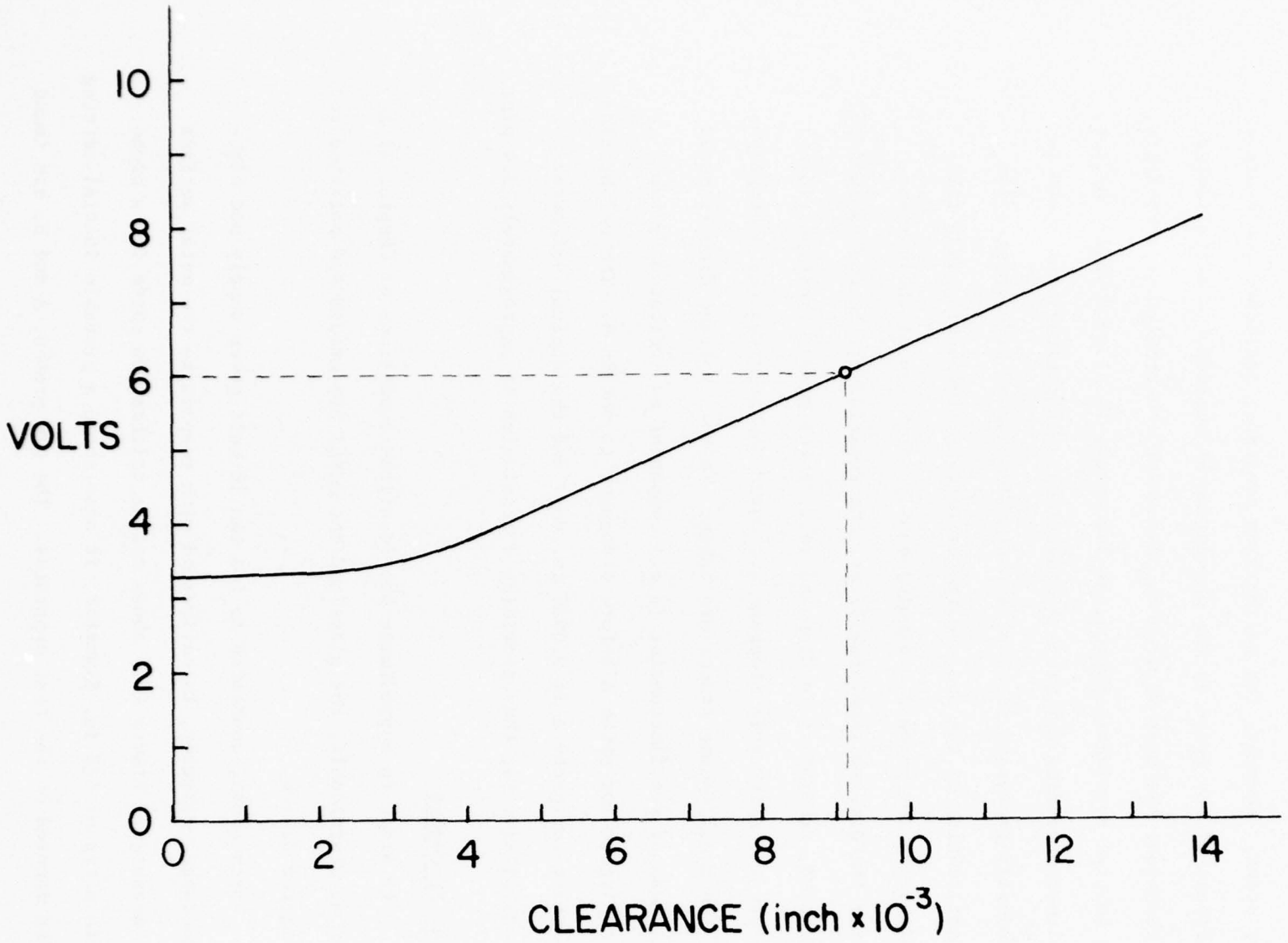

Figure 22. Calibration Curve for Probe A. The circle shows a typical initial setting.

to have slightly different calibration constants for a given metal cup.

The cup is mounted on the spindle and the glass slab on the gimbals. The two probes are attached and set to chosen initial gaps. The oscilloscope is then adjusted so that the signals from the two probes are displayed to the same scale (volts per inch of gap deviation). The oscilloscope is set to display the d.c. signal from probe B but the a.c. from probe A. Thus one observes the changes in the reading of probe B throughout the duration of the run, i.e., any slow rise and fall as well as any bounce or vibration of the cup as a whole are displayed. The trace for probe A, by contrast, shows only the surface profile relative to the mean.

The spindle is started from rest and the speed gradually increased, as explained in §3.3. Voltage readings from the voltmeters are recorded and simultaneous photographs of the oscilloscope traces are taken.

No attempt is made to control the film-thickness, it being determined by the operating conditions. When probe B indicates no bouncing of the cup, the time-dependent output of probe A is taken as the measurement of the contour of the surface passing over it. Temperature-dependent variations in such properties as the viscosity of the oil and coefficients of thermal conductivity and expansion of the metal are not considered. Therefore, no attempt is made to measure temperature variations. Instead, the bulk temperature of the oil is measured after shut-down by a simple thermometer so as to obtain an estimate of the overall viscosity of the oil (SAE 10) from viscosity charts. Pressures are not measured. The only evidence of thermoelastic instability being sought is macroscopic deformation of the surface.

3.5 Results and Observations

Sudden and very dramatic deformations of the surface are found to occur at a certain speed, interpreted as the critical. Prior to the onset of the instability, the surface wave grows steadily in magnitude, while the oscillogram for probe B shows no bounce or vibration. The film-thickness prior to the occurrence of the instability is measured as outlined in §3.3 and is plotted against the critical sliding speed as shown in fig. (23). In this figure, the data points are experimentally obtained, while the closed regime of instability is drawn on the basis of the derivations of Chapter II, but for the geometry used in the experiment. The physical parameters and material properties used are listed in Appendix C.

In the course of the experiments, the well known phenomenon of inward pumping (see, for instance, ref. [25]) has been repeatedly observed. Two somewhat unexpected observations are that, for a given load, a wider seal face requires a higher starting torque and an abundance of oil in the pool usually leads to higher values of film-thickness than when there is less oil. These effects perhaps merit further studies and some explanation, but are being ignored here because the critical condition alone is of interest.

In all the oscillograms that follow, the upper trace represents probe B, the lower trace probe A. An upward trend represents, in the upper trace, a rising of the cup from the glass; in the lower trace it represents a protruberance on the face of the cup.

Figure (24) shows the evolution of a surface profile from a low, subcritical speed (a) to a supercritical speed (e). Large spikes or

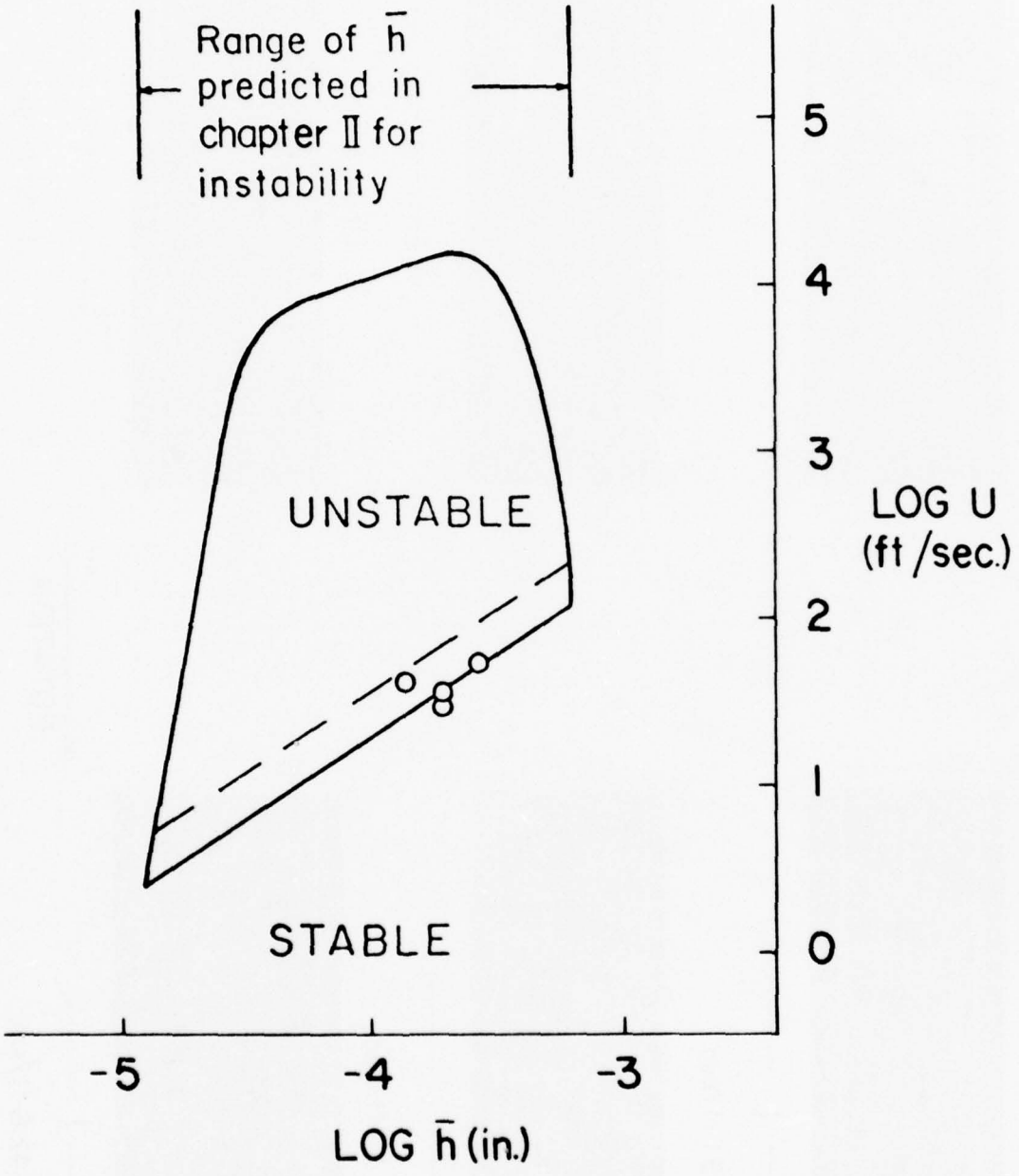

Figure 23. Comparison of Experimental Data (circles) with Prediction of Chapter II.

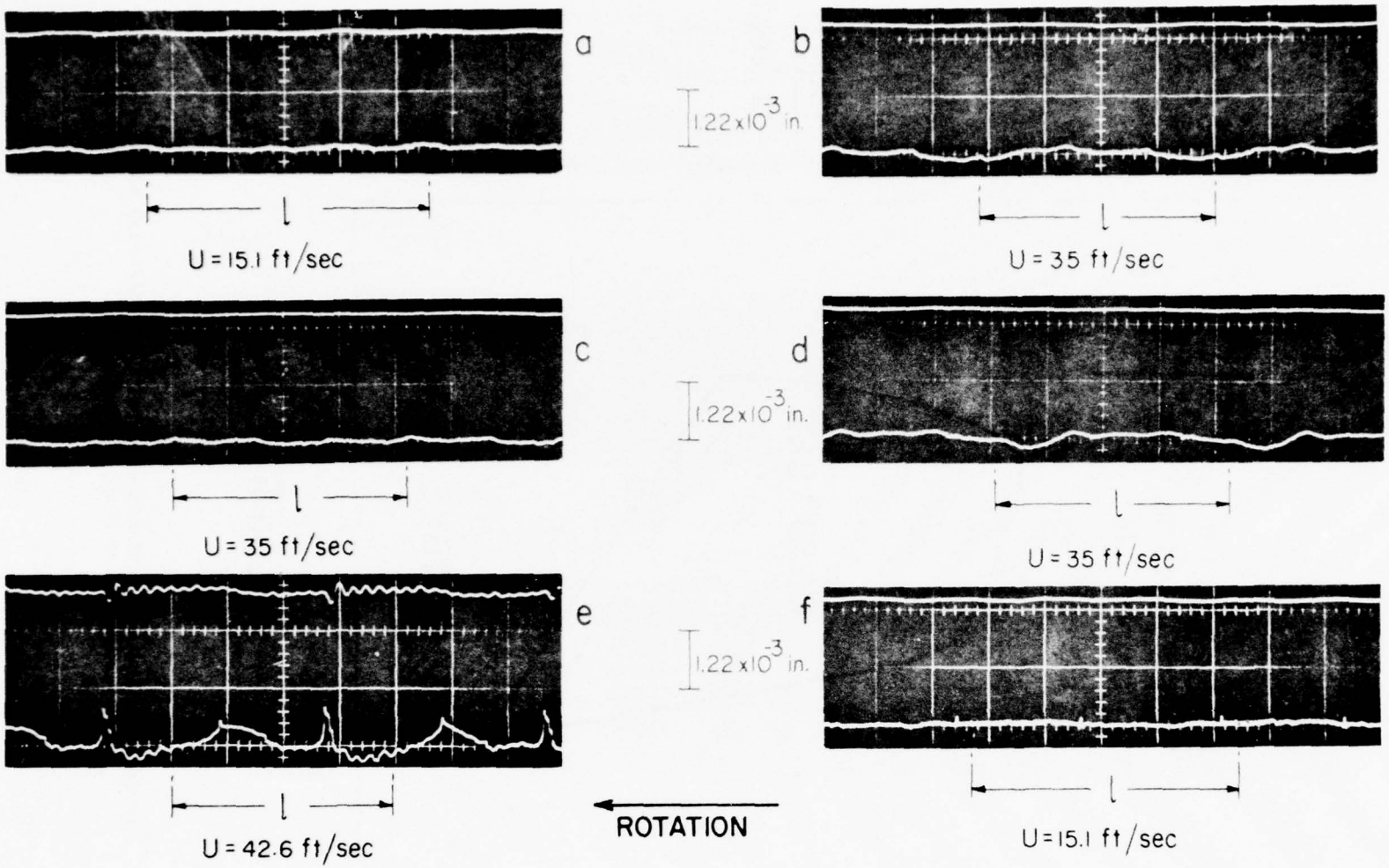

Figure 24. Oscillograms Showing Surface Profile at Different Sliding Speeds. ℓ = One Revolution

asperities are seen at the supercritical speed. As an asperity passes over probe A and dips into the slight depression above the probe, it sets off a vibration that is clearly indicated by the upper trace in fig. (24e). This is damped out until the next asperity passes over probe A and triggers another vibration. The lower trace records a vibration of the same phase and magnitude. The photographs of fig. (25) duplicate these aspects. That the asperities of fig. (24e) are of thermal origin, and not the manifestation of permanent surface damage, is proved by fig. (24f). This picture, taken after slowing down following brief operation in the deformed state, shows that the asperities have all but disappeared. Moreover, the surface profile closely resembles that in fig. (24a), taken at the same sliding speed but during start-up.

Examination of the metal face at the end of the experiment indicates that the asperities break through the oil film and rub directly against the glass. If only one asperity grows and touches the glass, static equilibrium requires that the glass plate must tilt and touch the metal face at a diametrically opposite point. The metal cup then rests on the glass on two "legs", the minimum required for dynamic equilibrium. Sometimes three "legs" are formed. Figure (26) shows an aluminum face with three black spots on it, the locations of three burnt asperities.

A very interesting feature of the operation at speeds just below the critical is the growth and movement of small surface disturbances. With the cup running at constant speed, small growths are seen to arise and traverse the face. The effect is very graphic when the oscilloscope trigger is set to commence the sweep at a particular point along the

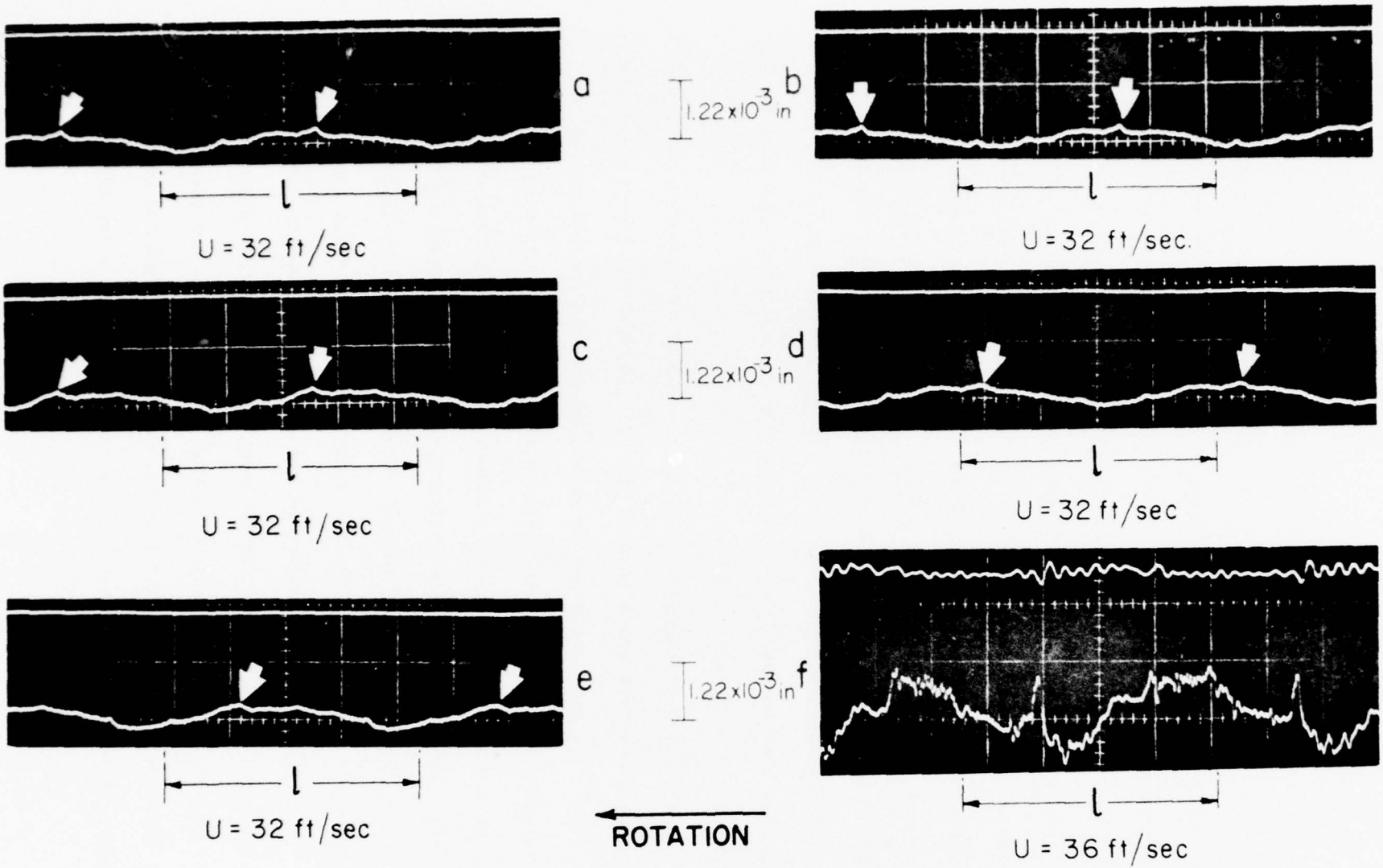

Figure 25. Oscillograms Showing Surface Profile at Different Sliding Speeds. Arrow Shows a Surface Blemish, Present at the Outset, Relative to Which Small Surface Irregularities are seen to Form and Move (a to e). ℓ = One Revolution

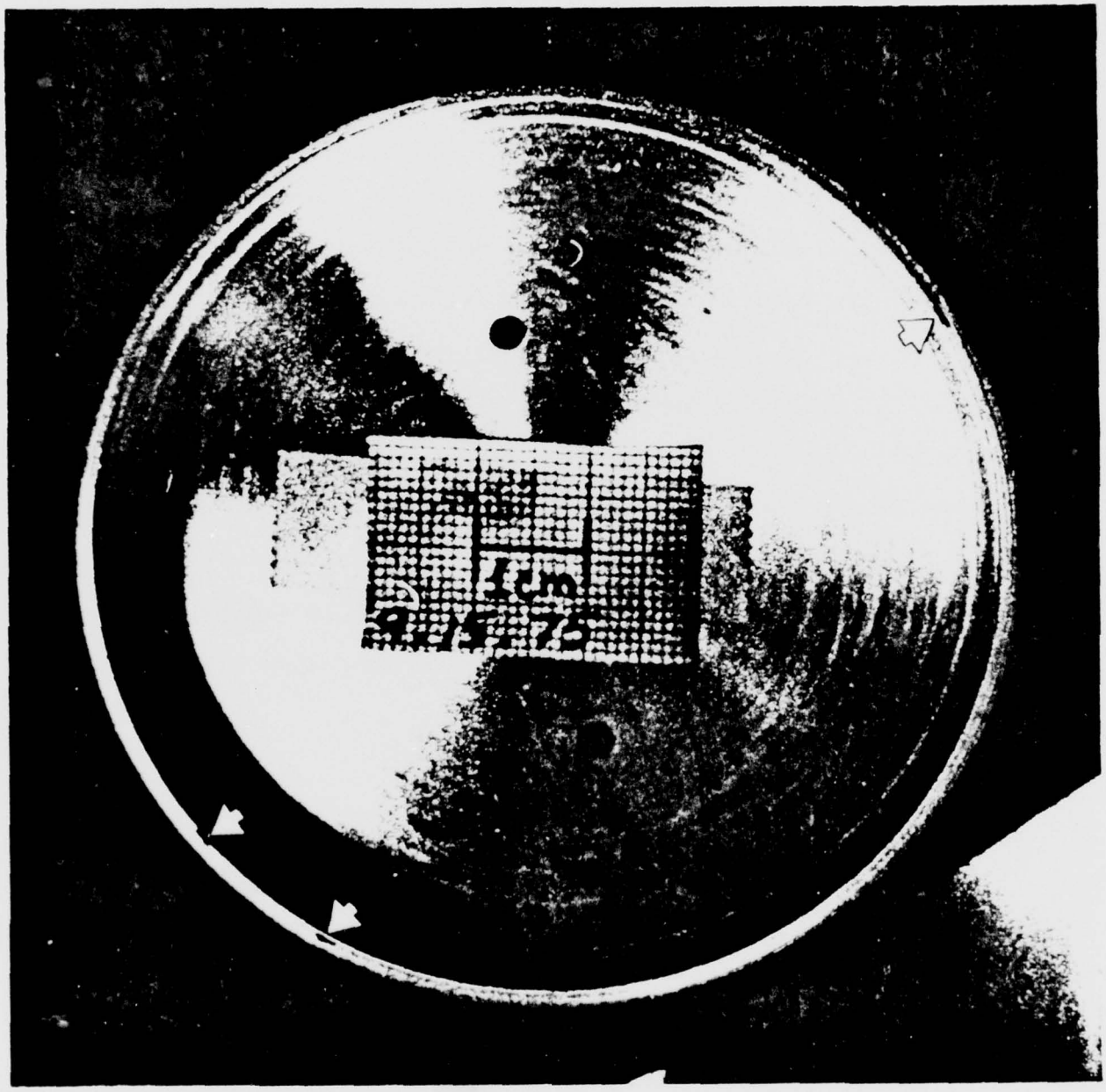

Figure 26. Photograph of Aluminum Face Showing Burnt Asperities (Arrows)

circumference of the cup. It has been repeatedly observed and is clearly a surface phenomenon. It is illustrated by fig. (24b,c,d). In fig. (25), the arrow marks a surface blemish that was present at the very outset and provides a convenient reference point relative to which moving features can be observed. The fact that the upper trace indicates no bounce proves that this is, indeed, a surface effect.

The close conformity between predicted and measured results (fig. 23) is startling. There is some uncertainty as to whether the circumference of the cup contains one surface wave or two (see, for instance, figs. 24c and e). In fig. (23), the solid line is for a single wave (κ = .66 in^{-1}) and the dashed line for two waves (κ = 1.33 in^{-1}) around the circumference. The pertinent dimensions and properties are listed in Appendix C.

On the basis of fig. (23), it is believed that the analysis presented in Chapter II, although idealized, does take proper account of the principal effects at work.

CHAPTER IV

INSTABILITY ANALYSIS FOR INITIALLY WAVY SURFACES

4.1 The Model

It was believed, even a few years ago, that physical contact between the faces of a seal was responsible for the prevention of leakage. Almost invariably, one face of a seal used to be made of graphite, whose self-lubricating property was possibly responsible for the satisfactory performance of face seals. With the advent of higher and higher duty requirements, however, the soft graphite faces began to perform with greater and greater unpredictability and harder alternative materials began to be sought. Research on seals was stepped up and gradually the realization dawned that some form of face lubrication was required for satisfactory operation. There was strong evidence linking failure of lubrication to seal failure.

Numerous theories have since been advanced in efforts to explain how a face seal supports load and effects sealing. One such theory, inadequately understood, is boundary lubrication, which is characterized by a degree of direct contact between the sliding surfaces and can be envisaged under conditions of very high load or when the sealed fluid is highly volatile. Nau [26] has reviewed the theories of lubricated face seals and concludes that, in general, face seals operate in the hydrodynamic regime, characterized by a coherent lubricating film separating the two surfaces.

Hamilton et al [27] have presented a theory of face lubrication depending on micro-asperities on the surface; the fluid flow is stated to generate positive pressures on the upstream side of these micro-asperities and cavitation pockets on the downstream side, thereby generating a net positive pressure. Reiner [28] has tried to explain the existence of a hydrodynamic film through the "inward-pumping" effect. This phenomenon, frequently observed, consists of a radial inflow across the faces of a seal; it implies some leakage and Reiner has attempted to explain it in terms of non-Newtonian effects in the film. Non-Newtonian models are difficult to formulate, but Tanner [29] has shown that they cannot adequately explain the ways in which a face-seal performs. Another theory postulates the generation of hydrodynamic pressure by faces that either have an angular misalignment or vibrate or oscillate with respect to each other [30,31].

Other theories consist of the "thermal wedge" in which circumferential temperature variations cause density and thence pressure variations, "pressure-viscosity" effects, radial eccentricity, and simply a radial hydrostatic pressure gradient between the sealed fluid and its "surroundings". More recently, attention has been focused on the strong likelihood of hydrodynamic pressure being generated by a mechanism that fits the classical theory of hydrodynamic lubrication presented by Reynolds in 1886. Stanghan-Batch and others [25,32] have shown that hydrodynamic pressures can be generated by wavy surfaces and that the operation of seals with wavy surfaces can be explained by Reynold's theory.

In Chapter II, it has been assumed that the two faces are perfectly flat initially. While that enables the use of analytical deductions,

it is a highly idealized configuration that does not occur in practice. Because the nominal film thickness $\bar{h}$ is very small in real face seals, even a very slight waviness is likely to be significant when compared with $\bar{h}$. Such waviness may comprise, in some instances, an angular misalignment of the two faces. As mentioned above, there are several possible modes of operation for a face seal, ranging from boundary lubrication to hydrodynamic action. A large number of applications fall in the latter category, and the generation of hydrodynamic pressures depends on surface waviness. While the flat face idealization may hold in a few real cases involving very small waviness and light face loading or a hydrostatic pressure gradient, an analysis of the wavy surface is essential to the understanding of thermoelastic effects in most real seals.

The upper surface in fig. (27) is a good thermal conductor with a waviness defined by h_o at a given operating condition. This waviness is not the initial, machined, surface profile, but rather the modified profile comprising the initial shape as well as subsequent thermal and elastic distortions compatible with the operating conditions. The stationary bottom surface is a flat thermal insulator. This surface is chosen as flat because it does not undergo thermal distortions and any initial waviness on it will remain the same because elastic effects are usually negligibly small. The face-load f, the sliding speed U, h_o and $\bar{h}$ together represent a quasi-static state or operating condition. Since f and U are nominally fixed in operation, departures from the quasi-static state will involve changes in either h_o or $\bar{h}$, or in both. Thus, in order to determine whether thermoelastic instabilities can

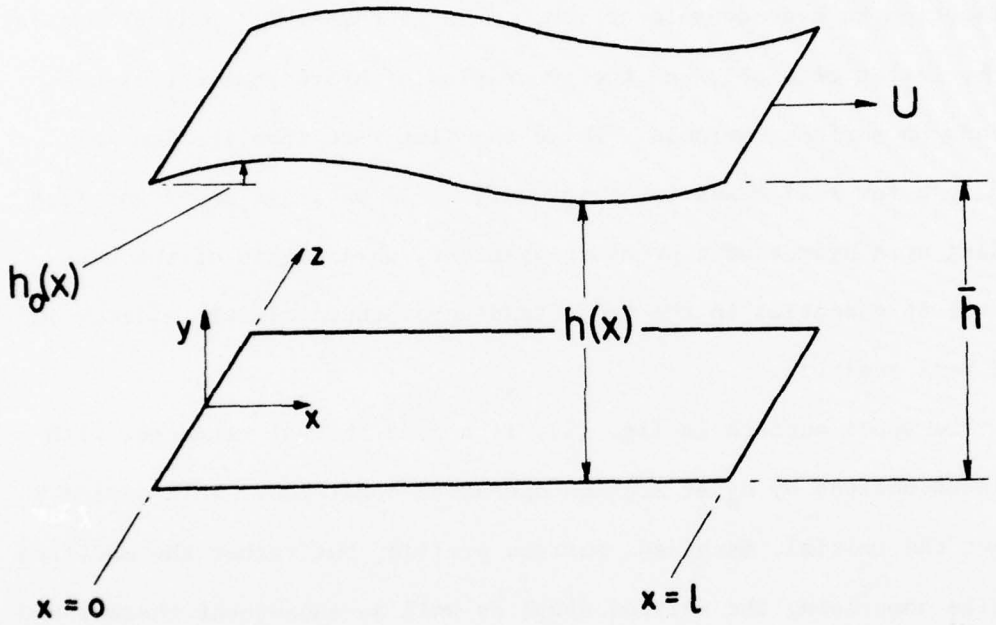

Figure 27. Definition Sketch for Operating Condition

occur, one may impose, as before, a small surface perturbation h' on h_o and examine whether the resulting changes in heat and pressure generation tend to increase the amplitude of h'. If so, the operating condition will be said to define an unstable state. If not, the seal will be said to be operating in a thermoelastically stable regime.

Most real face-type seals have low aspect ratios, i.e., the face-width is small compared to the inner radius. Therefore, the narrow-face geometry will be considered here. It is then possible to replace the cylinders (fig. 4) with flat blades as in Chapter II. Furthermore, because the pressure gradients in the x-direction are considerably smaller than those in the z-direction, a fair approximation of the flow is obtained by considering it to be purely Couette. This may not seem very obvious for sizable values of $|h_o|/\bar{h}$, but is true at least in those cases where the surface waviness has a large wavelength and the face width is small by comparison [33].

The velocity distribution for the x-direction is then given simply by

$$u = U \frac{y}{h} \tag{4-1}$$

where

$$h(x) = \bar{h} + \hat{h} + h_o(x) + h'(x) \tag{4-2}$$

h'(x) being the small perturbation whose decay or growth will indicate the stability or otherwise of the system. The introduction of h' will alter the hydrodynamic pressure distribution in the film, thus changing the net pressure or "load support" generated in the film. Since the face-loading f is constant for a given system and must be balanced by

the net pressure in the film, the two faces will tend to part or come closer to negate the increase or decrease of the net pressure. This relative axial motion between the two faces is represented, in eq. (4-2), by $\hat{h}$, which signifies a small change in $\bar{h}$, occasioned by the small change h' in h_o. It is assumed here that both faces are held in rigid mountings that permit axial motion without tilt. If one face is flexibly mounted, as in the experiments described in Chapter III, it will tilt in response to any asymmetry in the pressure wave resulting from the introduction of h'. The tilting case will be dealt with later.

4.2 Heat Generation

Viscous heat generation within the film is given by

$$q_g = \int_o^h \mu \left(\frac{\partial u}{\partial y}\right)^2 dy \tag{4-3}$$

in which eqs. (4-1) and (4-2) are to be substituted. In eq. (4-2), $\hat{h}$ and h' are perturbation (first order) quantities, while $\bar{h}$ and h_o are of zero order. One then has

$$q_g = \frac{\mu U^2}{h}$$

$$= \frac{\mu U^2}{(\bar{h} + h_o)\left(1 + \frac{h' + \hat{h}}{\bar{h} + h_o}\right)}$$

and, since $\frac{h' + \hat{h}}{\bar{h} + h_o} \ll 1$,

$$q_g = \frac{\mu U^2}{\bar{h} + h_o}\left(1 - \frac{h'}{\bar{h} + h_o} - \frac{\hat{h}}{\bar{h} + h_o}\right) \tag{4-4}$$

If one defines $q_g = q_o + q'$ where q_o denotes the zero order heating obtained in the unperturbed operating condition and q' the perturbation resulting from the introduction of h', one can write, from eq. (4-4),

$$q_o = \frac{\mu U^2}{\bar{h} + h_o} \tag{4-5}$$

$$q' = - \frac{\mu U^2}{(\bar{h} + h_o)^2} (h' + \hat{h}) \tag{4-6}$$

4.3 Heat Conduction and Convection

The heat generated in the film through the process of viscous dissipation is removed through convection and conduction. It was shown in Chapter II (see also Appendix A) that, for a narrow-face seal, convection has little effect on the temperature distribution in the metal. Georgopoulos [34] has proved this through a rigorous solution of the energy equation incorporating the convection term. It has been found that, for the narrow-face seal, the convected heat is only a very small percentage of that conducted. In view of the above, it will be assumed here that all the heat generated is conducted into the metal face. Thus, eqs. (4-4), (4-5) and (4-6) all represent the heat input into the metal.

4.4 Thermal Deformation

The relationship between the heat input to a surface and the corresponding surface curvature is given by

$$\frac{d^2 v}{dx^2} = \frac{\alpha_M q}{K_M} \tag{4-7}$$

where v denotes the thermal deformation of the surface. This applies to

plane-stress problems and was shown by Burton et al [9]; an erroneous multiplier of 2 was inadvertently introduced and later corrected [35]. In order that eq. (4-7) may reflect the fact that uniform heating will lead to zero curvature, an extra term should be introduced. In terms of the present nomenclature, eq. (4-7) may be rewritten as

$$\frac{d^2(\delta_{th})}{dx^2} = \frac{\alpha_M q'}{K_M} - C' \tag{4-8}$$

where

$$C' = \frac{1}{\ell} \int_o^{\ell} \frac{\alpha_M q'}{K_M} \, dx \tag{4-9}$$

Evidently, eqs. (4-8) and (4-9) are written in terms of perturbation quantities. The integration from $x = 0$ to $x = \ell$ implies summing around the circumference of the real seal. Using eqs. (4-6) and (4-9), in eq. (4-8), one obtains

$$\frac{d^2}{dx^2}(\delta_{th}) = -\frac{\alpha_M}{K_M} \frac{\mu U^2}{(\bar{h} + h_o)^2} (h' + \hat{h}) + \frac{\alpha_M}{K_M} \mu U^2 \frac{1}{\ell} \int_o^{\ell} \frac{h' + \hat{h}}{(\bar{h} + h_o)^2} \, dx \tag{4-10}$$

which, if integrated twice, will give $\delta_{th}(x)$.

4.5 Hydrodynamic Pressure

The tangential pressure distribution in the film is obtained as outlined in Chapter II. As mentioned earlier [see ref. 33], greater care is called for, in the case of the wavy surface, in applying the assumption of $\partial p/\partial x \ll \partial p/\partial z$. It should be emphasized, once again, that such an assumption is quite valid whenever the face-width is very small compared to the wavelength of the surface wave. Similar considerations

the basis of the well-known "short bearing" theory. Cameron [16] has shown that for $\lambda/L \geq 8$, the short bearing equations compare very well with results obtained from a numerical solution of the full Reynold's equation. The total pressure is given by

$$p = \frac{3\mu U}{h^3} \frac{dh}{dx} \left(z^2 - \frac{L^2}{4} \right) \tag{4-11}$$

Also

$$p_{max} = p_{z=0}$$

and the average pressure is given by (fig. 14)

$$\bar{p} = \frac{2}{3} p_{max}$$

so that one obtains

$$\bar{p} = - \frac{\mu U}{2h^3} L^2 \frac{dh}{dx} \tag{4-12}$$

in which h is as defined by eq. (4-2).

It should now be pointed out that, for a symmetric surface shape such as a sinusoidal wave, the pressure wave given by eq. (4-12) will also be symmetric because both h(x) and dh/dx are symmetric. Consequently, one will obtain positive pressures in the convergent portions of the liquid film, and symmetrically opposite (negative) pressures in the divergent portions, as indicated in fig. (28). The negative and positive parts of the pressure wave then cancel each other and the net pressure is zero, implying that no load can be supported.

In trying to explain how a face seal supports load, Stanghan-Batch et al [32] reported experiments which strongly suggested the existence of a hydrodynamic film between the two faces. The measured pressure waves showed positive peaks where the film converged, and essentially

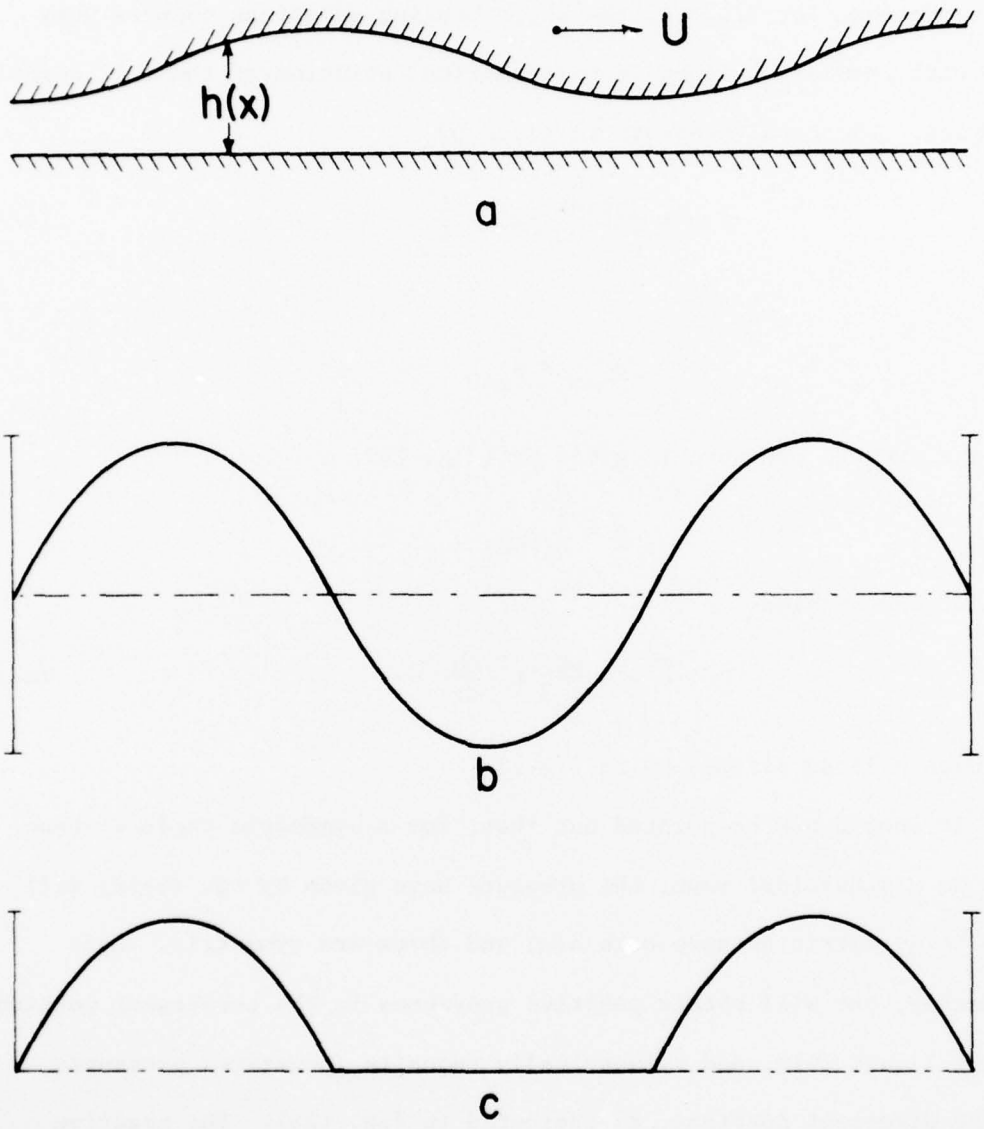

Figure 28. Circumferential Pressure Distribution

a) Sinusoidal Surface Shape giving symmetric h(x)
b) Corresponding theoretical pressure wave
c) Pressure wave with negative regions suppressed.

zero pressure where it diverged. Stanghan-Batch and Iny subsequently published a hydrodynamic theory for face seals [25]. It was shown that if one of the two faces was wavy, a hydrodynamic pressure wave was generated, but that cavitation occurred in the diverging portions of the film and extended into the converging regions as well (fig. 29). While it is known that filaments of fluid continue to flow through and around the cavity pockets, such flow is difficult to model or describe mathematically. Most commercial oils are known to release dissolved air at about four-fifths of atmospheric pressure. The authors found that, by analytically calculating the pressures and then simply suppressing the negative parts, a strikingly good approximation to experimentally measured values could be obtained, as shown in fig. (30). This information will be used in the present study.

Equation (4-12) can be expanded as

$$\bar{p} = - \frac{\mu U L^2}{2(\bar{h} + h_o)^3 \left(1 + \frac{\hat{h} + h'}{\bar{h} + h_o}\right)^3} \frac{d}{dx} (\bar{h} + h_o + \hat{h} + h')$$

and, since $\frac{\hat{h} + h'}{\bar{h} + h_o} \ll 1$ and $\frac{d\bar{h}}{dx} = 0 = \frac{d\hat{h}}{dx}$, one has

$$\bar{p} = - \frac{\mu U L^2}{2(\bar{h} + h_o)^3} \left[1 - \frac{3(\hat{h} + h')}{\bar{h} + h_o}\right] \left(\frac{dh_o}{dx} + \frac{dh'}{dx}\right) \qquad (4\text{-}13)$$

If one defines $\bar{p} = p_o + p'$ where p_o denotes the zero order (operating) pressure and p' the first order (perturbation) pressure, one obtains, from eq. (4-13),

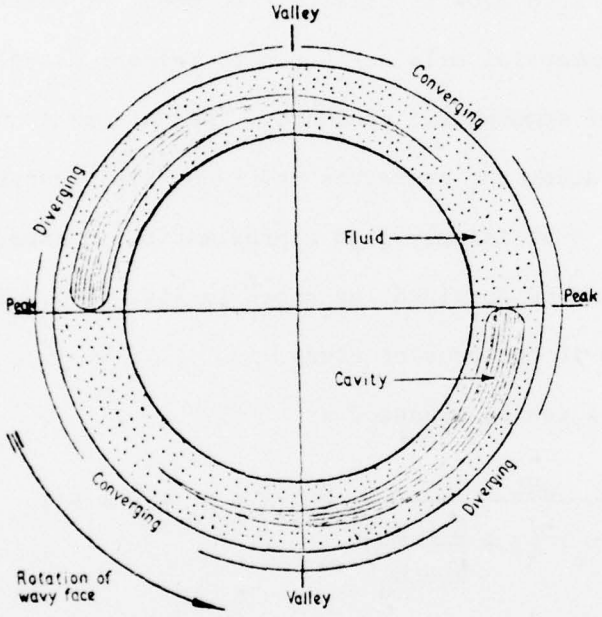

Figure 29. Typical Location of Cavitation Pockets
(Stanghan-Batch and Iny, ref. 25)

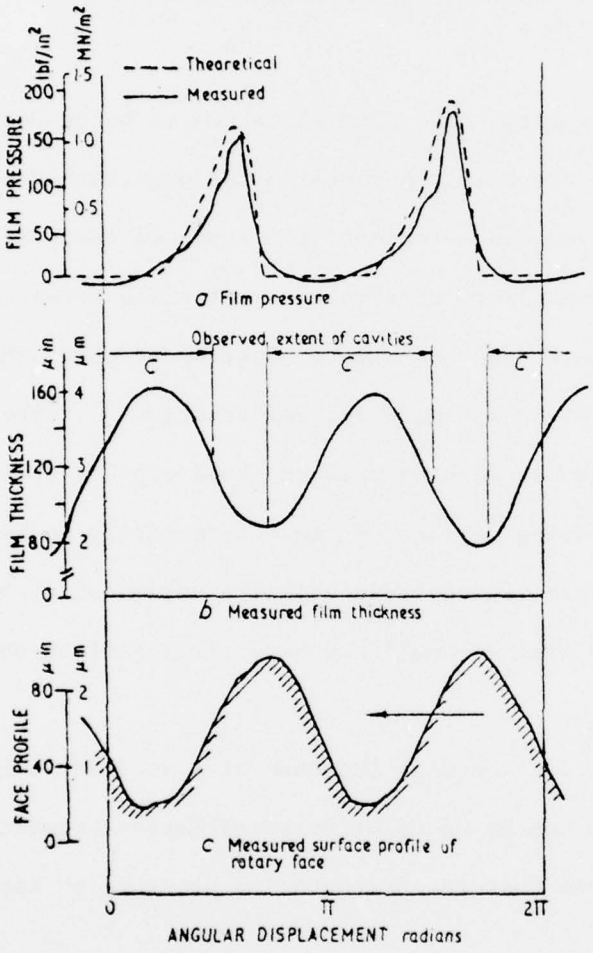

Figure 30. Characteristics of Profiled Cast-Iron Seal Face (Stanghan-Batch and Iny, ref. 25)

$$p_o = - \frac{\mu U L^2}{2(\bar{h} + h_o)^3} \frac{dh_o}{dx} \tag{4-14}$$

and

$$p' = - \frac{\mu U L^2}{2(\bar{h} + h_o)^3} \left[\frac{dh'}{dx} - \frac{3(\hat{h} + h')}{\bar{h} + h_o} \frac{dh_o}{dx} \right] \tag{4-15}$$

where all second order terms have been discarded as being small.

Since p_o denotes the film pressures in the unperturbed operating condition, its negative values indicate the zones of cavitation. It will be assumed, as stated earlier, that in the cavitating zones the film, for analytical purposes, does not exist. Everywhere else, the film exists and has positive pressures. The perturbation p' represents a small change in p_o and has meaning only in those regions where the film exists. In the cavitating regions, p' must necessarily be zero, while in the positive pressure regions even negative values of p' are permissible because they will be small and have little effect on the larger positive values of p_o.

One may consider for a moment the case of a seal whose faces are so mounted that there can be no relative axial motion between them, i.e., $\hat{h} \equiv 0$. It will be seen that the perturbation pressure p'' for such a set-up will be

$$p'' = - \frac{\mu U L^2}{2(\bar{h} + h_o)^3} \left(\frac{dh'}{dx} - \frac{3h'}{\bar{h} + h_o} \frac{dh_o}{dx} \right) \tag{4-16}$$

Using eq. (4-16) in eq. (4-15), one may write

$$p' = p'' - \hat{p} \tag{4-17}$$

where

$$\hat{p} = - \frac{3\mu U L^2}{2(\bar{h} + h_o)^4} \hat{h} \frac{dh_o}{dx} \tag{4-18}$$

It may then be argued that since p'' has a wave form, it can be thought of as composed of a zero-average wave and a constant. By definition, then, the zero-average component is incapable of supporting load, but capable of producing face distortion. The constant (uniform) component, on the other hand, is incapable of causing distortion, but produces a net force (positive or negative). Since, by definition, p_o supports the fixed load f on the face, any additional axial force generated within the film must be neutralized by relative axial motion between the faces (where the mechanical set-up allows such motion, as in almost all cases), and such motion is represented by $\hat{h}$. Thus, if one subtracts from p'' its constant component (as represented by the right-hand side of eq. (4-17)), one is left with its zero average component which, according to eq. (4-17), is p'. That means

$$\frac{1}{\ell}\int_{x=0}^{\ell} p'\,dx = 0$$

so that eq. (4-17) gives

$$\frac{1}{\ell}\int_{x=0}^{\ell} \hat{p}\,dx = -\hat{h}\left[\frac{1}{\ell}\int_{o}^{\ell} \frac{3\mu UL^2}{2(\bar{h}+h_o)^4}\frac{dh_o}{dx}\,dx\right] = \frac{1}{\ell}\int_{o}^{\ell} p''dx \qquad (4\text{-}19)$$

In eq. (4-19), the right hand side is known because p'' is defined, in eq. (4-16), in terms of operating conditions and an impressed h'. The only unknown on the left hand side is $\hat{h}$, which can then be calculated. In view of the fact that the film is supposedly non-existent in portions of the interval of integration, the definite integrals require some qualification, but that will be discussed later.

For the present, it is sufficient to recognize that the pressures that cause face distortion are given by p' and that these can be

AD-A047 926 NORTHWESTERN UNIV EVANSTON ILL F/G 20/11
THERMOELASTIC PHENOMENA IN LUBRICATED SLIDING CONTACT.(U)
JAN 77 B N BANERJEE , R A BURTON N00014-75-C-0761
UNCLASSIFIED 5341-427 NL

2 OF 2
AD
A047926

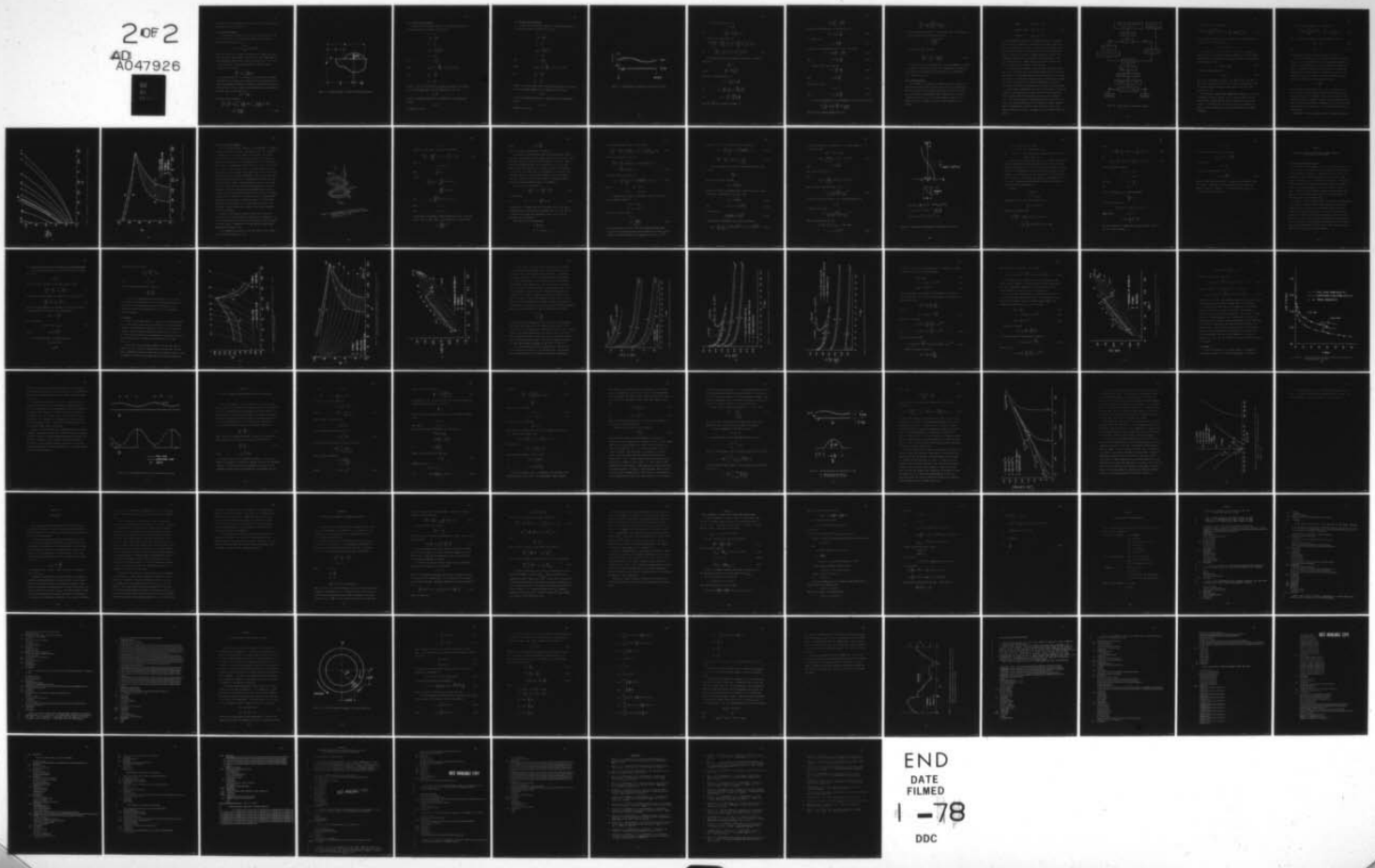

END
DATE FILMED
1 -78
DDC

determined by first obtaining p'' from eq. (4-16), then $\hat{h}$ from eq. (4-19), and then using eq. (4-17) for p'.

4.6 Elastic Deformation

As pointed out in the preceding section, elastic distortion of the face is caused by p'. The relationship between pressure and the deflection produced by it is [36]

$$v(x) = -\frac{2}{\pi E}\int_{\xi=a}^{\xi=b} p(\xi)\,\ell n|x-\xi|\,d\xi$$

where the interval a to b defines the extent of the loading zone, and ξ the location of a load element, as in fig. (31). This relationship is valid everywhere except for $\xi = x$, and so the region $(x-\epsilon) < \xi < (x+\epsilon)$ is excluded from it. Differentiating under the integral sign by Leibnitz's rule, one finds

$$\frac{d^2v}{dx^2} = \frac{2}{\pi E}\int_a^b \frac{p'(\xi)}{|x-\xi|^2}\,d\xi$$

As the region around $\xi = x$ is of interest here, this region is treated independently by exploiting the linearity of the load-displacement relationship and adding the component of curvature produced by a uniform load over this region. This is done by differentiating the corresponding displacement curve [36] and found to be

$$\varphi(\epsilon) = -\frac{4p'}{\pi E\epsilon}$$

It follows that, for small ϵ,

$$\frac{d^2v}{dx^2} \equiv \frac{d^2\delta_E}{dx^2} = \frac{2}{\pi E}\left[\int_o^{x-\epsilon} \frac{p'(\xi)}{|x-\xi|^2}\,d\xi + \int_{x+\epsilon}^{\ell} \frac{p'(\xi)}{|x-\xi|^2}\,d\xi - \frac{2p'}{\epsilon}\right]$$

$$\equiv \frac{2}{\pi E}\, I^*\left(\frac{p'(\xi)}{|x-\xi|^2}\right) \qquad (4\text{-}20)$$

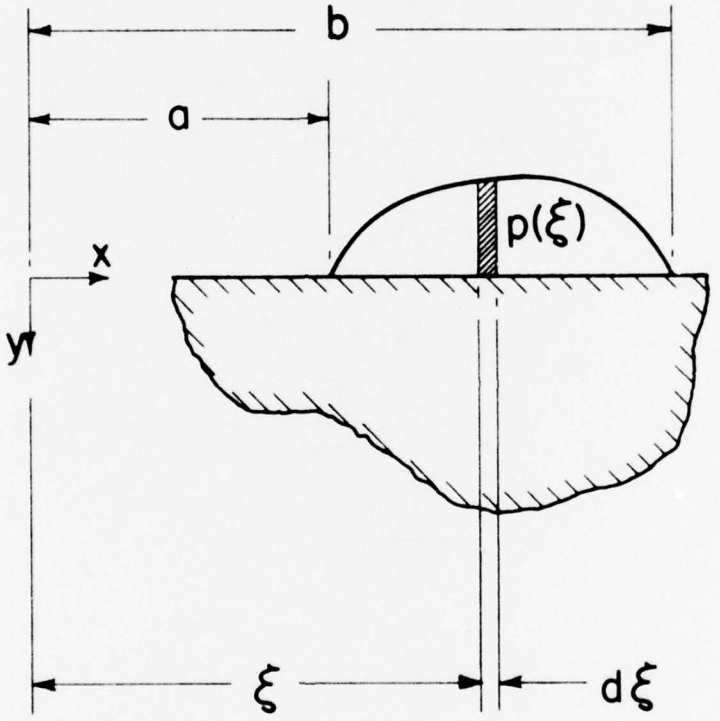

Figure 31. Definition Sketch for Elastic Deformation Equation

4.7 Normalization of Variables

To reduce all the preceding equations to non-dimensional form, the following dimensionless variables will be used:

$$X = \kappa x$$

$$Y(X) = \frac{h'(x)}{\bar{h}}$$

$$\hat{H} = \frac{\hat{h}}{\bar{h}}$$

$$H(X) = \frac{h_o(x) + \bar{h}}{\bar{h}}$$

$$\chi = \kappa\xi$$

and

$$u = \frac{U}{U_{crit}}$$

where $U_{crit} = \bar{h}\kappa \sqrt{\frac{\overline{K_M}}{\mu\alpha_M}}$ as in eq. (2-84).

Also,

$$\Delta_{th} = \frac{\delta_{th}}{\bar{h}}$$

$$\Delta_E = \frac{\delta_E}{\bar{h}}$$

Further, if both the surface wave h_o and the perturbation h' are defined to have a wavelength equal to the circumference ℓ of the seal,

$$\ell = \frac{2\pi}{\kappa}$$

so that the dimensional interval ℓ is replaced by the non-dimensional interval

$$2\pi = \kappa\ell$$

as shown in fig. (32).

4.7 Normalization of Variables

To reduce all the preceding equations to non-dimensional form, the following dimensionless variables will be used:

$$X = \kappa x$$

$$Y(X) = \frac{h'(x)}{\bar{h}}$$

$$\hat{H} = \frac{\hat{h}}{\bar{h}}$$

$$H(X) = \frac{h_o(x) + \bar{h}}{\bar{h}}$$

$$\chi = \kappa \xi$$

and

$$u = \frac{U}{U_{crit}}$$

where

$$U_{crit} = \bar{h}\kappa \sqrt{\frac{\overline{K_M}}{\mu \alpha_M}}$$ as in eq. (2-84).

Also,

$$\Delta_{th} = \frac{\delta_{th}}{\bar{h}}$$

$$\Delta_E = \frac{\delta_E}{\bar{h}}$$

Further, if both the surface wave h_o and the perturbation h' are defined to have a wavelength equal to the circumference ℓ of the seal,

$$\ell = \frac{2\pi}{\kappa}$$

so that the dimensional interval ℓ is replaced by the non-dimensional interval

$$2\pi = \kappa \ell$$

as shown in fig. (32).

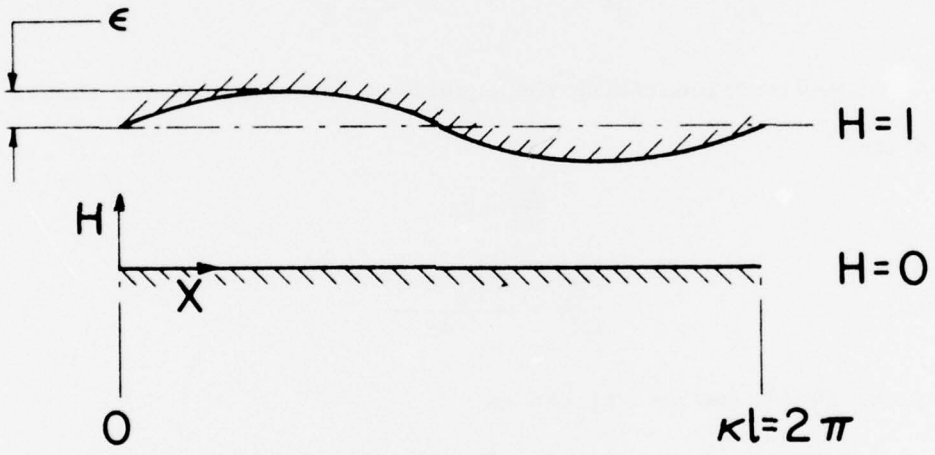

Figure 32. Non-Dimensional Coordinates for Operating Condition

It follows, from the above, that

$$dx = \frac{dX}{\kappa}$$

and $$\frac{d^2h'}{dx^2} = \bar{h}\kappa^2 \frac{d^2Y}{dX^2} \quad \text{etc.}$$

Equation (4-10) then reduces to

$$\bar{h}\kappa^2 \frac{d^2\Delta_{th}}{dX^2} = -\frac{\alpha_M \mu U^2}{K_M \bar{h}} \left(\frac{Y}{H^2} + \frac{\hat{H}}{H^2}\right) + \frac{\alpha_M \mu U^2}{K_M \bar{h}} \frac{1}{2\pi} \int_o^{2\pi} \left(\frac{Y}{H^2} + \frac{\hat{H}}{H^2}\right) dX$$

or, $$\frac{d^2\Delta_{th}}{dX^2} = -\frac{u^2}{H^2}\left(Y + \hat{H}\right) + \frac{u^2}{2\pi} \int_o^{2\pi} \frac{Y + \hat{H}}{H^2} dX \qquad (4\text{-}21)$$

In non-dimensionalizing the equations for pressure, it should be noted that

$$\frac{d\bar{h}}{dx} = 0$$

so that $$\frac{dh_o}{dx} = \frac{d(h_o + \bar{h})}{dx}$$

Then, eq. (4-14) may be written as

$$p_o = -\frac{\mu L^2}{2\bar{h}^3} \frac{U}{H^3} \bar{h}\kappa \frac{dH}{dX}$$

or, $$p_o = -\frac{\mu L^2 \kappa}{2\bar{h}^2} \frac{U}{U_{crit}} \bar{h}\kappa \sqrt{\frac{\bar{K}_M}{\mu \alpha_M}} \frac{1}{H^3} \frac{dH}{dX}$$

or, $$p_o = -\frac{L^2\kappa^2}{2\bar{h}} \sqrt{\frac{\overline{\mu K_M}}{\alpha_M}} \frac{u}{H^3} \frac{dH}{dX}$$

and, since $\frac{L^2\kappa^2}{12} = W$ as defined in Chapter II,

$$p_o \frac{\bar{h}}{W} \sqrt{\frac{\bar{\alpha}_M}{\mu K_M}} = - \frac{6u}{H^3} \frac{dH}{dX}$$

Defining the non-dimensional zero-order pressure as

$$P_o = p_o \frac{\bar{h}}{W} \sqrt{\frac{\bar{\alpha}_M}{\mu K_M}} \tag{4-22}$$

one finally gets

$$P_o = - \frac{6u}{H^3} \frac{dH}{dX} \tag{4-23}$$

Similarly, by non-dimensionalizing eq. (4-16), one obtains

$$P'' = - \frac{6u}{H^3} \left(\frac{dY}{dX} - 3 \frac{Y}{H} \frac{dH}{dX} \right) \tag{4-24}$$

where

$$P'' = p'' \frac{\bar{h}}{W} \sqrt{\frac{\bar{\alpha}_M}{\mu K_M}} \tag{4-25}$$

From eq. (4-18), it follows that

$$\hat{P} = - \frac{18u}{H^4} \hat{H} \frac{dH}{dX} \tag{4-26}$$

where

$$\hat{P} = \hat{p} \frac{\bar{h}}{W} \sqrt{\frac{\bar{\alpha}_M}{\mu K_M}} \tag{4-27}$$

and, from eq. (4-17),

$$P' = P'' - \hat{P} \tag{4-28}$$

where

$$P' = p' \frac{\bar{h}}{W} \sqrt{\frac{\bar{\alpha}_M}{\mu K_M}} \tag{4-29}$$

For the non-dimensional elastic deformation, one has, from eq. (4-20),

$$\bar{h} \kappa^2 \frac{d^2 \Delta_E}{dX^2} = \frac{2}{\pi E} \frac{W}{\bar{h}} \sqrt{\frac{\overline{\mu K_M}}{\alpha_M}} \kappa I^* \left(\frac{P'(\chi)}{|X-\chi|^2} \right)$$

where I^* has the meaning defined on pg. 86.

or,
$$\frac{d^2\Delta_E}{dX^2} = \frac{2}{\pi\bar{h}^2}\sqrt{\frac{\mu K_M W^2}{\alpha_M \kappa^2 E^2}}\, I^*\left(\frac{P'(\chi)}{|X-\chi|^2}\right)$$

It will be recalled from Chapter II that the lower limit of film-thickness for which instability was predicted was given by

$$h_1 = \left[\frac{96 K_M \mu W^2}{E^2 \alpha_M \kappa^2}\right]^{1/4}$$

If one defines $H_L = \frac{h_1}{\bar{h}}$, one finds

$$\frac{d^2\Delta_E}{dX^2} = \frac{H_L^2}{2\sqrt{6}\,\pi}\, I^*\left(\frac{P'(\chi)}{|X-\chi|^2}\right) \qquad (4\text{-}30)$$

In chapter II, it has been shown that h_1 is representative of the edge of the domain in which elastic effects are consequential to instability. In the present case, therefore, one would expect elastic deformation to be important for $H_L = 1$.

4.8 Stability Analysis

As in Chapter II, the question of whether or not the system is in thermoelastic stability will again be posed in terms of a perturbation. Will the introduction of the small perturbation Y(X) result in thermal (Δ_{th}) and elastic (Δ_E) deformations whose combined effect is greater in amplitude than $|Y|$? If so, the chosen operating condition is unstable; if not, it is stable. As before, three conditions can be defined:

$$\begin{aligned} &\text{stable:} && |\Delta_{th} + \Delta_E| < |Y| \\ &\text{neutrally stable:} && |\Delta_{th} + \Delta_E| = |Y| \\ &\text{unstable:} && |\Delta_{th} + \Delta_E| > |Y| \end{aligned} \tag{4-31}$$

The second condition represents the so-called threshold of instability that was sought in Chapter II by solving the corresponding equation for the case of initially flat surfaces. In the present case, such a solution by analytical means is unfeasible in view of the non-linearities present. Therefore, $Y(X)$ will be supplied and $\Delta_{th}(X)$ and $\Delta_E(X)$ will be separately computed from eqs. (4-21) and (4-30) respectively. Then $\Delta_{th}(X)$ and $\Delta_E(X)$ will be summed and $|\Delta_{th} + \Delta_E|$ will be compared with $|Y|$ to see which one of conditions (4-31) prevails.

In accounting for cavitation, it will be noted that some flow does occur in the cavitation zones, but that the heating effects of that flow are uncertain. One may say, however, that such effects will lie between the extremes of full-film heat generation and zero heating (corresponding to a truly non-existent film). Stability analyses will be made for both extremes and the true situation will be expected to fall in between.

The procedure is outlined in fig. (33). For the purpose of numerical computation, the derivatives are written in terms of the central difference formula, while the integrations are done by the trapezoidal rule. Since the film equations are meaningless where the film does not exist, the integrals between 0 and 2π are treated as improper integrals and the integrations are carried out only over those regions of the domain in which the film exists (analogous to the "half Sommerfeld" condition).

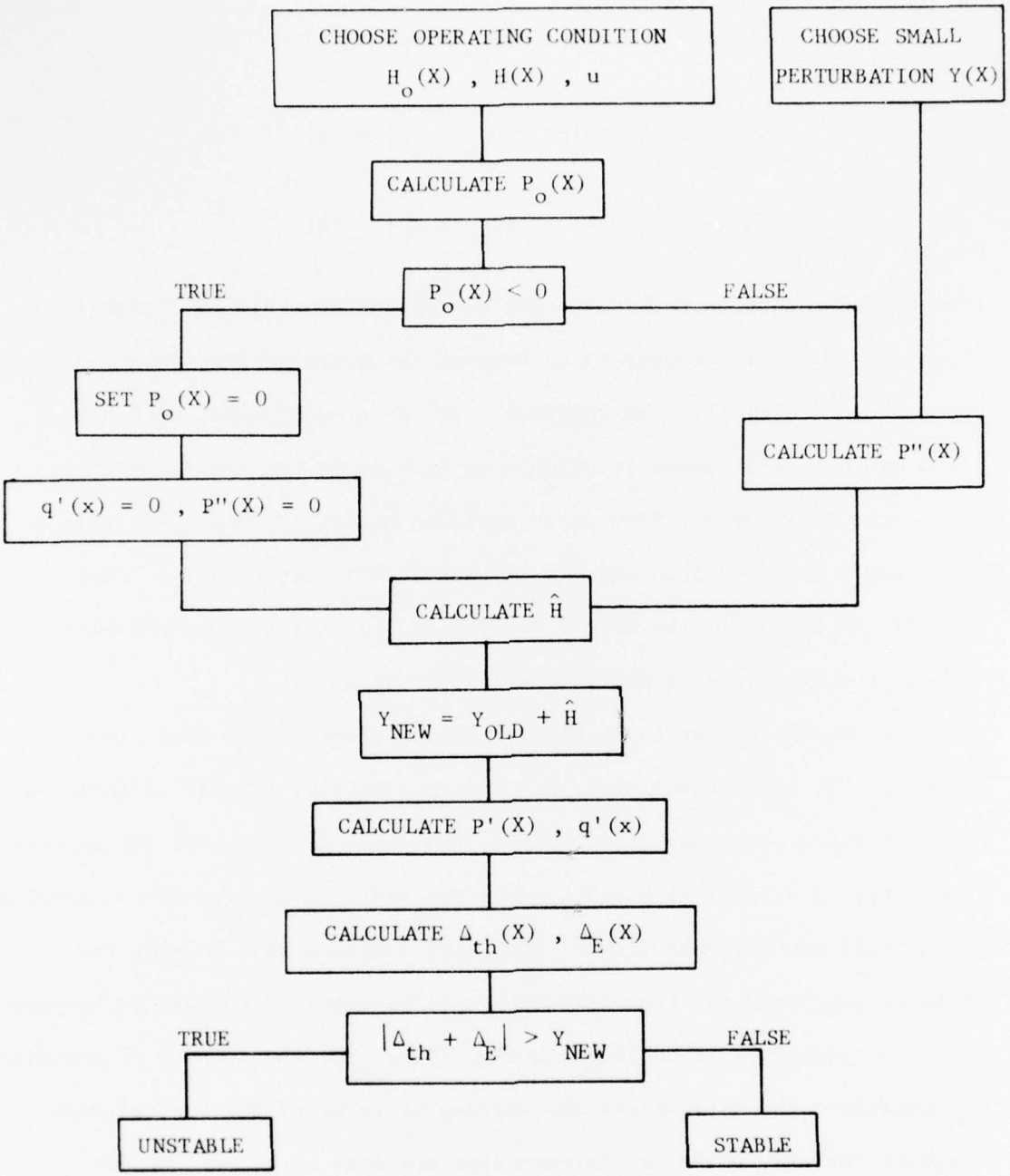

Figure 33. Block Diagram of Instability Analysis

Equation (4-21) is expanded as

$$\frac{(\Delta_{th})_{i+1} - 2(\Delta_{th})_{i} + (\Delta_{th})_{i-1}}{(DX)^2} = -u^2 \frac{Y_i}{H_i^2} + \frac{u^2}{(n-1)DX} \sum_{i=o}^{n} \frac{Y_i}{H_i^2} \tag{4-32}$$

where n denotes the number of pivotal points, DX the pivotal spacing and Y represents the corrected (or new)

$$(Y)_{new} = (Y)_{old} + \hat{H}$$

If one writes eq. (4-32) for all the i's, one gets n equations, of which two have to be replaced by boundary conditions. The first boundary condition derives from the fact that Δ_{th} must be single valued around the seal circumference. Thus

$$(\Delta_{th})_1 = (\Delta_{th})_n \tag{4-33}$$

The other boundary condition is

$$(\Delta_{th})_1 = 0 \tag{4-34}$$

which is not an arbitrary imposition. The idea is that, after Y(X) is corrected to include $\hat{H}$, there will be no rigid-body displacements, and the deformations may be measured relative to any fixed point, here chosen as the first.

The resulting n equations are solved for the unknown Δ_{th}'s by using a subroutine called MVS, which is one of a library package that goes under the name of MIDAS (Matrix, Inverse, Determinant, and Algebraic System). As stated earlier, two cases are solved, one assuming zero heating in the cavitating zones, the other assuming full-film heating throughout.

For the elastic deformations, eq. (4-30) gives

$$\frac{(\Delta_E)_{i+1} - 2(\Delta_E)_i + (\Delta_E)_{i-1}}{(DX)^2} = \frac{H_L^2}{\pi\sqrt{6}} I^*\left(\frac{P'_j}{|X_i - \chi_j|^2}\right) \tag{4-35}$$

where I^* represents a summation, with the boundary conditions

$$(\Delta_E)_1 = (\Delta_E)_n \tag{4-36}$$

and

$$(\Delta_E)_1 = 0 \tag{4-37}$$

The same pivotal spacings are used for the X_i's and the χ_j's.

In the actual event, the search for the threshold of instability ($|\Delta_{th} + \Delta_E| = |Y|$) has proved to be time-consuming and expensive. It has also been found that $\Delta_E(X)$ is orders of magnitude smaller than $\Delta_{th}(X)$. Consequently, elastic deformations have been dropped from consideration and stability analyses conducted on the basis of the dominant Δ_{th} alone. In so doing, plots have been made of $|\Delta_{th}|/|Y|$ versus u for a number of discreet values of ϵ where

$$\epsilon = \frac{|h_o|}{\bar{h}}$$

The resulting curves are shown in fig. (34). For each value of ϵ, the critical u is given by the point where the corresponding curve crosses the $|\Delta_{th}|/|Y| = 1$ ordinate. These critical values are then plotted on a ϵ versus u graph as shown in fig. (35), which also illustrates the difference between the assumptions of full-film heating and zero-heating in the cavitation zones. The true solutions lie in the shaded region.

Appendix D shows the program used in the computer calculations.

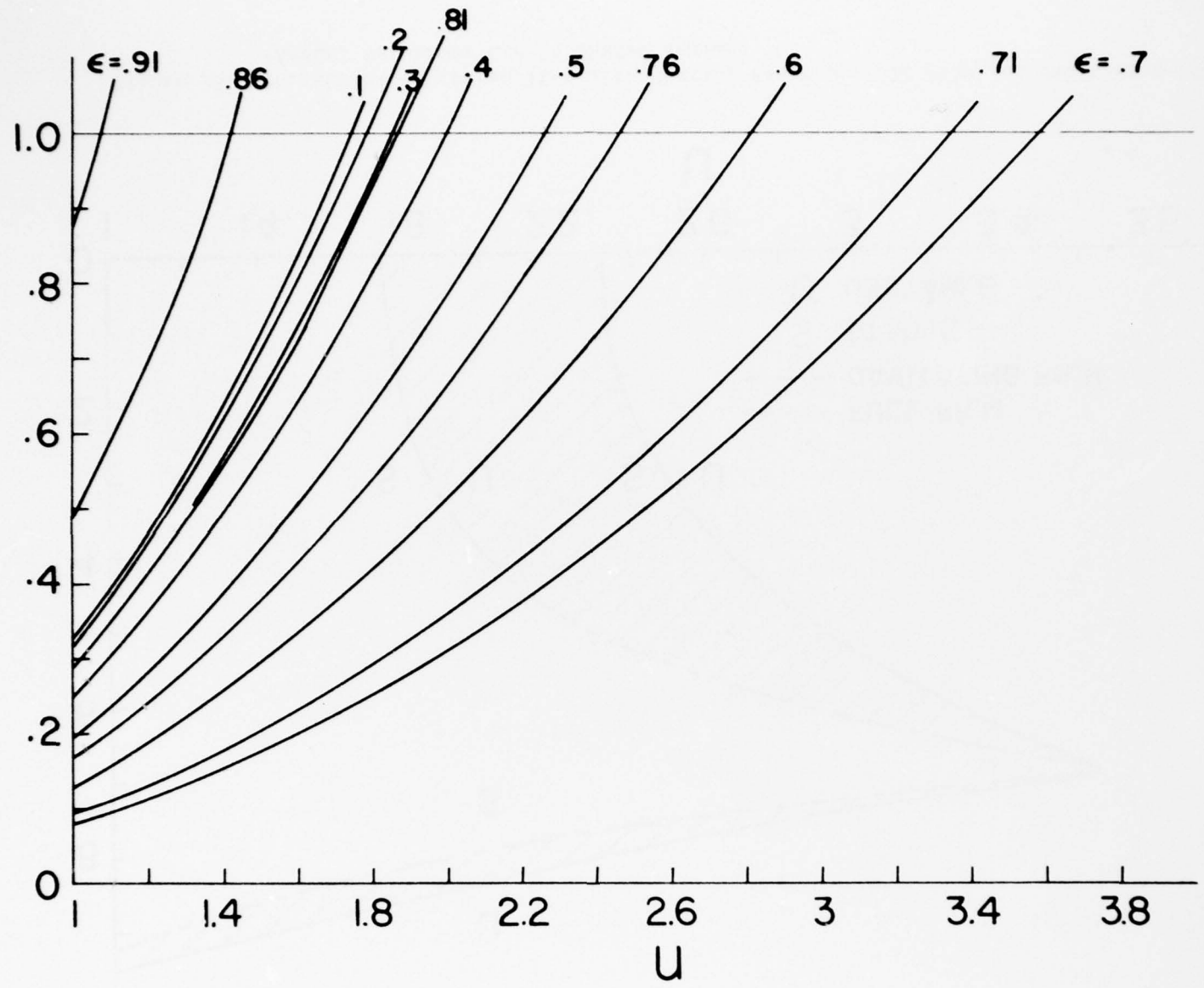

Figure 34. Determination of Non-Dimensional Critical Speed for Operating Surface Waviness

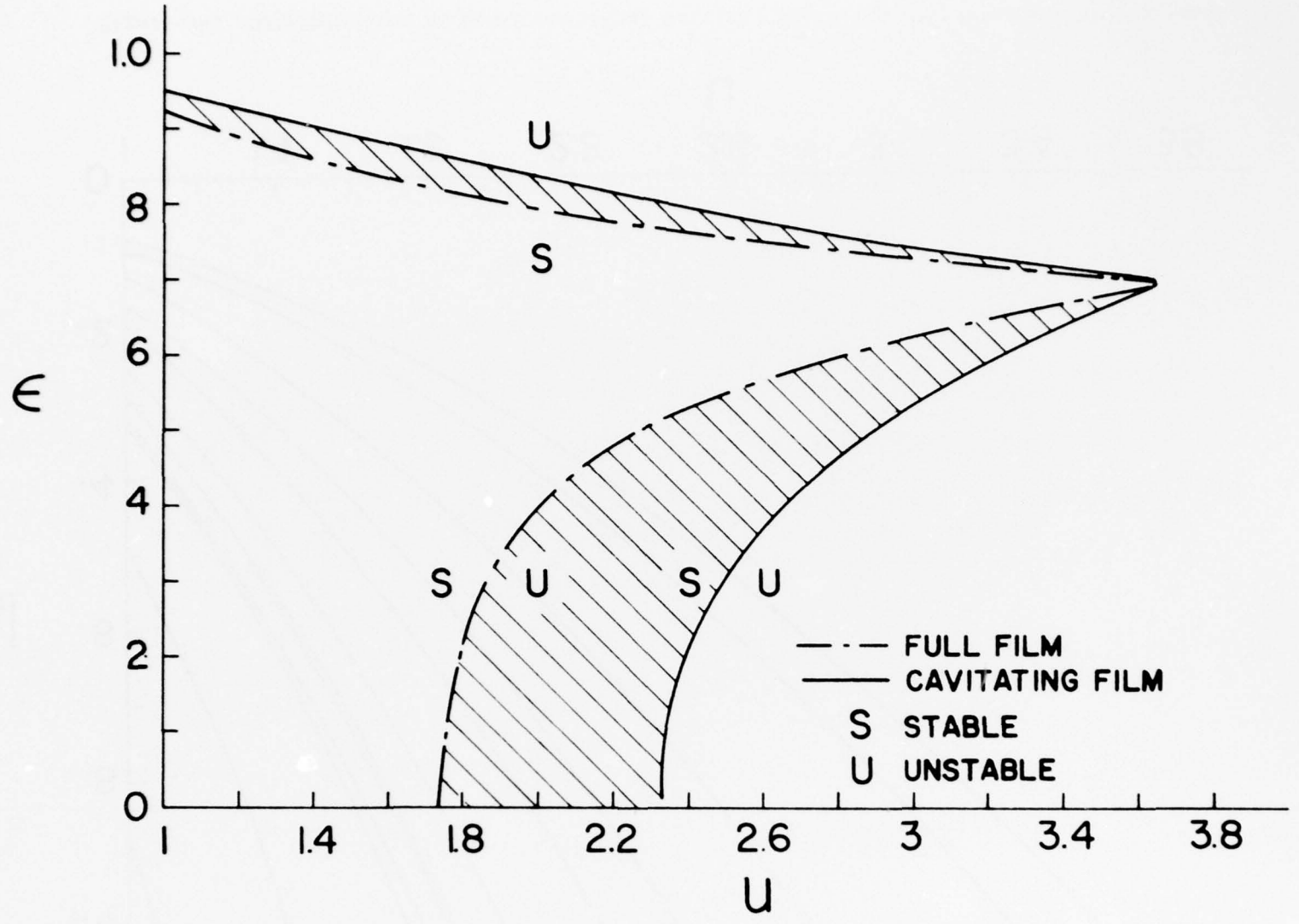

Figure 35. Thresholds of Instability with Heating Based on Full Film and Cavitating Film. (Actual Solutions Lie in Shaded Regime)

4.9 Notes on Various Parameters

One of the most important parameters is the wavelength. In Chapter II it has been shown that the largest wavelengths are the most susceptible to instability, i.e., have the lowest critical speeds. The results represented by fig. (35) are based on the assumption of a single wave around the circumference, i.e., a wavelength equal to the circumference. This is akin to a misalignment between two perfectly flat faces as shown in fig. (36). If one of the two faces is flexibly mounted, as is the common practice, the resultant single-lobed pressure wave will tilt that face and neutralize the initial misalignment. Thus, a single-lobed wave can exist only when both faces are rigidly mounted, allowing axial but not tilting motion. Where a flexible mounting is used, a surface wave must have at least two lobes in order that hydrodynamic pressure may be generated. Calculations show that with wavelength equal to half the circumference, the critical speeds plotted in fig. (35) will be doubled. As shown, fig. (35) provides the critical speeds for a rigidly mounted seal with a single-lobed wave; doubling the values of u will describe the threshold of instability for a flexibly mounted seal with a two-lobed wave. Each will represent the lowest critical speed obtainable for the given mounting.

An analysis was made and a computer program used to allow for tilting of the faces during operation, and are given in Appendix E. Use of this program, however, was discontinued subsequent to the realization of the above facts. A symmetrical two-lobed wave will always remain symmetrical and produce no tilt.

To test whether the equations for the wavy surface can be reduced to those derived in Chapter II, let

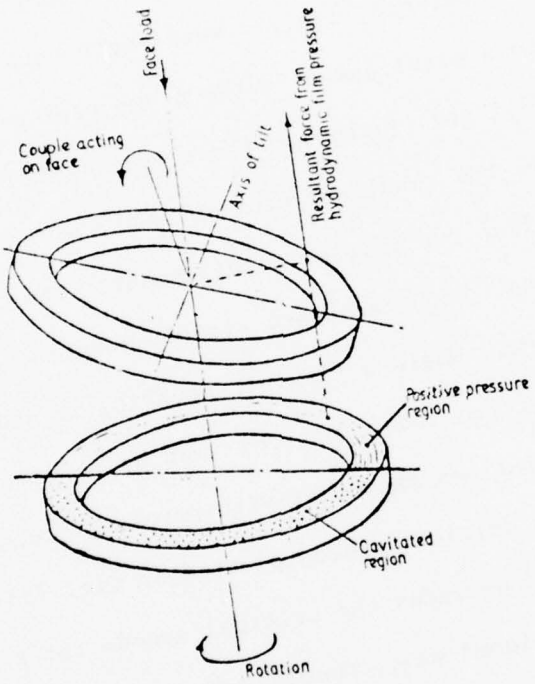

Figure 36. How Hydrodynamic Film Pressure Tends to Neutralize Relative Face Nutation (Stanghan-Batch and Iny, ref. 25)

$$h_o = 0$$

signifying a flat surface. Then eq. (4-10) becomes

$$\frac{d^2\delta_{th}}{dx^2} = -\frac{\alpha_M \mu U^2}{K_M \bar{h}^2}\left[(h' + \hat{h}) - \frac{1}{\ell}\int_o^{\ell}(h' + \hat{h})dx\right] \qquad (4\text{-}38)$$

Then, let

$$h' = A \sin \kappa x$$

whence

$$\int_o^{\ell} h'dx = 0$$

so that

$$\frac{d^2}{dx^2}(\delta_{th}) = -\frac{\alpha_M \mu U^2}{K_M \bar{h}^2}(h' + \hat{h} - \hat{h})$$

$$= -\frac{\alpha_M \mu U^2}{K_M \bar{h}^2} A \sin \kappa x$$

Thus,

$$\delta_{th} = \frac{\alpha_M \mu U^2}{K_M \bar{h}^2}\frac{A}{\kappa^2} \sin \kappa x + C_1 x + C_2$$

where

$$C_2 = 0$$

and

$$C_1 x + C_2 = 0$$

in keeping with the boundary conditions described by eqs. (4-33) and (4-34). Then, in order that δ_{th} may be equal to h', one must have

$$1 = \frac{\alpha_M \mu}{K_M \bar{h}^2 \kappa^2} U^2$$

whence $$U = \bar{h}\kappa \sqrt{\frac{\overline{K_M}}{\mu\alpha_M}}$$

which is the same as that obtained in Chapter II.

This linearized derivation shows that, with initially flat surfaces, vertical rigid-body motions, when allowed, do not affect the critical speed. This might lead one to believe that $\hat{h}$ has minimal or no effect. However, numerical solutions show that if $\hat{h}$ is assumed to be zero, U_{crit} gets smaller as $|h_o|$ gets larger, while the opposite occurs if $\hat{h}$ is allowed to be non-zero. This would seem to be an anomaly, because larger $|h_o|$'s should be expected to lead to greater disparities in $q'(x)$ along the film and, consequently, lower critical speeds. A linearized simplification of the heating equation suggests an explanation.

If $h_o \ll \bar{h}$, eq. (4-6) reduces to

$$q' = -\frac{\mu U^2}{\bar{h}^2}\left(h' + \hat{h} - \frac{2h_o h'}{\bar{h}} - \frac{2h_o \hat{h}}{\bar{h}}\right) \qquad (4\text{-}39)$$

It follows that,

for $$h_o \equiv 0 \quad , \quad q' = -\frac{\mu U^2}{\bar{h}^2}(h' + \hat{h}) \qquad (4\text{-}40)$$

in which case, as already shown, $\hat{h}$ does not affect the critical speed. On comparing eqs. (4-39) and (4-40), one might guess that, with non-zero h_o and $\hat{h}$, the last term in the parenthesis of eq. (4-39) is the one that makes all the difference.

Recalling eq. (4-21), and defining

$$Y = \frac{A}{\bar{h}} \sin X$$

$$H = 1 + \varepsilon \cos X \quad , \quad \varepsilon < 1$$

and stipulating, further, that $\hat{H}$ is zero, one has

$$\frac{d^2\Delta_{th}}{dX^2} = -\frac{u^2A}{\bar{h}}\left[\frac{\sin X}{(1+\epsilon\cos X)^2} - \frac{1}{2\pi}\int_0^{2\pi}\frac{\sin X}{(1+\epsilon\cos X)^2}\,dX\right] \tag{4-41}$$

This can be integrated to give [37]

$$\frac{d\Delta_{th}}{dX} = -\frac{u^2A}{\bar{h}\epsilon}\left\{\frac{1}{1+\epsilon\cos X} - \frac{1}{2\pi}\left[\frac{1}{1+\epsilon\cos X}\right]_0^{2\pi}\right\} + C_1$$

$$= -\frac{u^2A}{\bar{h}\epsilon}\frac{1}{1+\epsilon\cos X} + C_1 \tag{4-42}$$

Integrating again, one obtains [37]

$$\Delta_{th} = -\frac{u^2A}{\bar{h}\epsilon}\frac{\delta}{\sqrt{1-\epsilon^2}}\cos^{-1}\left[\frac{\epsilon+\cos X}{1+\epsilon\cos X}\right] + C_1X + C_2 \tag{4-43}$$

where

$$\delta = 1 \quad \text{for} \quad \sin X \geq 0$$

$$\delta = -1 \quad \sin X \leq 0$$

To determine the constants of integration C_1 and C_2, one has to use the boundary conditions

$$X = 0 \quad , \quad \Delta_{th} = 0$$

$$X = 2\pi \quad , \quad \Delta_{th} = 0$$

which give, from eq. (4-43),

$$C_2 = 0$$

$$C_1 = \frac{u^2A\delta}{\bar{h}\epsilon\sqrt{1-\epsilon^2}} \tag{4-44}$$

The implication of eq. (4-44) is that the maximum and minimum values of Δ_{th} will not correspond exactly with the peak and the trough of $Y(X)$, but will be displaced slightly, corresponding to the value of $\sqrt{1-\epsilon^2}$.

Returning to eqs. (4-43) and (4-42), one can now write

$$\Delta_{th} = - \frac{u^2 A}{h\epsilon} \frac{\delta}{\sqrt{1-\epsilon^2}} \left[\cos^{-1}\left(\frac{\epsilon + \cos X}{1 + \epsilon \cos X} \right) - X \right] \tag{4-45}$$

$$\frac{d\Delta_{th}}{dX} = - \frac{u^2 A}{h\epsilon} \left(\frac{1}{1 + \epsilon \cos X} - \frac{\delta}{\sqrt{1-\epsilon^2}} \right) \tag{4-46}$$

At the points where Δ_{th} attains its maximum and minimum values, one has

$$\frac{d\Delta_{th}}{dX} = 0$$

which, from eq. (4-46), requires

$$\cos X = \frac{\sqrt{1-\epsilon^2} - \delta}{\epsilon \delta}$$

from which it will be seen readily that, of the two values of δ, only the positive is admissible in this case. Thus,

$$\cos X = \frac{\sqrt{1-\epsilon^2} - 1}{\epsilon} \tag{4-47}$$

and

$$X = \cos^{-1}\left(- \frac{1 - \sqrt{1-\epsilon^2}}{\epsilon} \right) \tag{4-48}$$

so that one gets

$$\frac{\epsilon + \cos X}{1 + \epsilon \cos X} = \frac{1 - \sqrt{1-\epsilon^2}}{\epsilon} \tag{4-49}$$

Using the above relationships in eq. (4-45), one obtains

$$\Delta_{th} = - \frac{u^2 A}{h\epsilon} \frac{\delta}{\sqrt{1-\epsilon^2}} \left[\cos^{-1}\left(\frac{1 - \sqrt{1-\epsilon^2}}{\epsilon} \right) - \cos^{-1}\left(- \frac{1 - \sqrt{1-\epsilon^2}}{\epsilon} \right) \right] \tag{4-50}$$

in which the maximum Δ_{th} corresponds to $\delta = -1$ and the minimum to $\delta = 1$.

One can write, then,

$$|\Delta_{th}| = |\Delta_{max} - \Delta_{min}|$$

or
$$|\Delta_{th}| = \frac{2u^2 A}{\bar{h}\epsilon\sqrt{1-\epsilon^2}} \left|\cos^{-1}(\theta) - \cos^{-1}(-\theta)\right| \tag{4-51}$$

where
$$\theta = \frac{1 - \sqrt{1-\epsilon^2}}{\epsilon}$$

and, by definition, $\frac{2A}{\bar{h}} = |Y|$

Thus,

$$|\Delta_{th}| = \frac{u^2|Y|}{\epsilon\sqrt{1-\epsilon^2}} \left|\cos^{-1}(\theta) - \cos^{-1}(-\theta)\right|$$

and, for neutral stability ($|\Delta_{th}| = |Y|$)

$$u = \left[\frac{\epsilon\sqrt{1-\epsilon^2}}{\left|\cos^{-1}(\theta) - \cos^{-1}(-\theta)\right|}\right]^{1/2} \tag{4-52}$$

It will be seen that, for small ϵ, i.e., small amplitudes of h_o,

$$\theta = \frac{\epsilon}{2}$$

so that eq. (4-52) gives

$$u = \left[\frac{\epsilon\sqrt{1-\epsilon^2}}{\left|\cos^{-1}\left(\frac{\epsilon}{2}\right) - \cos^{-1}\left(-\frac{\epsilon}{2}\right)\right|}\right]^{1/2}$$

and, as illustrated by fig. (37),

$$\cos^{-1}\left(\frac{\epsilon}{2}\right) - \cos^{-1}\left(-\frac{\epsilon}{2}\right) = -\epsilon, \text{ for small } \epsilon$$

$$\therefore u = (1-\epsilon^2)^{1/4} \tag{4-53}$$

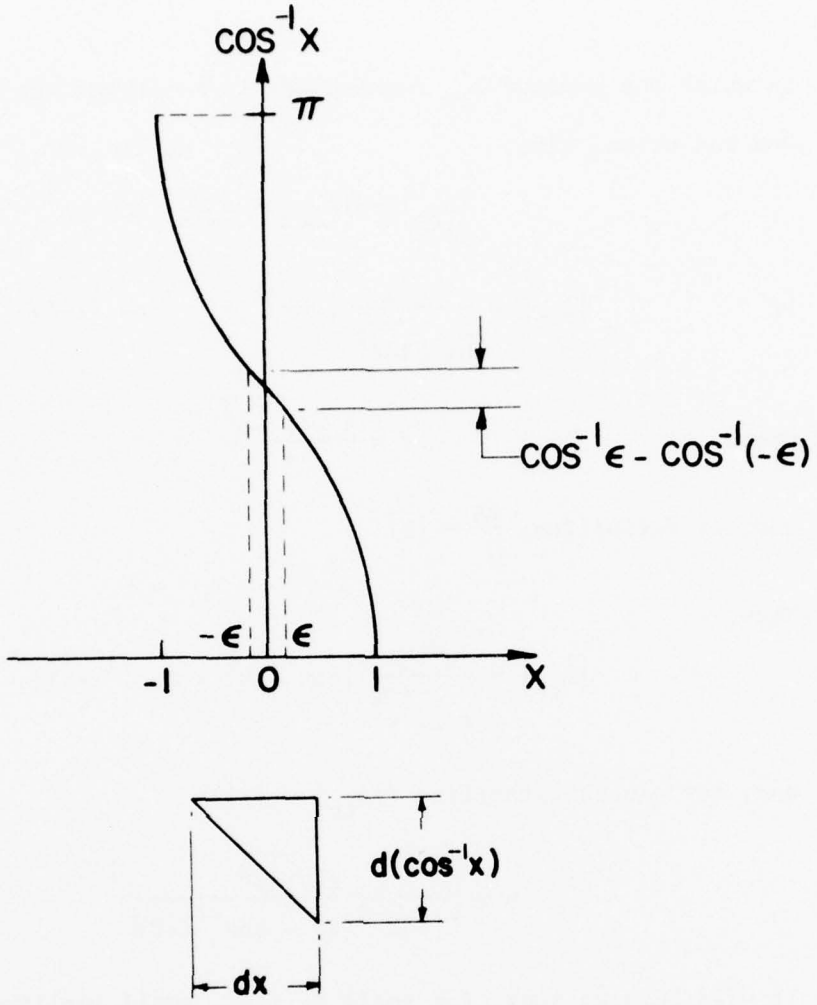

For small ϵ, $\frac{d}{dx}(\cos^{-1}x) = \frac{\cos^{-1}\epsilon - \cos^{-1}(-\epsilon)}{2\epsilon}$

or, $\cos^{-1}\epsilon - \cos^{-1}(-\epsilon) = -\frac{2\epsilon}{\sqrt{1-x^2}}\frac{dx}{dx}$

At $x = 0$, $\cos^{-1}\epsilon - \cos^{-1}(-\epsilon) = -2\epsilon$

Figure 37. Illustration of Trigonometric Relationship for Arc cos

It is clear from eq. (4-53) that

(i) $u = 1$ for a flat surface ($\epsilon = 0$)

and (ii) $u < 1$ for a wavy surface and larger values of ϵ give smaller values of u.

Returning now to the case where $\hat{H} \neq 0$, i.e., relative axial motion prevails between the two rigidly mounted faces, it will be seen that analytical integration of eq. (4-21) becomes very complicated. Furthermore, $\hat{H}$ can be evaluated only from the pressure distribution (see, for example, eq. (4-19)) and is best done numerically. Since the purpose, in this section, is to illustrate the nature of the dependence of u on $\hat{H}$, it will be appropriate and sufficient to simplify the analysis to include only very small values of ϵ.

Defining

$$Y = \frac{A}{h} \sin X$$

$$H = 1 + \epsilon \sin X$$

and using eq. (4-21), one notes that, for $\epsilon \ll 1$,

$$\frac{1}{H^2} = 1 - 2\epsilon \sin X$$

Equation (4-21) then becomes

$$\frac{1}{u^2} \frac{d^2 \Delta_{th}}{dX^2} = - \left(\frac{A}{h} \sin X + \hat{H} \right)(1 - 2\epsilon \sin X)$$

$$+ \frac{1}{2\pi} \int_0^{2\pi} \left(\frac{A}{h} \sin X + \hat{H} \right)(1 - 2\epsilon \sin X)\, dX$$

whence

$$\frac{1}{u^2}\frac{d\Delta_{th}}{dX} = \left(\frac{\bar{A}}{\bar{h}} - 2\epsilon\hat{H}\right)\cos X - \frac{\epsilon\bar{A}}{2\bar{h}}\sin 2X + C_1 \qquad (4\text{-}54)$$

and

$$\frac{1}{u^2}\Delta_{th} = \left(\frac{\bar{A}}{\bar{h}} - 2\epsilon\hat{H}\right)\sin X + \frac{\epsilon\bar{A}}{4\bar{h}}\cos 2X + C_1 X + C_2 \qquad (4\text{-}55)$$

Using the boundary conditions

$$X = 0 \quad : \quad \Delta_{th} = 0$$

$$X = 2\pi \quad : \quad \Delta_{th} = 0$$

one finds $C_2 = -\frac{\epsilon\bar{A}}{4\bar{h}}$

and $C_1 = 0$

At the points where Δ_{th} is maximum and minimum

$$\frac{d\Delta_{th}}{dX} = 0$$

so that eq. (4-54) gives

$$\left(\frac{\bar{A}}{\bar{h}} - 2\epsilon\hat{H}\right)\cos X - \frac{\epsilon\bar{A}}{\bar{h}}\sin X \cos X = 0$$

whence either $\cos X = 0$

or $\sin X = \frac{1}{\frac{\epsilon\bar{A}}{\bar{h}}}\left(\frac{\bar{A}}{\bar{h}} - 2\epsilon\hat{H}\right)$

The second condition is inadmissible because it yields $|\sin X| > 1$.

The first condition implies

$$X = \frac{\pi}{2} \quad , \quad \frac{3\pi}{2}$$

for which, using eq. (4-55), it is seen that

$$|\Delta_{th}| = \frac{2A}{\bar{h}} u^2 \left|1 - \frac{2\varepsilon\hat{\bar{H}}\bar{h}}{A}\right|$$

By definition,

$$|Y| = \frac{2A}{\bar{h}}$$

so that, for neutral stability and $\varepsilon \ll 1$,

$$u = \left(1 + \frac{2\varepsilon\hat{\bar{H}}\bar{h}}{A}\right)^{1/2} \tag{4-56}$$

Equation (4-56) shows clearly that u is always greater than unity when $\hat{H}$ is present. Furthermore, it has been numerically determined that $\hat{\bar{H}}\bar{h}/A$ gets larger as ε increases. It follows that larger values of ε will result in higher values of u.

CHAPTER V

PREDICTION OF INSTABILITY FROM GIVEN INITIAL CONDITIONS FOR THE INITIALLY WAVY SURFACE

5.1 Operating and Initial Conditions

It has been stated in section (4.1) that the surface waviness $h_o(x)$ is not the initial or machined profile, but rather the profile observed at any given moment of operation. Together with the face load f, the sliding speed U and the mean film-thickness $\bar{h}$, h_o describes a given operating condition, i.e., an assumed quasi-static state. The question asked and answered in the preceding chapter was whether this state was stable. The results represented by fig. (35) describe in effect, a series of neutrally stable operating conditions (though load has been ignored); they do not tell the designer how to avoid designing a seal that will operate in the unstable regime.

In order to be able to predict whether a given seal, as manufactured, will be stable in operation under a given load and at a given speed, the data of fig. (35) have to be "translated" so that they show the effect of the initial surface profile. It will be recalled that h_o represents the cumulative effects of thermal distortion on the initial waviness h_i. Thus, if one calculates the thermally produced component of $h_o(x)$ and subtracts it from $h_o(x)$, one will have the initial profile $h_i(x)$ which, together with the specified face load f and the operating speed U, will represent the initial conditions.

5.2 Determination of Initial Surface Profile, Load and Sliding Speed

In the assumed quasi-static state, the heat generation is given by eq. (4-5)

$$q_o = \frac{\mu U^2}{\bar{h} + h_o}$$

which corresponds to a thermally generated surface curvature

$$\frac{d^2\delta_{th}}{dx^2} = \frac{\alpha_M q_o}{K_M} - \frac{1}{\ell}\int_o^{\ell} \frac{\alpha_M q_o}{K_M}\, dx \tag{5-1}$$

Written in terms of non-dimensional quantities, eq. (5-1) becomes

$$\frac{d^2\Delta_{th}}{dX^2} = \frac{u^2}{H} - \frac{1}{2\pi}\int_o^{2\pi} \frac{u^2}{H}\, dX \tag{5-2}$$

and can be solved numerically as outlined in section (4.8), using the boundary conditions (4-33) and (4-34). Recalling that

$$H(X) = 1 + \frac{h_o(X)}{\bar{h}}$$

it is clear that

$$H_i(X) = H(X) - \Delta_{th}(X) - 1 \tag{5-3}$$

where $$H_i(X) = \frac{h_i(X)}{\bar{h}}$$

To determine the load f, it will be noted that

$$df = p_o(x)\cdot L\cdot dx$$

$$= p_o L \frac{dX}{\kappa}$$

Recalling eq. (4-22), one has

$$f = \frac{WL}{\bar{h}\kappa}\sqrt{\frac{\overline{\mu K_M}}{\alpha_M}}\int_o^{2\pi} P_o dX$$

whence

$$F = \int_o^{2\pi} P_o(X)dX \tag{5-4}$$

where the non-dimensional load is defined as

$$F = \left(\frac{\bar{h}\kappa}{WL}\sqrt{\frac{\overline{\alpha_M}}{\mu K_M}}\right) f \tag{5-5}$$

First, $P_o(X)$ is determined numerically from eq. (4-23). Then F is numerically calculated from eq. (5-4), the integration being carried out only over the non-cavitating regions of the fluid film. The dimensional load f is then obtained from eq. (5-5). The program is listed in Appendix F.

5.3 Results

In fig. (38) are shown graphs of u versus log F for different values of ϵ. Each point on each of the curves represents a possible operating condition. The threshold of instability is the locus of all operating conditions that are neutrally stable and is drawn from fig. (35). It is seen that while initially the non-dimensional critical speed increases with increasing ϵ and F, it decreases sharply beyond $\epsilon \approx 0.7$ and $\log F \approx 2.1$.

On fig. (35), one can now draw a number of constant load lines as shown in fig. (39). Using the computed values of H_i and figs. (38) and (39), a comprehensive map can be drawn (fig. 40) showing the effects of all the parameters and their relationship with the threshold of instability.

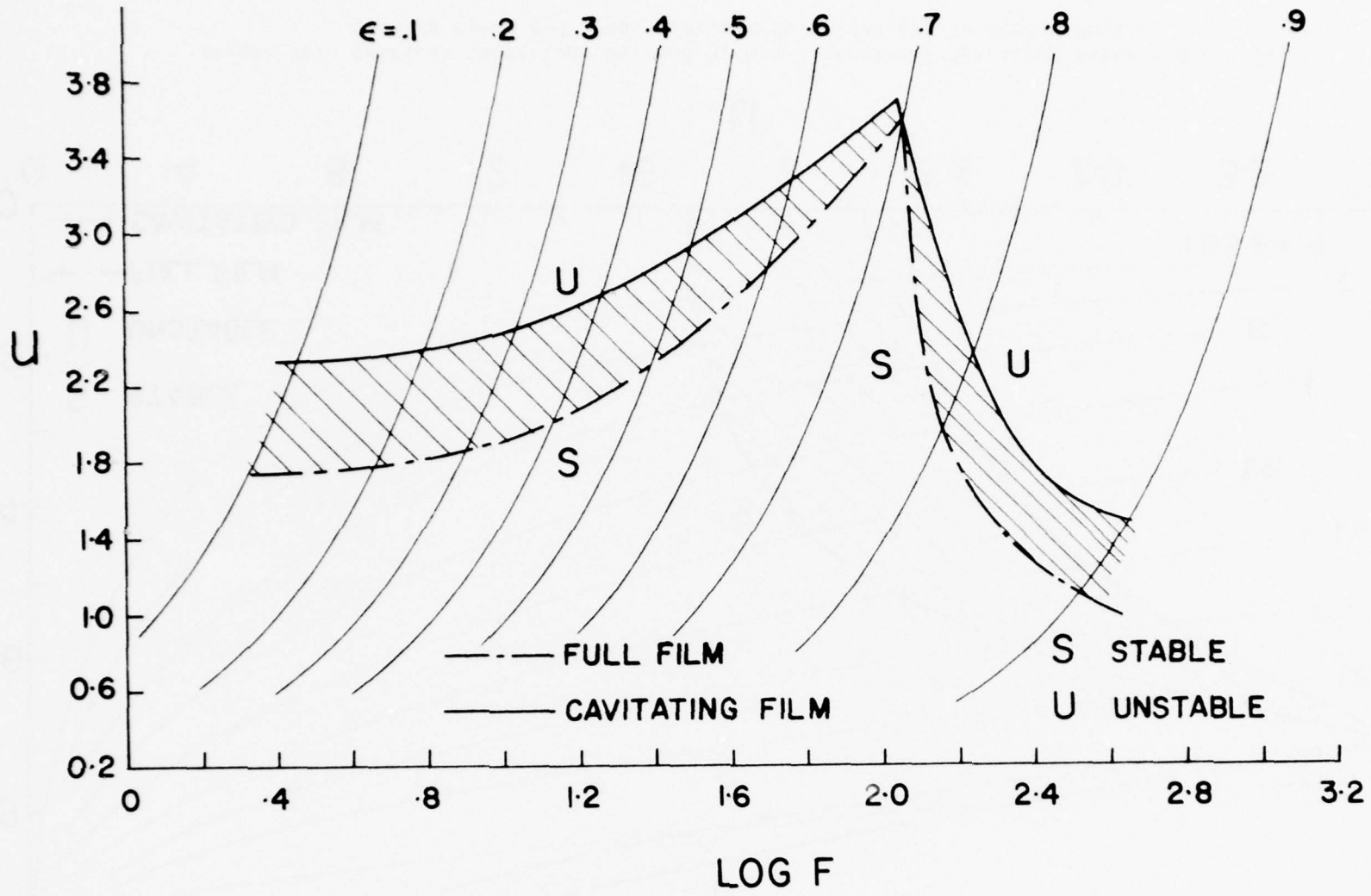

Figure 38. Non-Dimensional Critical Sliding Speeds for Non-Dimensional Loads. (Actual Solutions Lie in Shaded Regime)

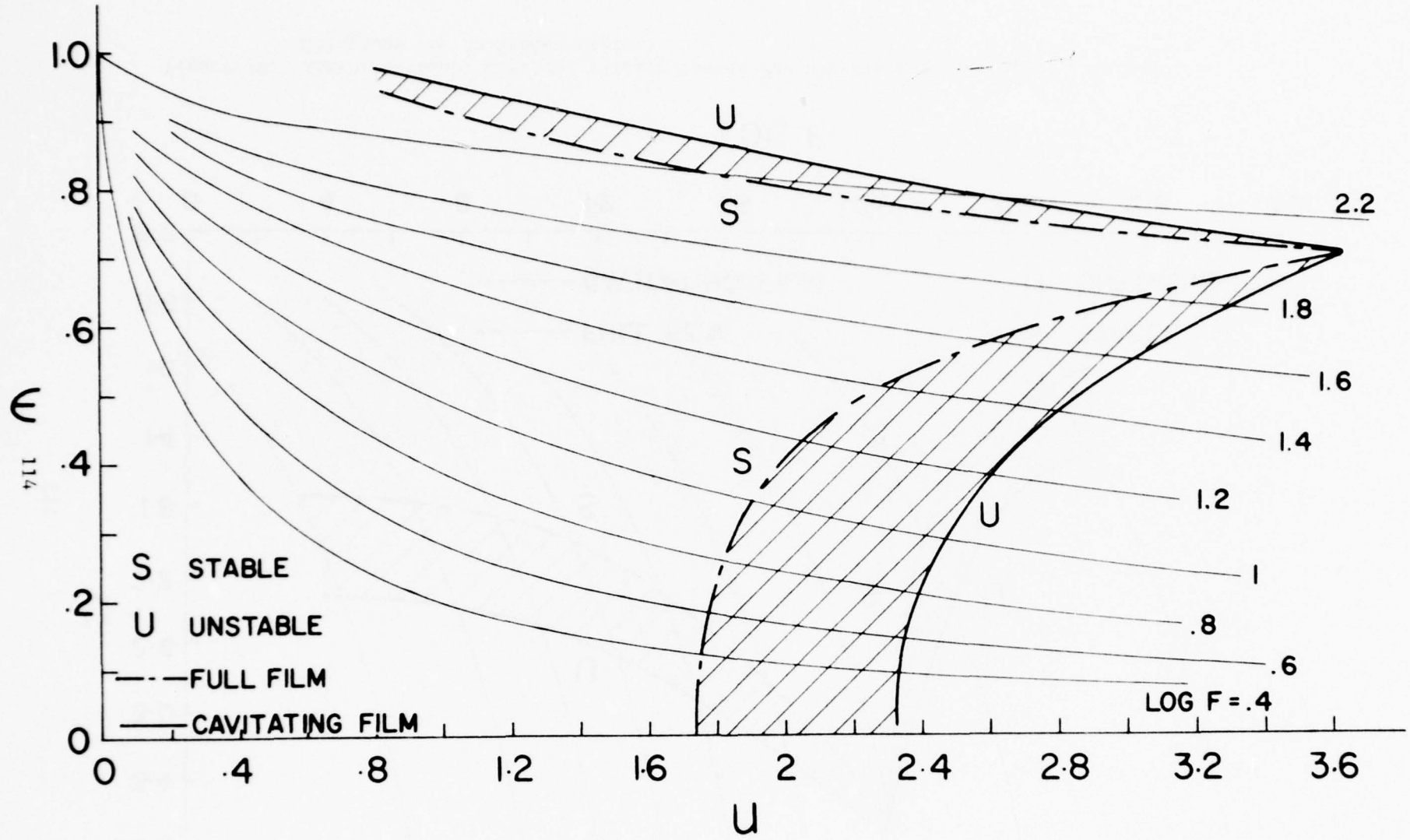

Figure 39. Critical Conditions Defined by Non-Dimensional Operating Surface Waviness, Sliding Speed and Load. (Actual Solutions Lie in Shaded Regime)

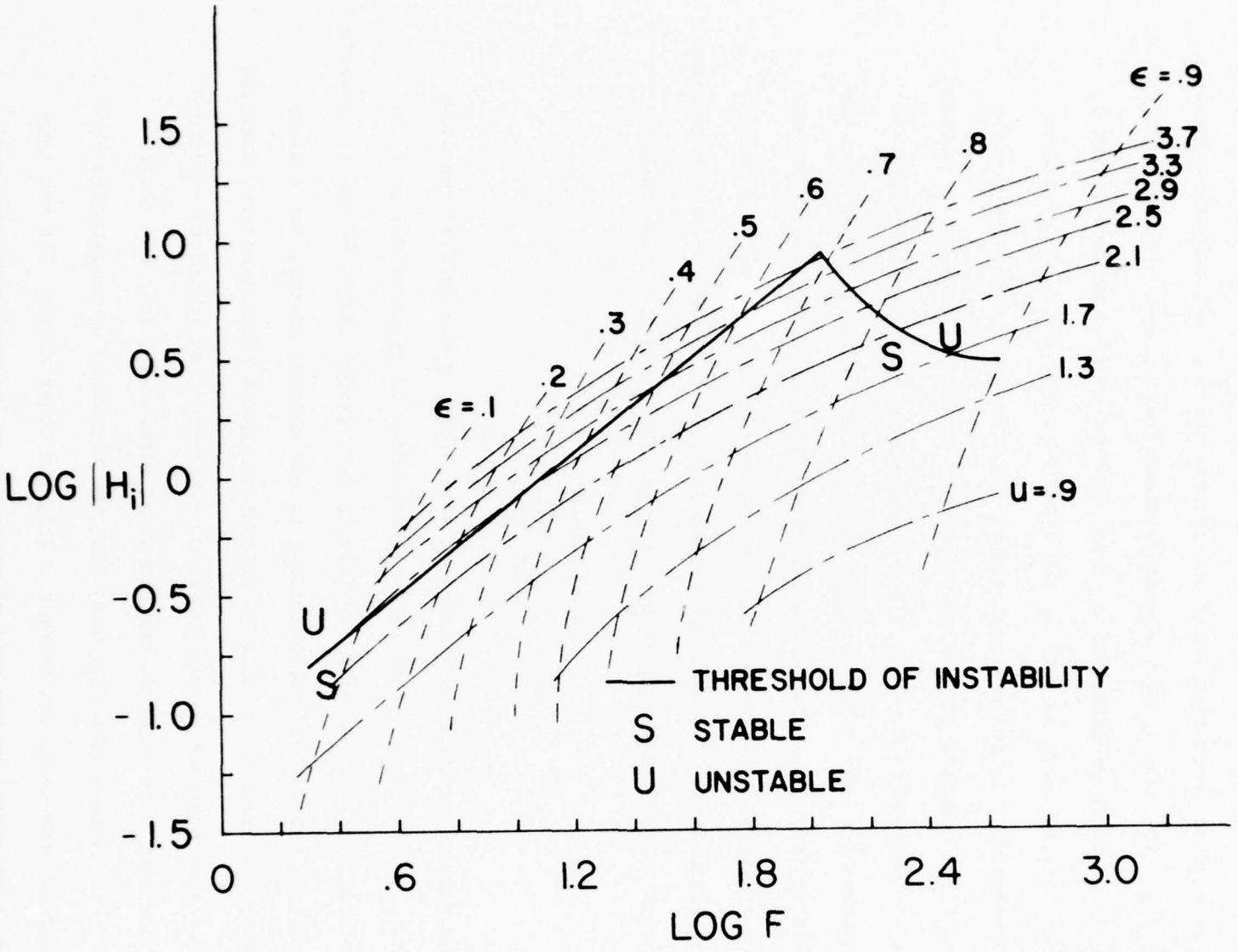

Figure 40. Chart Showing Operating Conditions and Threshold of Instability for Zero Heating in Cavitation Zones

Since the purpose is to define the critical threshold in terms of a given load, operating speed and initial surface waviness, the plots of fig. (40) have to be rendered in dimensional terms. It will then be possible to predict, for a given load and initial surface waviness, the critical speed as well as the film-thickness and surface waviness corresponding to the critical state. This has been done in two ways. The first consists of writing equations for the critical speed in terms of the parameters F, $|H_i|$, ϵ and then solving them simultaneously to eliminate $\bar{h}$. The other is a sequence of direct crossplotting from the data of fig. (40). In the latter approach, a value of $|h_i|$ is assumed and values of $\bar{h}$ are calculated for a number of points on the threshold of instability. For each of these points, $|h_o|$ is then readily determined, whence f and U can be found by using eq. (5-5) and the relationship

$$u = \frac{U}{\bar{h}\kappa \sqrt{\frac{\overline{K_M}}{\mu\alpha_M}}}$$

The results can then be plotted to show, for a given initial amplitude $|h_i|$, the critical values of U corresponding to given values of f, as in fig. (41). It is also possible to draw graphs (figs. 42 and 43) showing $\bar{h}$ and $|h_o|$ versus load corresponding to the neutral states, for a given $|h_i|$. In order to be able to predict the onset of instability, however, the first approach should be taken. The resulting empirical equations, of course, must generate the graphs of figs. (41), (42) and (43).

It is seen from fig. (40) that the threshold of instability consists of two legs, one below F $\approx$ 2.1, the other above. The two legs are represented by two sets of equations in terms of nondimensional

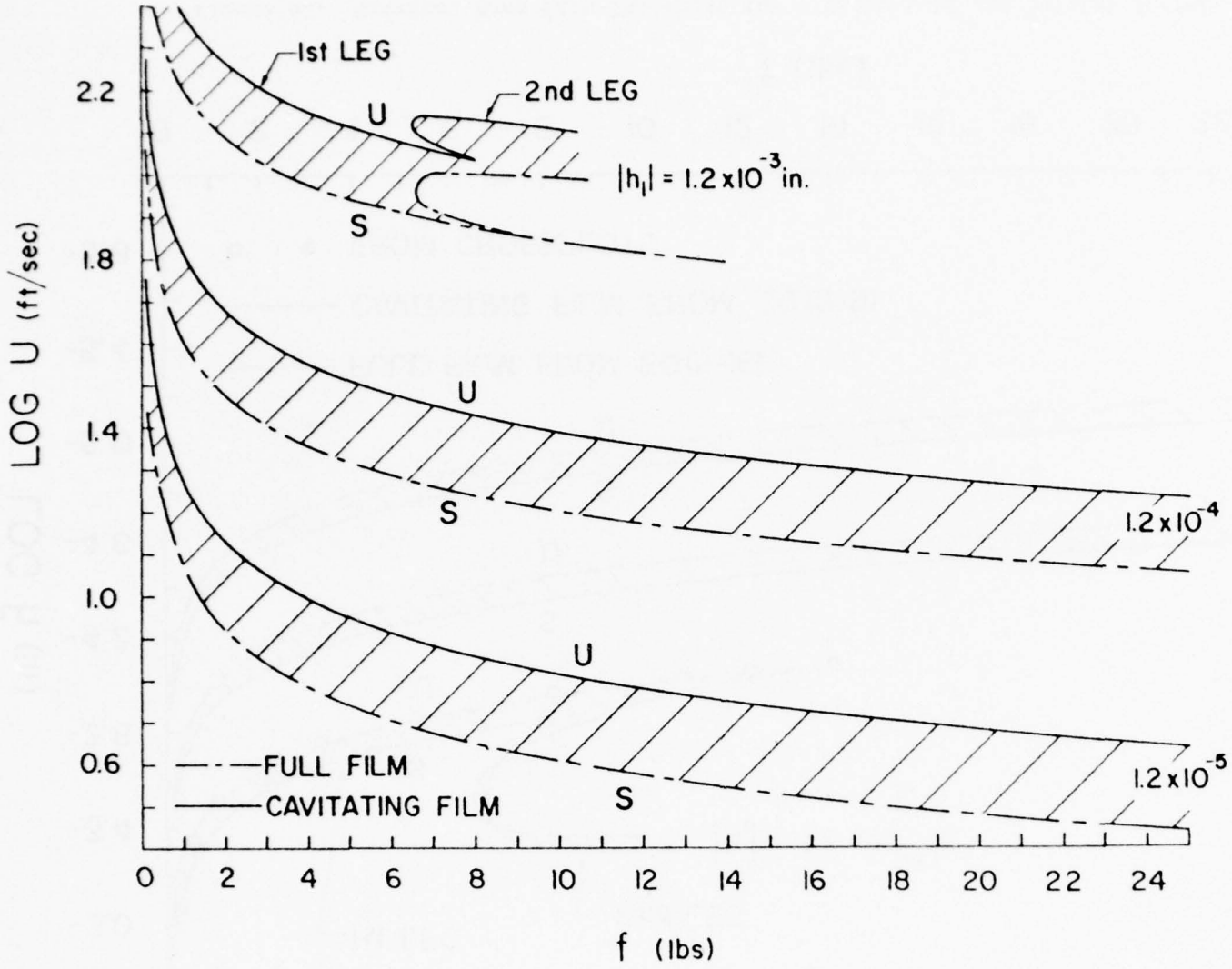

Figure 41. Critical Sliding Speed for a Given Load and Initial Surface Waviness

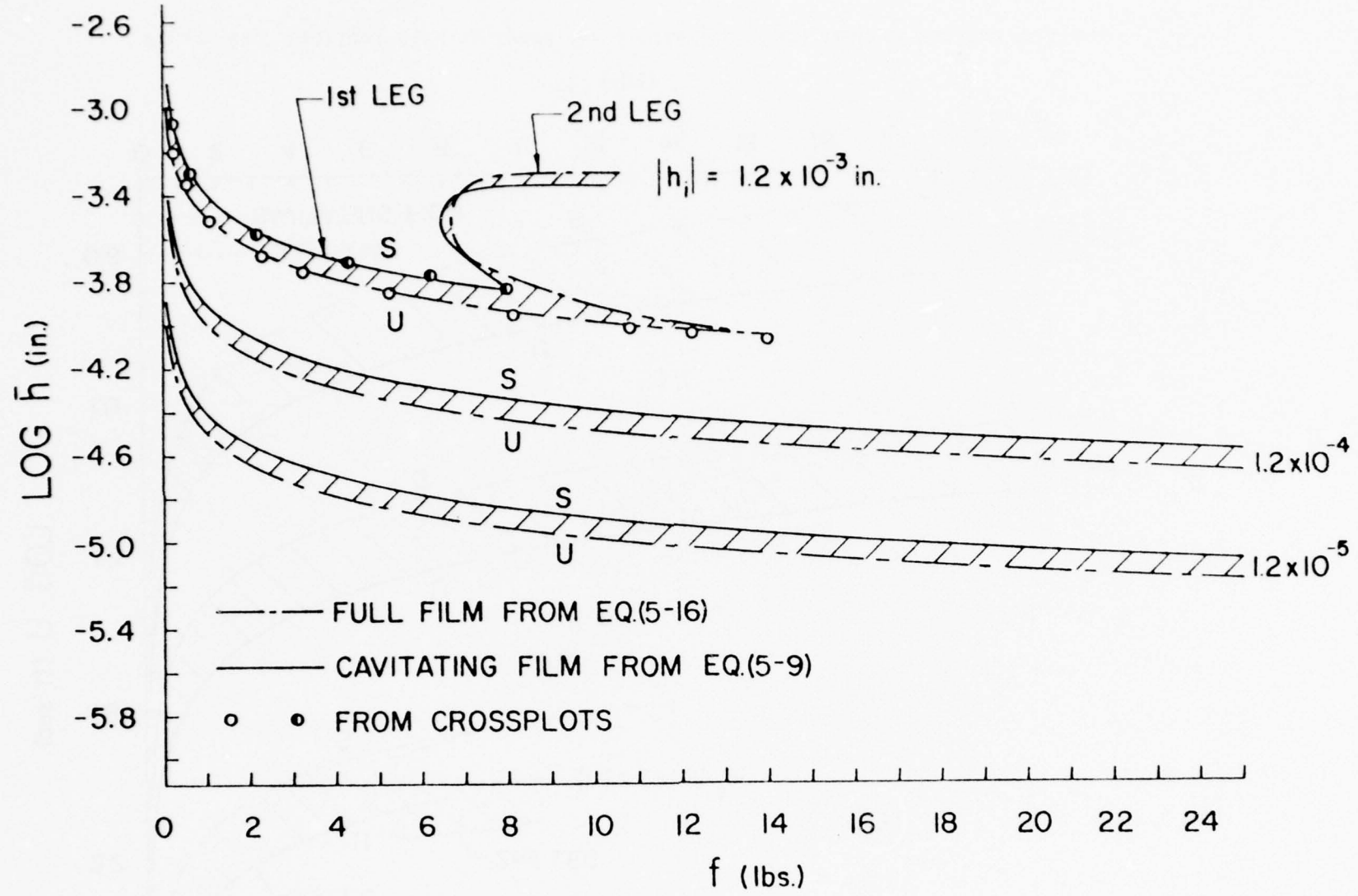

Figure 42. Critical Mean Film-Thickness for a Given Load and Initial Surface Waviness

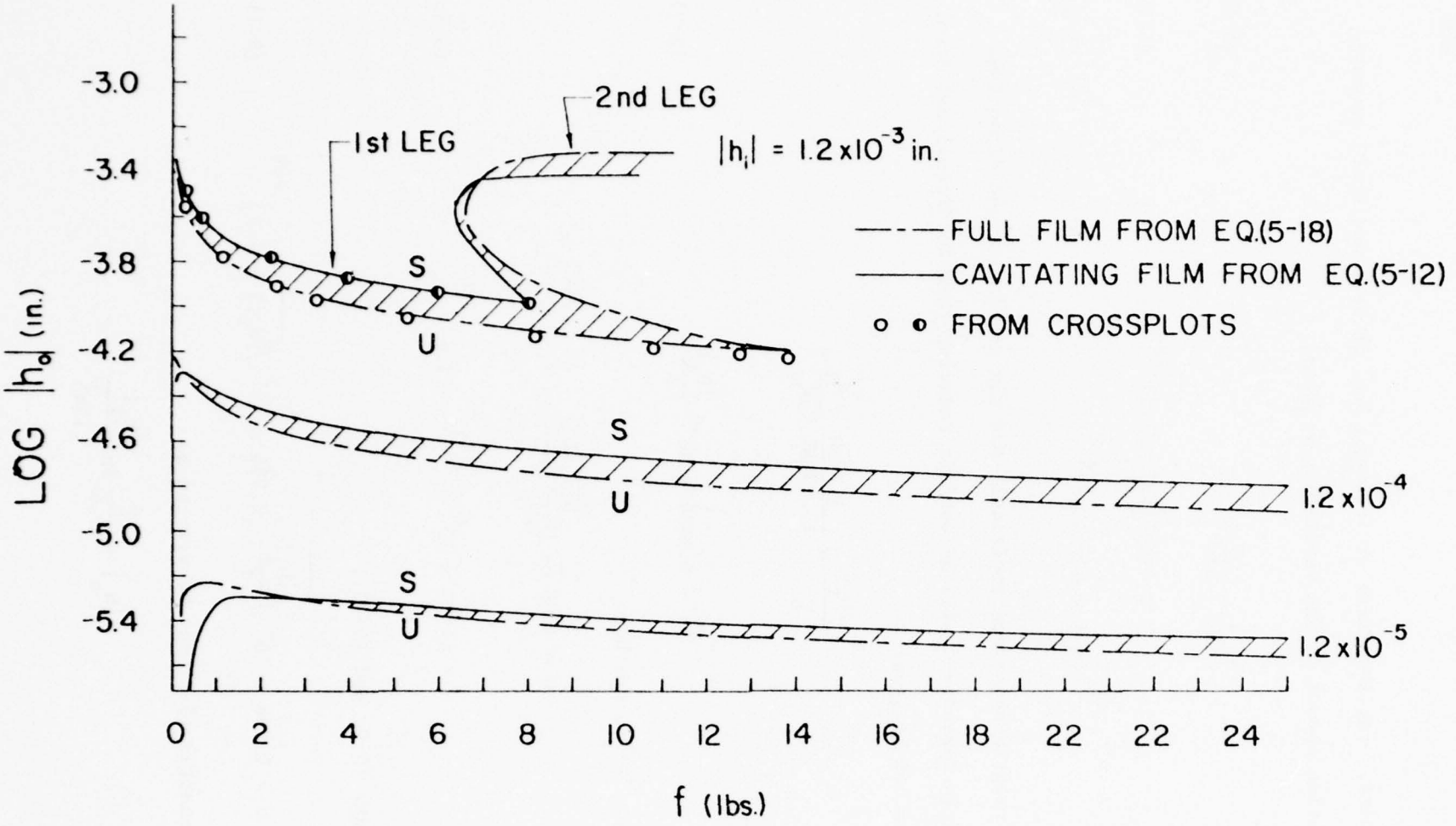

Figure 43. Critical Operating Surface Waviness for a Given Load and Initial Surface Waviness

variables. For the first or leftward leg, it is found that, assuming no heating occurs in the cavitating regions,

$$|H_i| = \frac{F}{13.33} \tag{5-6}$$

$$u = 1.96(|H_i| + 1.5)^{.286} \tag{5-7}$$

$$|H_i| = 0.158\, e^{5.6\epsilon} \tag{5-8}$$

These relationships are empirical, and the properties and dimensions listed in Appendix C will be used in reducing them to dimensional form. Equation (5-6) gives

$$\frac{|h_i|}{\bar{h}} = \frac{1}{13.33} \frac{\bar{h}\kappa}{WL} \sqrt{\frac{\overline{\alpha_M}}{\mu K_M}}\, f$$

whence,

$$\bar{h}^2 = 1.1454 \times 10^{-5} \frac{|h_i|}{f} \tag{5-9}$$

From Eq. (5-7), one has

$$U = 1.96\, \bar{h}\kappa \sqrt{\frac{\overline{K_M}}{\mu\alpha_M}} \left(\frac{|h_i|}{\bar{h}} + 1.5\right)^{.286}$$

or,

$$U = 4.691 \times 10^{6}\, \bar{h} \left(\frac{|h_i|}{\bar{h}} + 1.5\right)^{.286} \tag{5-10}$$

From eqs. (5-9) and (5-10),

$$U = 1.588 \times 10^{4} \sqrt{\frac{\overline{|h_i|}}{f}} \left(2.955 \times 10^{2} \sqrt{\overline{|h_i|} f} + 1.5\right)^{.286} \tag{5-11}$$

Equation (5-8) may be written as

$$|h_o| = \frac{\bar{h}}{5.6} \ln \frac{|h_i|}{.158\bar{h}}$$

and, substituting for $\bar{h}$ from eq. (5-9), one has

$$|h_o| = 6.0435 \times 10^{-4} \sqrt{\frac{|h_i|}{f}} \ln\left(1.87 \times 10^{3} \sqrt{|h_i| f}\right) \tag{5-12}$$

Thus, knowing $|h_i|$ and f and the dimensions and properties (such as those given in Appendix C) one can determine the mean film-thickness, the sliding speed and the amplitude of the surface waviness at the critical condition by using eqs. (5-9), (5-11) and (5-12).

For the case where heat generation is calculated on the basis of a full lubricating film (the pressure wave is still assumed to be comprised solely of positive values), the above approach leads to the following relationships (see figs. (38), (39), (44))

$$|H_i| = \frac{F}{8.51} \tag{5-13}$$

$$u = 1.246(|H_i| + 2.2)^{.378} \tag{5-14}$$

$$|H_i| = \frac{1}{8.9}\left(e^{6.75\varepsilon}\right) \tag{5-15}$$

Equation (5-13) gives

$$\bar{h}^2 = 8.51 \frac{WL}{\kappa} \sqrt{\frac{\mu K_M}{\alpha_M}} \frac{|h_i|}{f}$$

or, using the properties and dimensions of Appendix C,

$$\bar{h} = 2.7041 \times 10^{-3} \sqrt{\frac{|h_i|}{f}} \tag{5-16}$$

From eq. (5-14),

$$U = 1.246\, \bar{h}\kappa \sqrt{\frac{K_M}{\mu\alpha_M}} \left(\frac{|h_i|}{\bar{h}} + 2.2\right)^{.378}$$

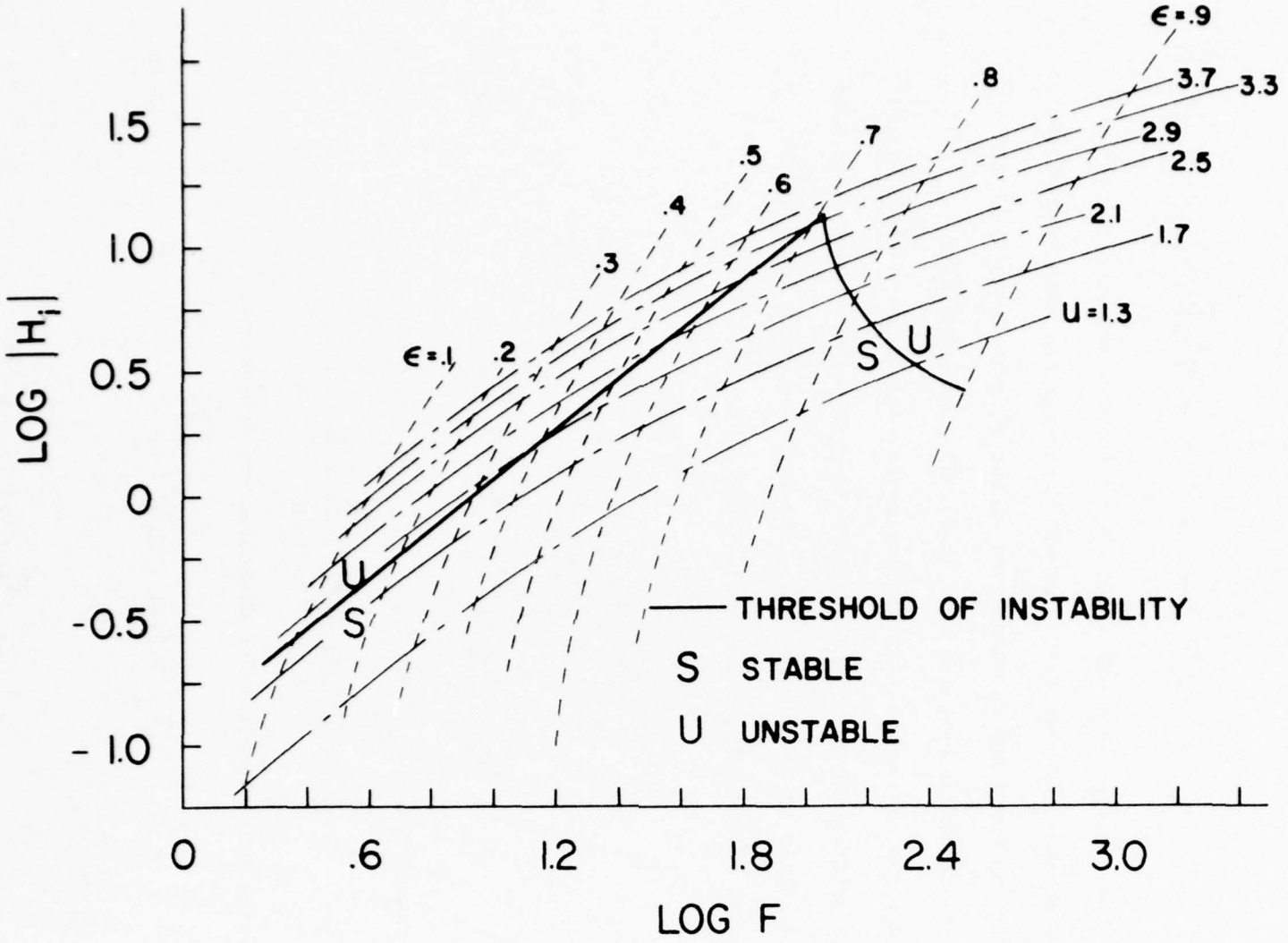

Figure 44. Chart Showing Operating Conditions and Threshold of Instability with Heating Based on Full Continuous Film

or, $$U = 2.982 \times 10^{6} \bar{h} \left[\frac{|h_i|}{\bar{h}} + 2.2 \right]^{.378}$$

whence, using eq. (5-16), one obtains

$$U = 8.0636 \times 10^{3} \sqrt{\frac{|h_i|}{f}} \left[3.698 \times 10^{2} \sqrt{|h_i| f} + 2.2 \right]^{.378} \qquad (5\text{-}17)$$

Finally, using eqs. (5-15) and (5-16), it is found that

$$|h_o| = 4.006 \times 10^{-4} \sqrt{\frac{|h_i|}{f}} \ell n \left[3.291 \times 10^{3} \sqrt{|h_i| f} \right] \qquad (5\text{-}18)$$

Figures (42), (43), (45) shows comparisons between the above relationships and corresponding curves obtained through direct cross-plotting.

Obtaining similar equations for the second leg of the threshold (fig. 40) proves to be a little more difficult. When heating is assumed to be zero in the cavitating portions of the film, it is found that, for all practical purposes, the sliding speed U, the mean film thickness $\bar{h}$ and the operating surface wave amplitude $|h_o|$ are independent of load for all loads greater than that at which the two legs of the threshold meet. For this reason, and also because of the complicated equations that are obtained for the second leg, these equations are not being presented. They are neither informative, nor useable. However, figs. (41), (42), (43) show the second leg as obtained by direct cross-plotting.

5.4 Remarks

The results presented in this chapter apply to "floating" but non-flexible mountings, i.e., the mean film-thickness can vary but

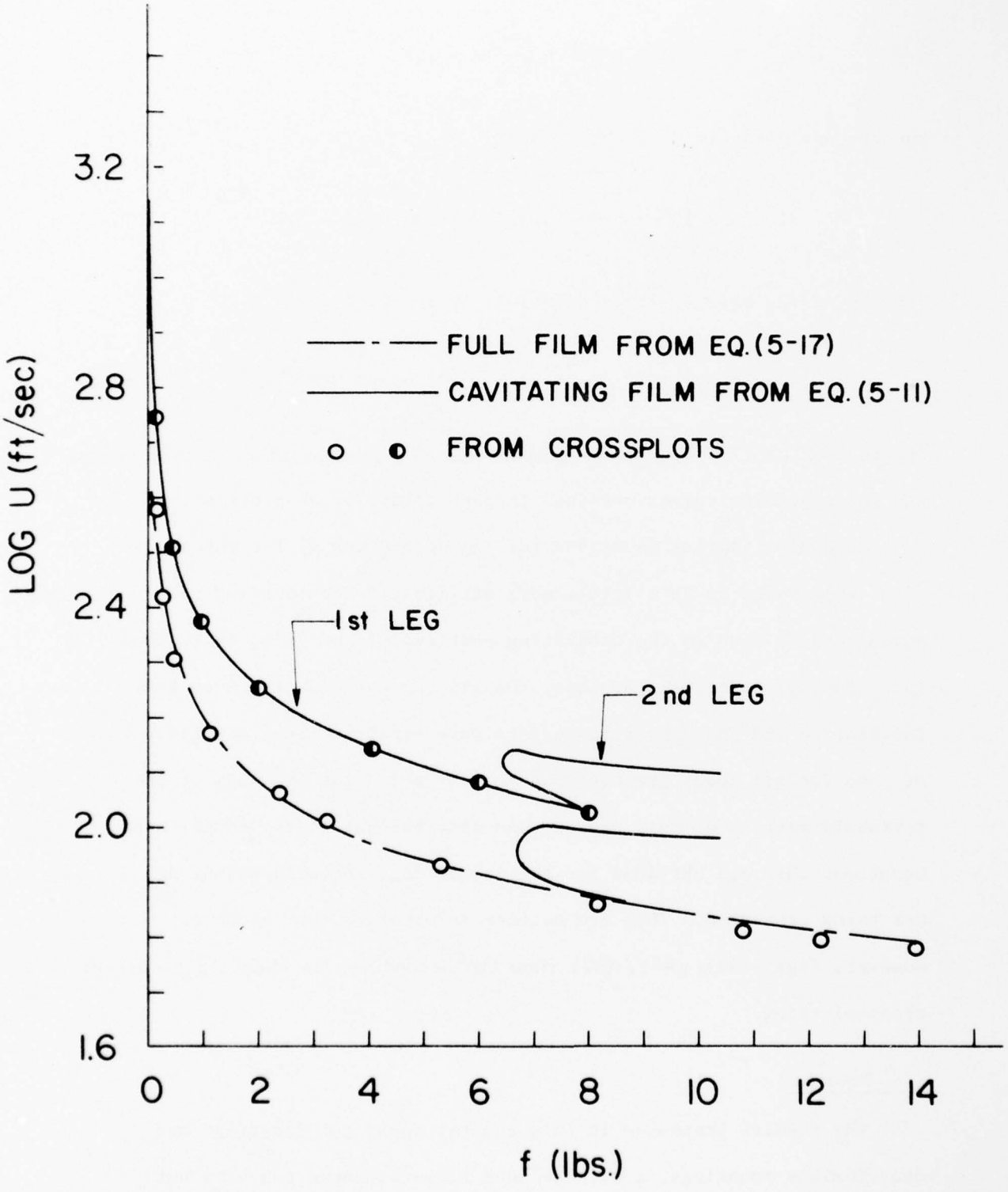

Figure 45. Comparison Between Calculated Critical Speeds and Corresponding Empirical Equations

neither face can tilt. Other operating parameters being identical, a flexibly mounted face must necessarily have at least a two-lobed profile and the critical sliding speeds will then be double those represented by fig. (41).

One might expect, intuitively, that the critical speeds will be greater for the case when full-film heating is assumed than for the case of zero heating in the cavitating regions, because the disparities in heating are more abrupt in the latter case than in the former, as illustrated in fig. (46). However, figs. (39) and (41) belie such expectations. The explanation is not apparent. At any rate, as has been stated earlier, the true solutions lie in between the two cases, in the shaded regimes shown in the figures.

Finally, it should be noted that, in obtaining the present results, a number of "operating conditions" were selected. While such operating conditions doubtlessly represent mathematically admissible quasi-static solutions, it cannot be said yet whether they do occur in practice, i.e., whether a given "initial condition" can evolve into its corresponding neutrally stable "operating condition". The following chapter seeks to answer that question.

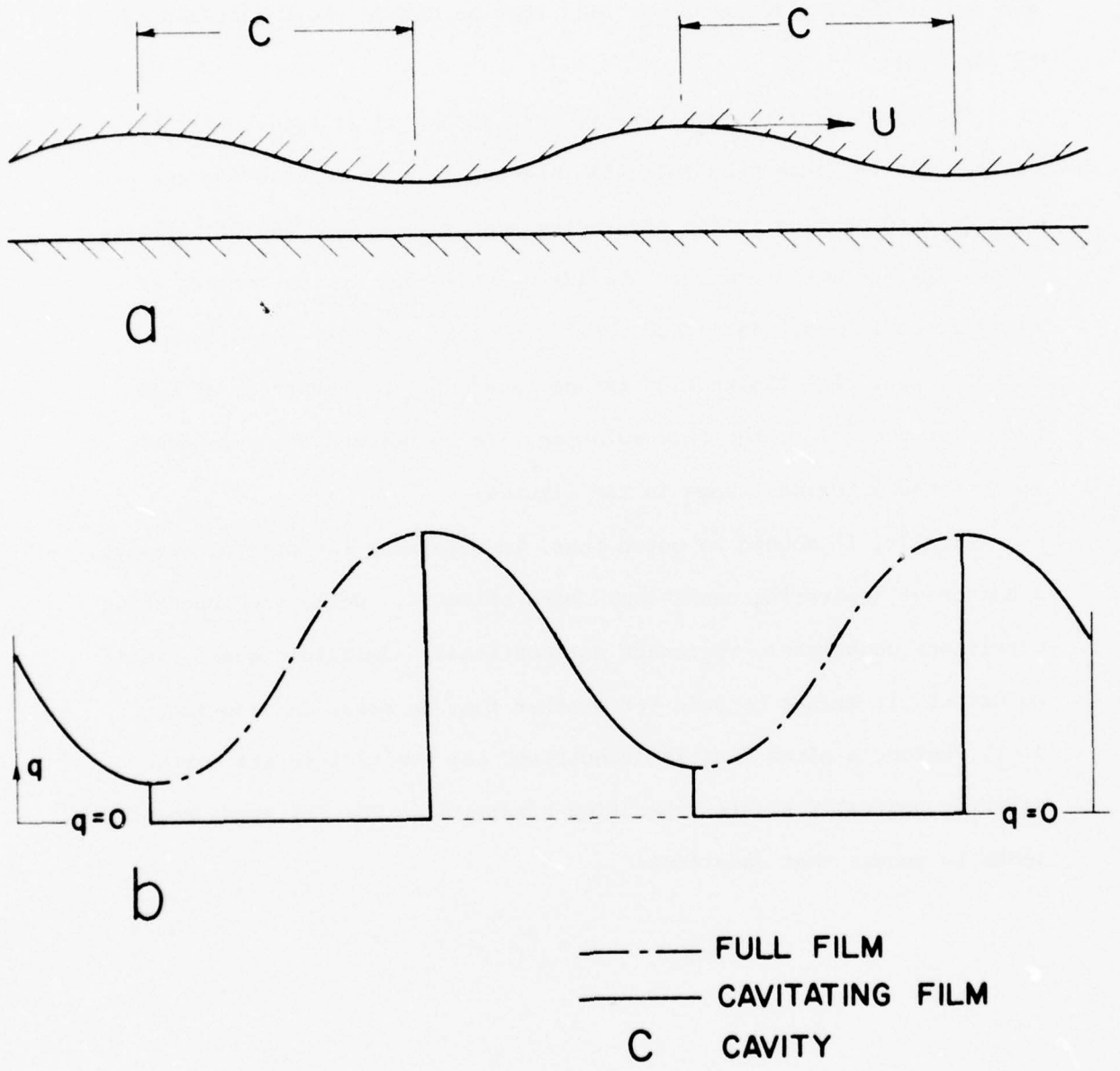

Figure 46. Heat Generation Based on Full Film and Cavitating Film

CHAPTER VI

EVOLUTION OF OPERATING CONDITIONS FROM GIVEN INITIAL CONDITIONS

In the last chapter, it has been shown that, for a given initial waviness and load, a neutrally stable operating condition can be defined in terms of sliding speed, mean film-thickness and surface waviness. To determine whether such an operating condition can actually be attained in practice, one needs to follow the growth of the thermal deformation as speed is increased from rest. This involves the integration of eq. (4-8) which, written in terms of the zero-order quantities, is

$$\frac{d^2v}{dx^2} = \frac{\alpha_M q_o}{K_M} - C \tag{6-1}$$

where v denotes the thermal deformation. Using eq. (4-5) and the normalizing procedure of section (4.7), eq. (6-1) can be written as

$$\frac{d^2V}{dX^2} = \frac{u^2}{H} - C \tag{6-2}$$

where $$C = \frac{1}{2\pi} \int_o^{2\pi} \frac{u^2}{H} \, dX$$

If one knows H and u, one can, presumably, determine V from eq. (6-2). However, this equation is difficult to integrate when H is the independent variable. This difficulty can be circumvented by choosing V as the independent variable and then asking what the corresponding H must be.

Let $$V = V_o \cos X$$

Then $$\frac{d^2V}{dX^2} = - V_o \cos X$$

so that eq. (6-2) can be written as

$$C - V_o \cos X = \frac{u^2}{H}$$

whence, $$H = \frac{u^2}{C}\left(\frac{1}{1 - \frac{V_o}{C}\cos X}\right) \qquad (6\text{-}3)$$

Now, by definition (see fig. 27),

$$\bar{h} \equiv \frac{1}{\ell}\int_o^{\ell} h \, dx$$

or, in non-dimensional terms (fig. 32),

$$1 = \frac{1}{2\pi}\int_o^{2\pi} H \, dX \qquad (6\text{-}4)$$

Substitution of H from eq. (6-3) into eq. (6-4) gives

$$1 = \frac{u^2}{2\pi C}\int_o^{2\pi} \frac{dX}{1 - \frac{V_o}{C}\cos X}$$

and, following integration

$$1 = \frac{u^2}{C\sqrt{1 - \left(\frac{V_o}{C}\right)^2}}$$

whence $$C = \left(u^4 + V_o^2\right)^{1/2} \qquad (6\text{-}5)$$

From eq. (6-3), it is seen that

$$\frac{dH}{dX} = - \frac{u^2 V_o \sin X}{\left(C - V_o \cos X\right)^2} \tag{6-6}$$

The amplitude ϵ of the surface wave will be the difference between the maximum and minimum values of H, for which

$$\frac{dH}{dX} = 0$$

Equation (6-6) then shows that, for H to have its maximum and minimum values,

$$\sin X = 0$$

which implies $\cos X = \pm 1$

Then, in keeping with the definition of ϵ (see fig. 32),

$$\epsilon = \frac{1}{2} \left| H_{max} - H_{min} \right|$$

$$= \frac{1}{2} \left| \frac{u^2}{C - V_o} - \frac{u^2}{C + V_o} \right|$$

or

$$\epsilon = \left| \frac{V_o u^2}{C^2 - V_o^2} \right|$$

whence, using eq. (6-5), it follows that

$$\epsilon \approx \frac{V_o}{u^2} \tag{6-7}$$

Rewriting eq. (5-3),

$$H_i = H - V - 1$$

or,

$$H_i = \frac{u^2}{C - V_o \cos X} - V_o \cos X - 1 \tag{6-8}$$

from which

$$\frac{dH_i}{dX} = - \frac{u^2 V_o \sin X}{\left(C - V_o \cos X\right)^2} + V_o \sin X \qquad (6\text{-}9)$$

If $$\frac{dH_i}{dX} = 0$$

equation (6-9) gives either

$$\sin X = 0 \qquad (6\text{-}10)$$

or $$u = \pm (C - V_o \cos X) \qquad (6\text{-}11)$$

From eq. (6-11), it follows that

$$|H_i| = 2u$$

which cannot be correct because it calls for an unique u for a given $|H_i|$. Equation (6-10) implies that

$$|H_i| = \frac{1}{2} \left| \frac{u^2}{C - V_o} - 1 - V_o - \frac{u^2}{C + V_o} + 1 - V_o \right|$$

which reduces to

$$|H_i| = \left| \frac{u^2}{C^2 - V_o^2} - 1 \right| V_o$$

and, upon substituting for C from eq. (6-5),

$$|H_i| = \left| \frac{1 - u^2}{u^2} \right| V_o$$

or, $$V_o = |H_i| \left| \frac{u^2}{1 - u^2} \right|$$

In the last equation, $|H_i|$ is, by definition, the amplitude of the initial waviness of the surface. The second modulus symbol, however,

was introduced to get around the question of which of the two values of H_i, corresponding to zero slope (eq. (6-10)), was the maximum and which the minimum. This modulus symbol should be dropped now to allow V_o to have positive and negative values, which imply opposite phases. Thus

$$V_o = \frac{u^2}{1 - u^2} |H_i| \tag{6-12}$$

or,

$$|H_i| = \frac{1 - u^2}{u^2} V_o \tag{6-13}$$

which shows that H_i and V will be in or out of phase accordingly as u is less than or greater than unity.

Combining eqs. (6-7) and (6-12), one obtains

$$\epsilon = \frac{|H_i|}{1 - u^2} \tag{6-14}$$

which shows how ϵ will evolve with changing u, for a given $|H_i|$. Equation (6-14) also shows that if u is equal to unity, i.e., the sliding speed is the critical defined by eq. (2-84), ϵ will be infinite for finite initial waviness. For $u < 1$, ϵ will be positive. For $u > 1$, ϵ will be negative. This means that, as u increases, the surface waviness ϵ increases while remaining in phase with $H_i(X)$, until u becomes unity. For $u > 1$, $H_o(X)$ suddenly goes out of phase with $H_i(X)$ and then ϵ gets smaller as u gets larger. If ϵ does, indeed, become infinite when u reaches unity, it might mean that the two surfaces will touch and the analyses of Chapter IV will break down. However, such a conclusion cannot be drawn from eq. (6-14) because all the variables in it are normalized with respect to $\bar{h}$, and the behavior of a face seal in

practice will depend upon changes in $\bar{h}$. To determine whether or not the system can actually attain unit u, and how it behaves if it does, eq. (6-14) will have to be rendered in terms of dimensional variables. Then Reynold's equation will have to be employed to determine pressure variations and consequent variations in the mean film-thickness.

Written in terms of dimensional quantities, eq. (6-14) becomes

$$|h_o| = \frac{|h_i|}{1 - \frac{U^2 \mu \alpha_M}{\bar{h}^2 \kappa^2 K_M}} \tag{6-15}$$

where it should be remembered that the modulus symbol represents an amplitude but does not preclude a sign, positive or negative.

As shown in section (5.2), the load f is given by

$$df = p_o L \, dx$$

which, integrated over the full-film domain, becomes (fig. 47)

$$f = \int_{x_1}^{x_1 + \frac{\lambda}{2}} p_o L \, dx$$

where λ is the wavelength. Then, recalling p_o from eq. (4-14), one has

$$f = -\frac{\mu U L^3}{2} \int_{x_1}^{x_1 + \frac{\lambda}{2}} \frac{1}{(\bar{h} + h_o)^3} \frac{d(\bar{h} + h_o)}{dx} \, dx$$

If there is only one wave around the seal circumference, one can write (see fig. 47)

$$f = -\frac{\mu U L^3}{2} \int_{\bar{h} + |h_o|}^{\bar{h} - |h_o|} \frac{d(\bar{h} + h_o)}{(\bar{h} + h_o)^3}$$

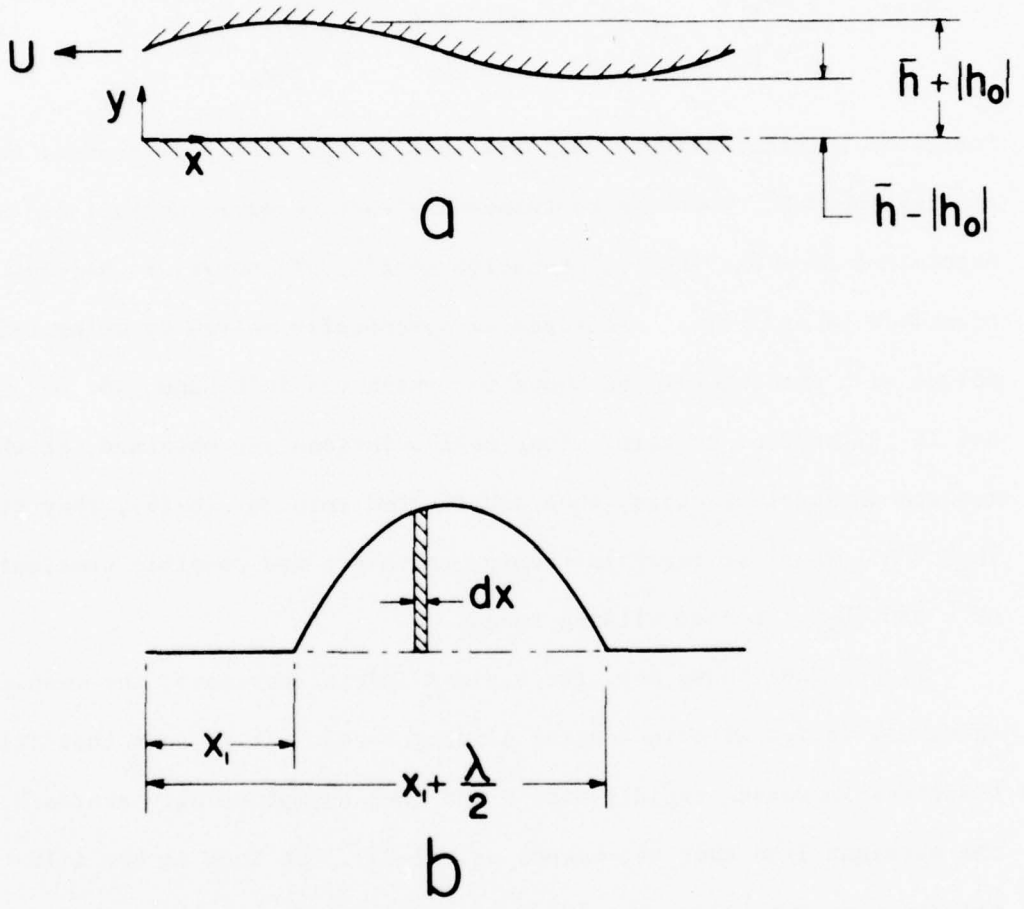

Figure 47. Definition Sketch for Calculation of Load

a) Operating Surface Profile
b) Corresponding Pressure Wave

which reduces to

$$\frac{\bar{h}^2 - |h_o|^2}{\bar{h}|h_o|} = \frac{\mu U L^3}{f} \tag{6-16}$$

Equations (6-15) and (6-16) can be combined to give, after some rearranging,

$$\left[\bar{h}^2\left(1 - \frac{U^2\mu\alpha_M}{\bar{h}^2\kappa^2 K_M}\right)^2 - |h_i|^2\right]^2 - \frac{\mu U L^3}{f}\bar{h}\left(1 - \frac{U^2\mu\alpha_M}{\bar{h}^2\kappa^2 K_M}\right)^3 |h_i| = 0 \tag{6-17}$$

For given initial waviness $|h_i|$ and load f, eq. (6-17) gives $\bar{h}$ at any sliding speed U. Then the corresponding surface waviness $|h_o|$ can be determined from eq. (6-16). Equation (6-17), of course, is hardly tractable by analytical means and is numerically solved by using trial values of $\bar{h}$ and determining those for which the left hand side of eq. (6-17) reduces to zero. Four real solutions are obtained, of which two are untenable because, when substituted into eq. (6-16), they give $|h_o| > \bar{h}$. Thus, at least in theory, there are two possible combinations of $\bar{h}$ and $|h_o|$ for most sliding speeds.

Figure (48) shows how, for a given initial waviness, the mean film-thickness varies with increasing sliding speed. It is seen that film-thickness increases rapidly with U and then asymptotically approaches the straight line that represents eq. (2-84). So long as the film-thickness evolves along the lower curve, the system will not attain a neutrally stable state described in Chapter V. However, since the lower curve hugs the straight line, instability, if and when it occurs, must always fall on the line representing family IV in fig. (15). This might explain the closeness between the predictions of Chapter II and experimental results, as shown in fig. (23).

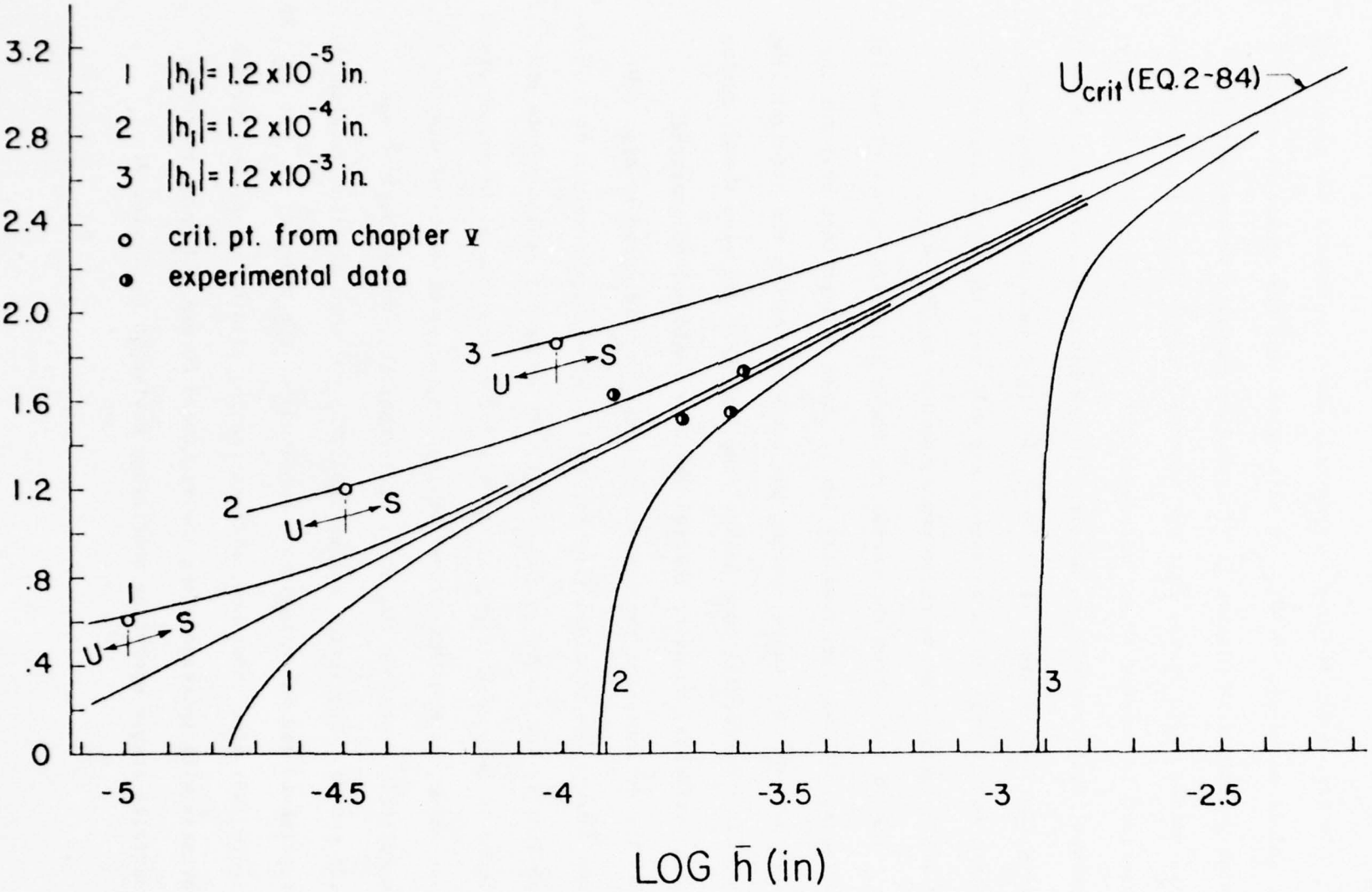

Figure 48. Evolution of Mean Film-Thickness with Increasing Sliding Speed (f = 10 lbs.)

In fig. (48), the upper asymptotic curve represents the second set of solutions to eq. (6-17). On this curve lies the neutrally stable point described in Chapter V. Instability prevails to the left of this point. This proves that the neutrally stable operating conditions described in Chapter IV are mathematically obtainable. It is unlikely, however, that they will be attained in practice. The system will evolve along the lower curve. If "jolted", it might jump over to the upper curve, but it will still be stable and will pass through a succession of states very close to those represented by eq. (2-84).

Figure (48) shows the curves for three different values of initial waviness, but the same load (10 lbs.). Load is important only for the early part of each curve, before the curve approaches the straight line. The four experimental data points from fig. (23) are also shown; during the experiments, however, initial waviness could not be measured.

The evolution of the surface waviness $|h_o|$ is shown in fig. (49). These curves are obtained from eq. (6-15) by using the values of $\bar{h}$ corresponding to the curves of fig. (48). The neutrally stable points predicted in Chapter V (figs. 41 and 43) for a face load of 10 pounds are also shown, as are the points obtained in the experiments of Chapter III, immediately preceding the onset of instability, where the load was 6.25 pounds. The latter suggest that the polished aluminum face in the experiments had an initial wave amplitude of the order of 10^{-4} to 10^{-5} in. Figure (49) also shows how, with increasing sliding speed, the surface waviness will increase along the rightward curves and never reach the neutrally stable operating conditions envisaged in Chapter V.

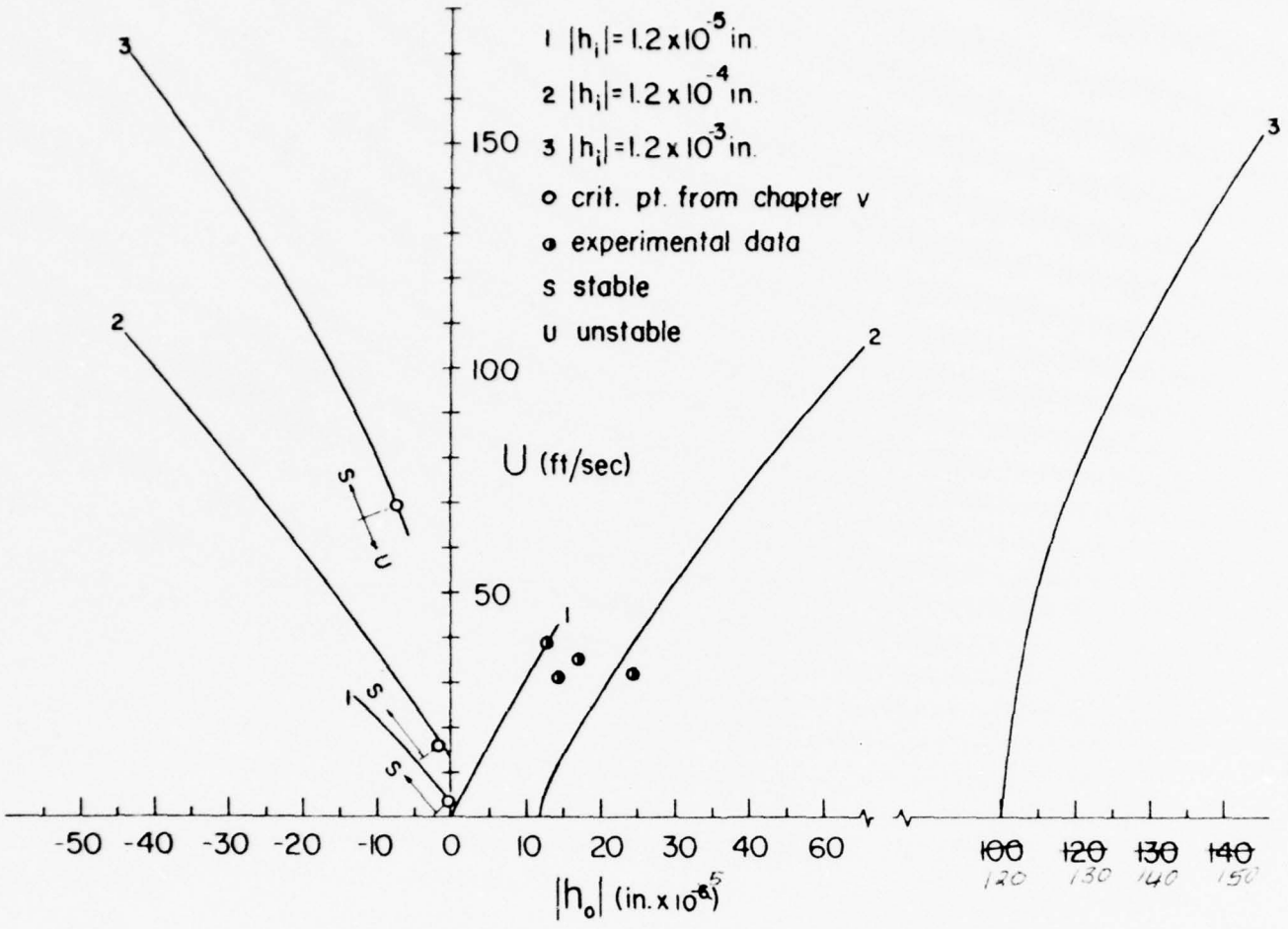

Figure 49. Evolution of Operating Surface Waviness with Increasing Sliding Speed (f = 10 lbs. Positive and Negative Signs Signify Opposite Phases)

The experimental points in fig. (49) lend added credibility to the analysis. The metal face was held by hand and polished on a wheel. The inferred magnitudes of the initial waviness seem very realistic.

CHAPTER VII

CONCLUSIONS

When a thermally conducting body slides on a thermal insulator, thermoelastic instability is found to occur under certain conditions. Small disturbances on the conducting surface grow and the surface undergoes macroscopic deformation.

If both surfaces are perfectly flat and separated by a film of viscous liquid, the regime of instability is determined by the mean film-thickness and the width of the sliding interface. When the width is large enough for cross-flow to be neglected, the instability will not occur at any sliding speed of practical interest. The sliding speed at which neutral stability prevails is called the critical and is given by

$$U_{crit} = \bar{h}\kappa \sqrt{\frac{\overline{K_M}}{\mu\alpha_M}}$$

The instability occurs for only a range of $\bar{h}$, and at sliding speeds greater than U_{crit}.

Experiments conducted with a polished aluminum face sliding on a polished, flexibly mounted, glass surface, where the surfaces can move apart from each other, show that the aluminum face develops a large waviness which grows very dramatically at a certain sliding speed. This speed is found to be very close to U_{crit}. The sudden, dramatic, growth of the surface undulation into spikes or asperities is interpreted as the occurrence of thermoelastic instability. These spikes break through

the lubricant film and rub directly against the glass. On slowing down from the unstable state, the metal face is seen to regain its original profile.

If the conducting face is wavy at the very outset, theoretical considerations show that thermoelastic instability, defined as the growth of a small disturbance, can occur only at sliding speeds considerably higher than U_{crit}. The initial surface profile changes with sliding speed and grows continuously through successive operating conditions. If both faces are rigidly mounted, a larger operating waviness corresponds to a lower critical speed. If the faces can move normal to each other, the growth of the surface waviness causes such motion and a larger operating waviness gives a higher critical speed. The critical speed in this case depends on the face load, the face width, and the amplitude of the initial waviness. Viscous heating is calculated with the film considered full throughout and also with the film assumed to be non-existent in the cavitating regions. The general thermoelastic behavior is seen to be the same in the two cases, the difference being in the magnitudes of the critical sliding speed.

An analysis of the continuous thermal distortion of the conducting face shows that, as sliding speed increases, the amplitude of the face profile also increases. The mean film-thickness increases too, and the sliding speed is then found to be very close to U_{crit}, but never greater. The surface waviness and mean film-thickness thus grow with the sliding speed and asymptotically with the threshold defined by U_{crit}. For the given initial waviness and load, the neutrally stable operating conditions mentioned in the preceding paragraph lie across this threshold

and are never attained in practice, although they are mathematically admissible quasi-static solutions. This means that if and when instability does occur, it occurs at a sliding speed very close to U_{crit}. As to the precise mechanism that triggers the instability, several possibilities exist. These possibilities are not discussed because, without supportive analyses, they are speculative in the main, and such analyses have not been conducted.

The last statement notes one of a few questions that have been raised but not answered. It is worthy of note, however, that the different facets of the present work are mutually supportive. The flat surface and initially wavy surface analyses and the experimantal data fit together very well to form a comprehensive picture.

APPENDIX A

THE VALIDITY OF A PARABOLIC TEMPERATURE DISTRIBUTION

In section (2.6), it is stated that the temperature profile in the oil film is approximated by a polynomial of the second degree. It is worthwhile to assess the departure of this approximation from the correct temperature distribution.

The energy equation for an incompressible flow in a thin film is as written in eq. (2-26) where T is the temperature perturbation. In writing eq. (2-26) account was taken of the fact that, for a narrow-face seal of the kind studied here and for a small perturbation,

$$\frac{\partial^2 T}{\partial y^2} \gg \frac{\partial^2 T}{\partial x^2} \quad , \quad \frac{\partial^2 T}{\partial z^2}$$

$$u = u_2 + u_1$$

where

$$u_1 \ll u_2$$

$$\frac{\partial p}{\partial x} \ll \frac{\partial p}{\partial z}$$

$$u_1 \ll w$$

$$\left(\frac{\partial w}{\partial y}\right)^2 \sim O(2) \text{ in the perturbation} \quad ,$$

where u_2 refers to the Couette component and u_1 to the pressure-generated component of the composite flow. It should be noted in particular that, for the narrow-lip configuration and a small perturbation, the contribution of u_1 (i.e., $\frac{\partial p}{\partial x}$) to the frictional heating term is so small that

it can be discarded from the energy equation. Equation (2-26) may be rewritten in differential form:

$$\rho C \left\{ \frac{\partial T}{\partial t} + u_2 \frac{\partial T}{\partial x} \right\} - K_{oil} \frac{\partial^2 T}{\partial y^2} = \frac{\mu U^2}{\bar{h}^2} \left(2 \frac{h'}{\bar{h}} \right) \qquad \text{(A-1)}$$

Recognizing that in this problem

$$\frac{\partial T}{\partial t} = - c \frac{\partial T}{\partial x}$$

this term in eq. (A-1) will be small whenever $\frac{c}{U}$ is small. Then eq. (A-1) may be rewritten

$$\rho C u_2 \frac{\partial T}{\partial x} - K_{oil} \frac{\partial^2 T}{\partial y^2} = \frac{2\mu U^2}{\bar{h}^2} \left(\frac{h'}{\bar{h}} \right) \qquad \text{(A-2)}$$

In most lubrication studies, the convection term on the left hand side is left out because it is usually very small compared to the conduction term. In that case the temperature profile will be precisely a second-degree polynomial, as assumed.

If convection is non-zero but still small relative to conduction, and one wishes to allow for it, one may write

$$T = \hat{T} + T'$$

where $\hat{T}$ is the parabolic temperature profile that corresponds precisely to the case of zero convection and T' is a correction on it to account for the small convection. The energy equation (A-2) may then be written as

$$\frac{\rho C U}{\bar{h}} y \frac{\partial}{\partial x} (\hat{T} + T') - K_{oil} \frac{\partial^2}{\partial y^2} (\hat{T} + T') = \frac{2\mu U^2}{\bar{h}^2} \left(\frac{h'}{\bar{h}} \right) \qquad \text{(A-3)}$$

where, by definition,

$$- K_{oil} \frac{\partial^2 \hat{T}}{\partial y^2} = \frac{2\mu U^2}{\bar{h}^2} \left(\frac{h'}{\bar{h}}\right) \tag{A-4}$$

Equation (A-3), written in the integral form, becomes

$$\frac{\rho C U}{\bar{h}} \int_{y_1}^{y_2} y \left(\frac{\partial \hat{T}}{\partial x} + \frac{\partial T'}{\partial x}\right) dy - K_{oil} \int_{y_1}^{y_2} \frac{\partial^2}{\partial y^2} (\hat{T} + T') = q_g \tag{A-5}$$

or,
$$\frac{\rho C U}{\bar{h}} \int_{y_1}^{y_2} y \left(\frac{\partial \hat{T}}{\partial x} + \frac{\partial T'}{\partial x}\right) dy - K_{oil} \left[\frac{\partial T}{\partial y}\right]_{y_1}^{y_2} = q_g$$

Since

$$\frac{\partial T'}{\partial x} \ll \frac{\partial \hat{T}}{\partial x}$$

and, as long as convection is much smaller than conduction,

$$\frac{\rho C U}{\bar{h}} \int_{y_1}^{y_2} y \frac{\partial T'}{\partial x} dy \ll - K_{oil} \left[\frac{\partial T'}{\partial y}\right]_{y_1}^{y_2}$$

Then, using the boundary condition given by eq. (2-23), one can write

$$\frac{\rho C U}{\bar{h}} \int_{y_1}^{y_2} y \frac{\partial \hat{T}}{\partial x} dy - q_g = K_{oil} \left.\frac{\partial T}{\partial y}\right|_{y=y_2} \tag{A-6}$$

It should be noted that in eq. (A-6) q_g is independent of the temperature distribution; so also is $\left.\frac{\partial T}{\partial y}\right|_{y=y_2}$, which is provided by an independent boundary condition (eq. 2-22). Thus the only term dependent on the temperature profile is the convection term and, according to eq. (A-6), the parabolic profile of $\hat{T}$ provides the appropriate evaluation of convection when $T' \ll \hat{T}$. Stated differently, given q_g, a parabolic temperature distribution in eq. (A-6) will provide the correct temperature gradient at the conducting surface.

The above analysis cannot be extended directly to the case where convection is comparable to conduction. In that case, the correct temperature profile will contain terms in the third and higher powers of y. One may still replace the correct profile with a parabolic one that meets the same boundary conditions and also satisfies eq. (2-26). The sacrifice in the shape of the temperature profile will induce a small error in the magnitude of the temperature and, in the integrated energy equation, $\left.\frac{\partial T}{\partial y}\right|_{y=y_2}$ and q_g will remain unchanged while the convection term, integrated across the film, will undergo a small change. One set of calculations with sizable convection indicated that the error induced by the parabolic approximation is less than 30% of T'.

An order of magnitude analysis shows that, for the range of family IV in fig. (15), the ratio of convection to conduction is of the order of 10^{-6} for $\bar{h} = 1.20 \times 10^{-5}$ in. and 10^{-1} for $\bar{h} = 3.4 \times 10^{-4}$ in. At the right hand extremity of this range, convection becomes important, as evidenced by eqs. (2-72), (2-73). From the foregoing arguments it would appear that for almost the entire range of the solution represented by family IV, which is the threshold of principal interest, the parabolic approximation is quite appropriate.

Georgopoulos [34] has rigorously solved the energy equation and shown that convection has little effect on the temperature at the metal surface.

APPENDIX B

EDGE DISPLACEMENT OF A SEMI-INFINITE PLATE UNDER NORMAL STRESS

Let the x-coordinate lie along the edge of a semi-infinite plate with the y-coordinate lying in the plane of the plate and pointing into it. Suppose, also, that a normal pressure p, defined as a general harmonic function, acts on this edge and that

$$\sigma_y\Big|_{y=0} = -\,p = A \sin \kappa x + B \cos \kappa x$$

The stress-function φ must satisfy the equation

$$\frac{\partial^4 \varphi}{\partial x^4} + 2\,\frac{\partial^4 \varphi}{\partial x^2 \partial y^2} + \frac{\partial^4 \varphi}{\partial y^4} = 0 \tag{B-1}$$

and the boundary conditions

$$\sigma_y\Big|_{y=0} = \frac{\partial^2 \varphi}{\partial x^2}\Big|_{y=0} = A \sin \kappa x + B \cos \kappa x \tag{B-2}$$

$$\varphi \to 0 \quad \text{as} \quad y \to \infty \tag{B-3}$$

$$\tau_{xy}\Big|_{y=0} = -\,\frac{\partial^2 \varphi}{\partial x\, \partial y}\Big|_{y=0} = 0 \tag{B-4}$$

The last two boundary conditions assure that σ_y vanishes at $y \to \infty$ and that the only stress at y=0 is the normal stress $\sigma_y\Big|_{y=0}$.

As a trial solution to eq. (B-1), let

$$\varphi = F(y)\left[C \sin \kappa x + D \cos \kappa x\right]$$

which, when substituted in eq. (B-1), gives

$$\left[\kappa^4 F(y) - 2\kappa^2 \frac{\partial^2 F(y)}{\partial y^2} + \frac{\partial^4 F(y)}{\partial y^4}\right] (C \sin \kappa x + D \cos \kappa x) = 0$$

whence, for the non-trivial solution,

$$\kappa^4 F(y) - 2\kappa^2 \frac{\partial^2 F(y)}{\partial y^2} + \frac{\partial^4 F(y)}{\partial y^4} = 0$$

The solution for F(y) is then

$$F(y) = \left(Pe^{-\kappa y} + Qye^{-\kappa y} + Me^{\kappa y} + Nye^{\kappa y} \right)$$

so that, now,

$$\varphi = \left(Pe^{-\kappa y} + Qye^{-\kappa y} + Me^{\kappa y} + Nye^{\kappa y} \right) (C \sin \kappa x + D \cos \kappa x)$$

Evidently, in order that boundary condition (B-3) may be satisfied,

$$M = N = 0$$

Thus,

$$\varphi = e^{-\kappa y}(P + Qy)(C \sin \kappa x + D \cos \kappa x)$$

$$\tau_{xy} = -\frac{\partial^2 \varphi}{\partial x \, \partial y}$$

$$= \kappa(C \cos \kappa x - D \sin \kappa x)\left[-\kappa e^{-\kappa y}(P + Qy) + Qe^{-\kappa y} \right]$$

In order to satisfy boundary condition (B-4),

$$\kappa(C \cos \kappa x - D \sin \kappa x)(-\kappa P + Q) = 0$$

$\therefore$ either $C \cos \kappa x - D \sin \kappa x = 0$

or $Q - \kappa P = 0$

If the first condition is true, boundary condition (B-2) will be satisfied only in the special case of

$$A \sin \kappa x = -B \cos \kappa x$$

and not in all cases. This suggests that

$$C \cos \kappa x - D \sin \kappa x \neq 0$$

but that

$$Q - \kappa P = 0$$

or,

$$Q = \kappa P$$

Then

$$\varphi = e^{-\kappa y}(1 + \kappa y)(PC \sin \kappa x + PD \cos \kappa x)$$

or,

$$\sigma_y = \frac{\partial^2 \varphi}{\partial x^2} = - e^{-\kappa y}(1 + \kappa y)\kappa^2 (PC \sin \kappa x + PD \cos \kappa x)$$

$$\sigma_y\Big|_{y=0} = - \kappa^2 (PC \sin \kappa x + PD \cos \kappa x)$$

Boundary condition (B-2) then requires

$$-(PC)\kappa^2 = A$$

$$-(PD)\kappa^2 = B$$

Then φ becomes:

$$\varphi = - e^{-\kappa y}(1 + \kappa y) \frac{1}{\kappa^2} (A \sin \kappa x + B \cos \kappa x)$$

It follows that

$$\sigma_x = \frac{\partial^2 \varphi}{\partial y^2} = e^{-\kappa y}(1 - \kappa y)(A \sin \kappa x + B \cos \kappa x)$$

$$\sigma_y = \frac{\partial^2 \varphi}{\partial x^2} = e^{-\kappa y}(1 + \kappa y)(A \sin \kappa x + B \cos \kappa x)$$

The deflection at the edge of the plate is then given by

$$\frac{\partial \delta}{\partial y} = \frac{1}{E}\left(\sigma_y - \nu \sigma_x\right)$$

or,

$$\delta = \frac{1}{E}\left[\int_{\infty}^{o}\left(\sigma_y - \nu\,\sigma_x\right) dy\right]$$

$$= -\frac{1}{E}\left[e^{-\kappa y}\left(y + \frac{2}{\kappa} + \nu y\right)\right]_{\infty}^{o} (A \sin \kappa x + B \cos \kappa x)$$

$$= -\frac{2}{\kappa E} (A \sin \kappa x + B \cos \kappa x)$$

or

$$\delta = -\frac{2}{\kappa E} (-p)$$

or,

$$\delta = \frac{2p}{E\kappa} \qquad \text{(B-5)}$$

APPENDIX C

PHYSICAL PROPERTIES AND PARAMETERS

The following dimensions and material properties have been used everywhere, except in Chapter II.

Metal face: aluminum, 3 in. diameter

.066 in. width

$K_M = 28.743$ in-lbs/sec-in-^oF

$k_M = 0.133$ in^2/sec

$E = 1 \times 10^7$ lb/in^2

$\alpha_M = 1.24 \times 10^{-5}$ $^oF^{-1}$

Oil: SAE 10 at 150^{o}F, $\mu = 1.8 \times 10^{-7}$ lb-sec/in^2

$k_{oil} = 1.01 \times 10^{-4}$ in^2/sec

$K_{oil} = 0.016$ in-lbs/sec-in-^oF

Parameters: $W = 1.613 \times 10^{-4}$

$f = 6.25$ lbs

$\kappa = 0.67$ in^{-1} for one complete wave

$\kappa = 1.33$ in^{-1} for two complete waves

In Chapter II, the diameter is 2 in. and

$\kappa = 1$ in^{-1}

APPENDIX D

PROGRAM FOR DETERMINING CRITICAL OPERATING CONDITIONS
FOR THE INITIALLY WAVY SURFACE

```
C         THIS PROGRAM ALLOWS FOR UNIFORM CHANGES IN HBAR
C         HHAT IS THE NONDIMENSIONAL SMALL CHANGE IN HBAR
C         HHATDIM IS THE DIMENSIONAL SMALL CHANGE IN HBAR
C
C
      DIMENSION X(51), HO(51),Y(51),PP(51),P1(51),HT(51)
      DIMENSION H(51), A(51,51), B(51,1), XS(51,1), G(51,51), IR(51)
      DIMENSION PF(51),PL(51),P2(51),BB1(51),XI(51),BB(51,1),XX(51,1)
      DIMENSION YY(51),B0(51,1),XL(51,1)
      HHAT1=0.0
      HBAR=1.0E-05
      DX=2.0*3.141592654/50.0
      DO 13 I=1,51
      DO 13 J=1,51
   13 A(I,J)=0.0
      DO 16 I=2,50
      A(I,I)=-2.0
      A(I,I+1)=1.0
      A(I,I-1)=1.0
   16 CONTINUE
      A(1,1)=1.0
      A(51,51)=-1.0
      A(51,1)=1.0
      DO 01 I=1,51
      XI(I)=+DX*(I-1)
      X(I)=+DX*(I-1)
   01 CONTINUE
C
C         U IS THE SLIDING SPEED, NONDIMENSIONALIZED WITH RESPECT TO
C       THE THEORETICAL CRITICAL SPEED FOR INITIALLY FLAT SURFACES
C
      U=1.0
      IND=1
      YO=HBAR*0.01
      YPR=(YO/100.0)/HBAR
 5555 CONTINUE
C
C         HO(I) IS THE NON-DIMENSIONAL SURFACE PROFILE, H(I) THE FILM-
C       THICKNESS AND Y(I) A SMALL PERTURBATION ON HO(I)
C
      DO 02 I=1,51
      HO(I)=-YO*SIN(X(I))
      H(I)=(HO(I)+HBAR)/HBAR
   02 CONTINUE
      DO 04 I=1,51
      Y(I)=-YPR*SIN(X(I))
      HT(I)=Y(I)
   04 CONTINUE
```

```
      NUM=1
 6666 CONTINUE
      PRINT 111,NUM,U
  111 FORMAT(1H0,10X,*NUM=*,I2,5X,*U=*,F5.2)
      KNUM=1
 7777 CONTINUE
C
C        P1(I) REFERS TO THE ZERO ORDER PRESSURE IN THE FILM.  WHEREVER
C
C     P1 IS NEGATIVE, THE FILM IS CONSIDERED BROKEN AND P1 SET TO ZERO.
C     P2(I) IS THE NON-DIMENSIONAL PRESSURE PERTURBATION AND IS SET TO
C     ZERO WHEREVER THE FILM IS BROKEN.
C
      P1(1)=-3.0*U*(H(2)-H(50))/(DX*H(1)**3.0)
      IF(P1(1).LT.0.0)501,502
  502 CONTINUE
      PL(1)=(UP-3.0*U*(Y(1)/H(1)))*(H(2)-H(50))
      GO TO 50
      PF(1)=U*(Y(2)-Y(50))
      P2(1)=-3.0*(PL(1)+PF(1))/(DX*H(1)**3.0)
      PP(1)=(1.0/H(1)**4.0)*(H(2)-H(50))/(2.0*DX)
  501 P1(1)=0.0
      P2(1)=0.0
      PP(1)=0.0
   50 CONTINUE
      P1(51)=P1(1)
      P2(51)=P2(1)
      PP(51)=PP(1)
      DO 30 I=2,50
      P1(I)=-3.0*U*(H(I+1)-H(I-1))/(DX*H(I)**3.0)
      IF(P1(I).LT.0.0)503,504
  504 CONTINUE
      PF(I)=U*(Y(I+1)-Y(I-1))
      PL(I)=(UP-3.0*U*(Y(I)/H(I)))*(H(I+1)-H(I-1))
      P2(I)=-3.0*(PF(I)+PL(I))/(DX*H(I)**3.0)
      PP(I)=(1.0/H(I)**4.0)*(H(I+1)-H(I-1))/(2.0*DX)
      GO TO 32
  503 CONTINUE
      P1(I)=0.0
      P2(I)=0.0
      PP(I)=0.0
   32 CONTINUE
   30 CONTINUE
  420 CONTINUE
      PAV1=0.0
      DO 101 I=2,50
      PAV1=PAV1+P2(I)
  101 CONTINUE
C
C        PAV IS THE UNIFORM (AVERAGE) COMPONENT OF P2 THAT CAUSES THE
C     VERTICAL LIFT WHAT WITH A FLOATING MOUNTING.
C
```

```
      PAV=(0.5*(P2(1)+P2(51))+PAV1)/50.0
      PRINT 918,PAV
  918 FORMAT(10X,*AVERAGE PRESSURE=*,E12.5)
      IF(KNUM.GT.1)419,400
  400 CONTINUE
      HAV1=0.5*(PP(1)+PP(51))
      HAV2=0.0
      DO 401 I=2,50
      HAV2=HAV2+PP(I)
  401 CONTINUE
      HAV=HAV1+HAV2
      PRINT 407,HAV
  407 FORMAT(10X,*HAV=*,E15.5)
      HHAT=-(50.0*PAV)/(18.0*U*HAV)
      DO 414 I=1,51
  416 PP(I)=PP(I)*18.0*U*HHAT
  417 CONTINUE
      P2(I)=P2(I)+PP(I)
  414 CONTINUE
      KNUM=KNUM+1
      GO TO 420
  419 CONTINUE
C
C        HERE P2 BECOMES THE ZERO AVERAGE, DEFORMATION CAUSING, COMPONENT
C      OF P2.
C
      DO 402 I=1,51
      P2(I)=P2(I)-PAV
      Y(I)=Y(I)+HHAT
  402 CONTINUE
      HHATDIM=HHAT*HBAR
      PRINT 403,(HHAT,HHATDIM,HBAR)
  403 FORMAT(10X,*HHAT=*,E15.5,5X,*HHATDIM=*,E15.5,5X,*HBAR=*,E15.5)
      HHAT1=HHAT1+HHATDIM
  103 CONTINUE
  405 CONTINUE
      B1=0.5*(Y(1)/(H(1)**2.0)+Y(51)/(H(51)**2.0))
      B2=0.0
      DO 06 I=2,50
      B2=B2+(Y(I)/H(I)**2.0)
   06 CONTINUE
      DO 10 I=1,51
      B(I)=((U*U*DX)/(2.0*3.141592654)*(B1+B2)-U*U*Y(I)/H(I)**2.0)
      B(I)=B(I)*DX**2.0
   10 CONTINUE
      B(1)=0.0
      B(51)=0.0
C
C        XS(I) ARE THE THERMOELASTIC DISPLACEMENTS CAUSED BY THE SMALL
C      PERTURBATION Y(I).  B(I) ARE THE RIGHT HAND SIDES OF EQ.(4-32) OF
C      THE TEXT.  HERE, HEATING IS CALCULATED ON THE BASIS OF A FULL,
C      COHERENT FILM THROUGHOUT.  XSAMP AND YAMP ARE AMPLITUDES.
C
```

```
      CALL MVS(A,51,51,B,1,XS,DET,IDET,G,IR,IER)
      PRINT 500,IER
  500 FORMAT(10X,*IER=*,I2)
      IF(IER.EQ.1)GO TO 2222
      XSMAX=AMAX1(XS(1),XS(2),XS(3),XS(4),XS(5),XS(6),XS(7),XS(8),
     1 XS(9),XS(10),XS(11),XS(12),XS(13),XS(14),XS(15),XS(16),XS(17),
     2 XS(18),XS(19),XS(20),XS(21),XS(22),XS(23),XS(24),XS(25),XS(26),
     3 XS(27),XS(28),XS(29),XS(30),XS(31),XS(32),XS(33),XS(34),XS(35),
     4 XS(36),XS(37),XS(38),XS(39),XS(40),XS(41),XS(42),XS(43),XS(44),
     5 XS(45),XS(46),XS(47),XS(48),XS(49),XS(50),XS(51))
      XSMIN=AMIN1(XS(1),XS(2),XS(3),XS(4),XS(5),XS(6),XS(7),XS(8),
     1 XS(9),XS(10),XS(11),XS(12),XS(13),XS(14),XS(15),XS(16),XS(17),
     2 XS(18),XS(19),XS(20),XS(21),XS(22),XS(23),XS(24),XS(25),XS(26),
     3 XS(27),XS(28),XS(29),XS(30),XS(31),XS(32),XS(33),XS(34),XS(35),
     4 XS(36),XS(37),XS(38),XS(39),XS(40),XS(41),XS(42),XS(43),XS(44),
     5 XS(45),XS(46),XS(47),XS(48),XS(49),XS(50),XS(51))
      XSAMP=ABS(XSMAX-XSMIN)
      YMAX=AMAX1(Y(1),Y(2),Y(3),Y(4),Y(5),Y(6),Y(7),Y(8),Y(9),Y(10),
     1 Y(11),Y(12),Y(13),Y(14),Y(15),Y(16),Y(17),Y(18),Y(19),Y(20),
     2 Y(21),Y(22),Y(23),Y(24),Y(25),Y(26),Y(27),Y(28),Y(29),Y(30),
     3 Y(31),Y(32),Y(33),Y(34),Y(35),Y(36),Y(37),Y(38),Y(39),Y(40),
     4 Y(41),Y(42),Y(43),Y(44),Y(45),Y(46),Y(47),Y(48),Y(49),Y(50),
     5 Y(51))
      YMIN=AMIN1(Y(1),Y(2),Y(3),Y(4),Y(5),Y(6),Y(7),Y(8),Y(9),Y(10),
     1 Y(11),Y(12),Y(13),Y(14),Y(15),Y(16),Y(17),Y(18),Y(19),Y(20),
     2 Y(21),Y(22),Y(23),Y(24),Y(25),Y(26),Y(27),Y(28),Y(29),Y(30),
     3 Y(31),Y(32),Y(33),Y(34),Y(35),Y(36),Y(37),Y(38),Y(39),Y(40),
     4 Y(41),Y(42),Y(43),Y(44),Y(45),Y(46),Y(47),Y(48),Y(49),Y(50),
     5 Y(51))
      YAMP=ABS(YMAX-YMIN)
      PRINT 112,XSAMP,YAMP
  112 FORMAT(1H0,10X,*XSAMP=*,E15.6,5X,*YAMP=*,E15.6)
      IF(XSAMP.LT.YAMP)GO TO 3333
      GO TO 9999
 3333 CONTINUE
      NUM=NUM+1
      DO 03 I=1,51
      Y(I)=Y(I)-HHAT
   03 CONTINUE
      U=U+0.2
     IF(U.GT.1.8)9999,6666
 8888 CONTINUE
 9999 CONTINUE
      U=1.0
      IND=IND+1
      YO=YO+HBAR*0.03
      IF(IND.GT.3)2222,5555
 2222 CONTINUE
      STOP
      END
```

APPENDIX E

THE FLEXIBLY MOUNTED, INITIALLY WAVY, SEAL FACE

In practice, one of the faces is usually flexibly mounted to accommodate axial misalignment. If both faces are nominally flat but axial misalignment prevails, the fluid pressure creates a couple that tilts the flexibly mounted face and corrects the misalignment (fig. 36). If, however, the faces are axially aligned, tilting will still occur if one face is wavy and the wavelength is equal to the circumference of the seal. If there are two identical waves around the circumference, there will be no tilt because the circumferential pressure distribution will be symmetric. If, however, the face deforms during operation so as to destroy this symmetry, tilting moments will arise to counteract the asymmetry in the pressure distribution.

The following analysis appertains to the response of a flexibly mounted system to small perturbations. It is assumed that a steady, non-tilting, configuration prevails and is then disturbed slightly. The subsequent pressure fluctuation and tilting moment are, therefore, of the order of the perturbation. The tilting moment may be resolved into its components about the A and B axes (fig. E-1) as follows:

$$d\tau_A = p_t'(L \cdot dx) r \sin\theta$$

$$d\tau_B = p_t'(L \cdot dx) r \cos\theta \qquad \text{(E-1)}$$

where p_t' is the appropriate pressure perturbation. In terms of non-dimensional variables, the components of the net tilting moment become

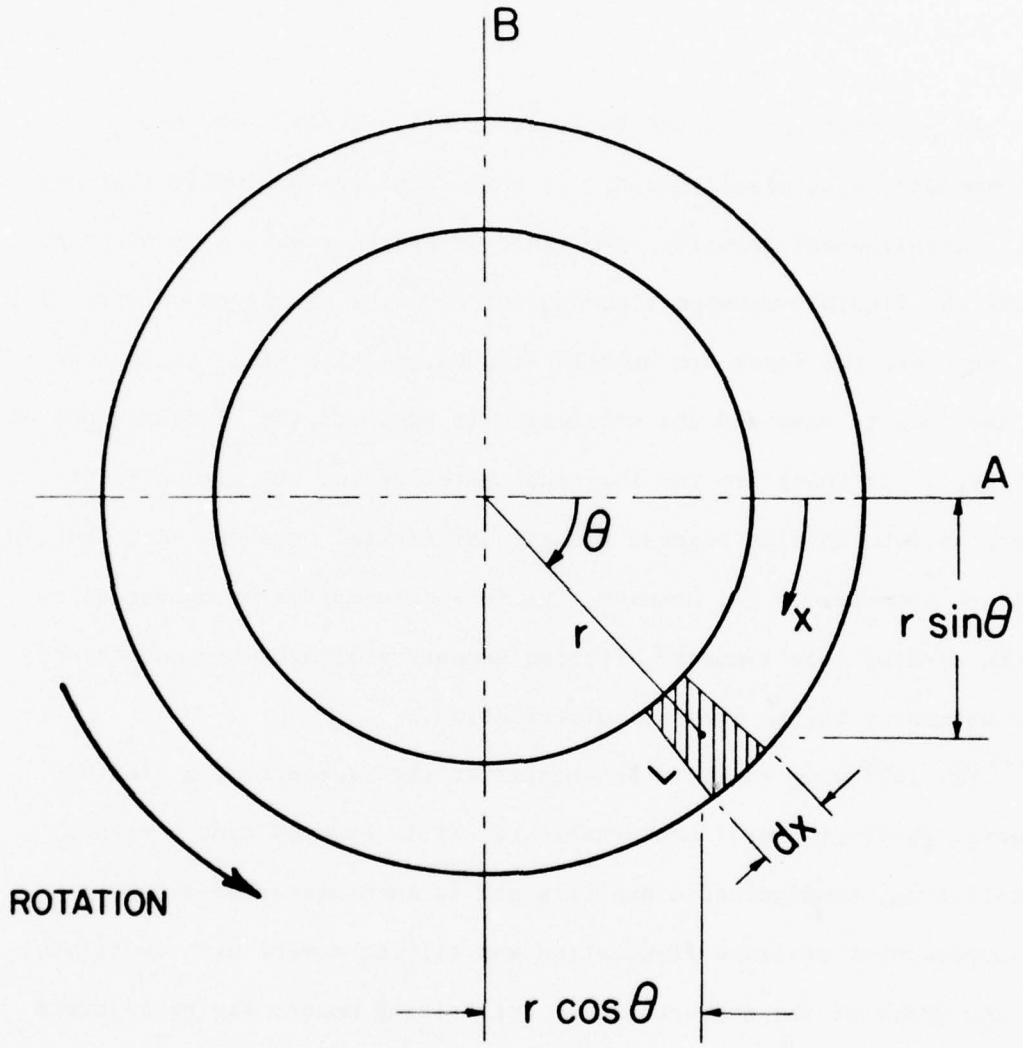

Figure E-1. Definition Sketch for Analysis of Flexibly Mounted Face

$$T_A = \int_o^{2\pi} P'_t \sin X \, dX \tag{E-2}$$

$$T_B = \int_o^{2\pi} P'_t \cos X \, dX \tag{E-3}$$

These components tilt the face so that the film-thickness changes shape. Such changes are also of the order of the perturbation and are denoted by

$$\tilde{H}_A \equiv H_A \sin X \tag{E-4}$$

$$\tilde{H}_B \equiv H_B \cos X \tag{E-5}$$

The faces can also have relative axial motion ($\hat{h}$) so that the non-dimensional film thickness is

$$\tilde{H}(X) = H(X) + \hat{H} + Y(X) + \tilde{H}_A(X) + \tilde{H}_B(X) \tag{E-6}$$

The non-dimensional pressure perturbation is

$$P'_t = P'' - \hat{P} - \frac{6u}{H^3}\left(\frac{d}{dX}\left(\tilde{H}_A + \tilde{H}_B\right) - \frac{3\left(\tilde{H}_A + \tilde{H}_B\right)}{H}\frac{dH}{dX}\right) \tag{E-7}$$

where P'' and $\hat{P}$ are as defined by eqs. (4-24) and (4-26).

The tilting moment is neutralized by the tilt defined by $\tilde{H}_A$ and $\tilde{H}_B$. Thus, using eqs. (E-2) and (E-3), one has the conditions

$$T_A = \int_o^{2\pi} P'_t \sin X \, dX = 0 \tag{E-8}$$

and

$$T_B = \int_o^{2\pi} P'_t \cos X \, dX = 0 \tag{E-9}$$

It has been explained in section (4.5) that the pressure perturbation p' must have a zero average. In the present case, by analogy, P_t' must have a zero average. Thus a third condition to be satisfied is

$$\frac{1}{2\pi}\int_0^{2\pi} P_t' \, dX = 0 \qquad \text{(E-10)}$$

Equations (E-8), (E-9) and (E-10) contain the three unknowns $\hat{H}$, H_A and H_B. They cannot be solved simultaneously by analytical means. To solve them numerically, they are first reduced, by a straightforward but cumbersome process, to

$$H_A = \frac{\Phi_1}{6u\Phi_2} \qquad \text{(E-11)}$$

$$\hat{H} = \frac{\Phi_3}{\Phi_4} H_A - \frac{\Phi_5}{6u\Phi_4} \qquad \text{(E-12)}$$

$$H_B = \frac{1}{\Phi_7}\left(\Phi_6 H_A - \Phi_8 \hat{H} - \frac{\Phi_9}{6u}\right) \qquad \text{(E-13)}$$

where

$$\Phi_1 = \Phi_9\Phi_{20} - \Phi_{10} + \Phi_5\Phi_{19} - \Phi_5\Phi_{18}$$

$$\Phi_2 = \Phi_6\Phi_{20} - \Phi_{16} + \Phi_3\Phi_{19} - \Phi_3\Phi_{18}$$

$$\Phi_3 = \Phi_{14} - \frac{\Phi_6}{\Phi_7}\Phi_{15}$$

$$\Phi_4 = \Phi_{12} - \frac{\Phi_8}{\Phi_7}\Phi_{15}$$

$$\Phi_5 = \Phi_{11} - \frac{\Phi_9}{\Phi_7}\Phi_{15}$$

$$\Phi_6 = \int_o^{2\pi} \frac{1}{H^3} \left(\cos X \sin X - \frac{3}{H} \frac{dH}{dX} \sin^2 X \right) dX$$

$$\Phi_7 = \int_o^{2\pi} \frac{1}{H^3} \left(\sin^2 X + \frac{3}{H} \frac{dH}{dX} \sin X \cos X \right) dX$$

$$\Phi_8 = 3 \int_o^{2\pi} \frac{1}{H^4} \frac{dH}{dX} \sin X \, dX$$

$$\Phi_9 = \int_o^{2\pi} P'' \sin X \, dX$$

$$\Phi_{10} = \int_o^{2\pi} P'' \, dX$$

$$\Phi_{11} = \int_o^{2\pi} P'' \cos X \, dX$$

$$\Phi_{12} = 3 \int_o^{2\pi} \frac{1}{H^4} \frac{dH}{dX} \cos X \, dX$$

$$\Phi_{13} = 3 \int_o^{2\pi} \frac{1}{H^4} \frac{dH}{dX} \, dX$$

$$\Phi_{14} = \int_o^{2\pi} \frac{1}{H^3} \left(\cos^2 X - \frac{3}{H} \frac{dH}{dX} \sin X \cos X \right) dX$$

$$\Phi_{15} = \int_o^{2\pi} \frac{1}{H^3} \left(\sin X \cos X + \frac{3}{H} \frac{dH}{dX} \cos^2 X \right) dX$$

$$\Phi_{16} = \int_o^{2\pi} \frac{1}{H^3} \left(\cos X - \frac{3}{H} \sin X \frac{dH}{dX} \right) dX$$

$$\Phi_{17} = \int_0^{2\pi} \frac{1}{H^3} \left(\sin X + \frac{3}{H} \cos X \frac{dH}{dX} \right) dX$$

$$\Phi_{18} = \frac{\Phi_8}{\Phi_4} \Phi_{20}$$

$$\Phi_{19} = \frac{\Phi_{13}}{\Phi_4}$$

$$\Phi_{20} = \frac{\Phi_{17}}{\Phi_7}$$

Equations (E-11), (E-12) and (E-13) are solved numerically for H_A, $\hat{H}$ and H_B.

To analyze the flexibly mounted seal for thermoelastic instability, eq. (4-21) is solved as described in chapter IV, where Y includes $\tilde{H}_A$ and $\tilde{H}_B$.

In describing the experiments in Chapter III, it has been observed that, as a consequence of the onset of instability, the two faces come into direct contact (fig. 26). To test whether this can be obtained in theory, an experimental profile has been measured at an operating condition just preceding the onset of instability. The non-dimensional critical speed has been taken as unity. A small sinusoidal perturbation is imposed on the metal surface and eq. (4-21) is solved for Δ_{th}. It is found that $|\Delta_{th}| > |Y|$. The following definitions are then introduced:

$$Y_{new}(X) = \alpha |\Delta_{th}| \sin X$$

where $$\alpha \approx .05$$

and $$H_{new}(X) = H_{old}(X) + \Delta_{th}(X) - Y_{new}(X)$$

The solution is repeated, with the new overall film thickness H_{new} and the new perturbation Y_{new}. This cycle is repeated over and over again and it is found that the surfaces do, indeed, touch. Such a solution has been obtained for the case of the floating but non-tilting mounting as well as the floating and tilting mounting. The results are shown in fig. (E-2).

It has to be pointed out that this procedure does not take full account of the dynamics of operation and therefore must not be regarded as a simulation of the long-term growth of a disturbance. It does, however, simulate the short-term growth of a surface perturbation and proves that if one surface comes very close to the other, it can then also touch.

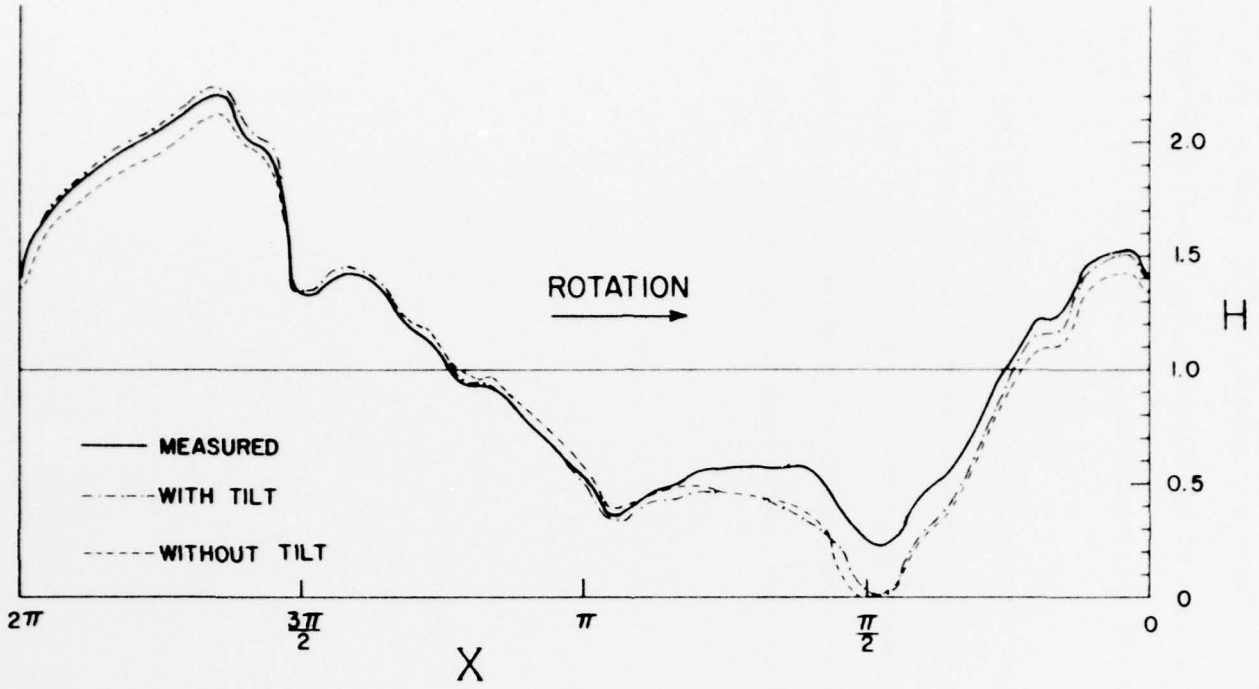

Figure E-2. Experimentally Measured Film-Thickness and Subsequent Theoretical Change by Perturbation until Surfaces Touch, for Flexible (Tilt) and Floating (without Tilt) Mountings

```
      PROGRAM ATLAST(INPUT,OUTPUT)
C
C
C        THIS PROGRAM ALLOWS FOR A NET LIFT (HHAT) AS WELL AS A TILT (COMPOSED
C      OF (HAHAT)SINX+(HBHAT)COSX).
C        P1(I) REFERS TO THE TOTAL ZERO ORDER PRESSURE THAT DETERMINES THE
C      REGIONS OF CAVITATION.  IN THE CAVITATING REGIONS, NONE OF THE EQUATIONS
C      APPLY.  P2(I) IS THE COMPONENT OF THE FIRST ORDER PERTURBATION ARISING
C      FROM THE SURFACE PERTURBATION Y(I) ALONE, AND P5(I) IS THE COMPONENT FROM
C      TILT AND NET LIFT.  WHEREVER P1 IS ZERO, P2 AND P5 ARE SET TO ZERO.
C      FINALLY, P2 AND P5 ARE ADDED TO PRODUCE A NEW P2, WHICH IS THE TOTAL
C      PERTURBATION PRESSURE AND HAS A ZERO AVERAGE AND PRODUCES ZERO TILT.  THE
C      CONDITION OF ZERO-AVERAGE P2, TOGETHER WITH THE ZERO TILT CONDITION,
C      PROVIDE THREE EQUATIONS FOR HHAT, HAHAT, HBHAT.
C        THE NEW P2 IS USED DIRECTLY FOR DETERMINING ELASTIC DEFORMATION.
C
C
      DIMENSION X(51), H0(51),Y(51),PP1(51),PP2(51),PP3(51),P1(51)
      DIMENSION H(51), A(51,51), B(51,1), XS(51,1), G(51,51), IR(51)
      DIMENSION PF(51),PL(51),P2(51),BB1(51),XI(51),BB(51,1),XX(51,1)
      DIMENSION YY(51),HT(51),A3(51),B3(51),F2(51),G2(51)
      DIMENSION P3(51),P4(51),P5(51),A1(51),A2(51),B1(51),B2(51)
      DIMENSION C2(51),D2(51),HAWAVE(51),HBWAVE(51),HMWAVE(51),C1(51)
      DIMENSION TA(51),TB(51)
      UP=0.0
      HBAR=1.48609E-05
      DX=2.0*3.14159265/50.0
      HS=3.12792E-04
      DO 13 I=1,51
      DO 13 J=1,51
   13 A(I,J)=0.0
      DO 16 I=2,50
      A(I,I)=-2.0
      A(I,I+1)=1.0
      A(I,I-1)=1.0
   16 CONTINUE
      A(1,1)=1.0
      A(51,51)=-1.0
      A(51,1)=1.0
      DO 01 I=1,51
      XI(I)=+DX*(I-1)
      X(I)=+DX*(I-1)
      P5(I)=0.0
   01 CONTINUE
 5555 CONTINUE
      U=-1.0
      NUM=1
      YO=HBAR/10.0
```

```
C
C          READ IN EXPERIMENTALLY MEASURED DIMENSIONAL SURFACE PROFILE
C       PRECEDING THE UNSTABLE STATE
C
        READ 409,(H0(I),I=1,51)
  409   FORMAT(6E12.5)
        DO 02 I=1,51
        H0(I)=H0(I)+6.1125E-06
        H(I)=(H0(I)+HBAR)/HBAR
   02   CONTINUE
        YPR=H(13)/25.0
        DO 04 I=1,51
        Y(I)=-YPR*SIN(X(I))
   04   CONTINUE
        PRINT 313,(H(I),I=1,51)
  313   FORMAT(/,51(/,10X,E15.5))
 6666   CONTINUE
        PRINT 111,NUM
  111   FORMAT(1H1,10X,*NUM=*,I2)
        KNUM=1
        MNUM=1
 7777   CONTINUE
        P1(1)=-3.0*U*(H(2)-H(50))/(DX*H(1)**3.0)
        IF(P1(1).LT.0.0)501,502
  502   CONTINUE
        PF(1)=U*(Y(2)-Y(50))
        PL(1)=(UP-3.0*U*(Y(1)/H(1)))*(H(2)-H(50))
        P2(1)=-3.0*(PL(1)+PF(1))/(DX*H(1)**3.0)
        PP3(1)=(1.0/H(1)**4.0)*(H(2)-H(50))/(2.0*DX)
        A3(1)=COS(X(1))
        B3(1)=SIN(X(1))
        F2(1)=(A3(1)-(3.0/H(1))*B3(1)*((H(2)-H(50))/(2.0*DX)))/H(1)**3.0
        G2(1)=(B3(1)+(3.0/H(1))*A3(1)*((H(2)-H(50))/(2.0*DX)))/H(1)**3.0
        GO TO 50
  501   CONTINUE
        P1(1)=0.0
        P2(1)=0.0
        PP3(1)=0.0
        F2(1)=0.0
        G2(1)=0.0
   50   CONTINUE
        P1(51)=P1(1)
        P2(51)=P2(1)
        A3(51)=A3(1)
        B3(51)=B3(1)
        PP3(51)=PP3(1)
        F2(51)=F2(1)
        G2(51)=G2(1)
        DO 30 I=2,50
        P1(I)=-3.0*U*(H(I+1)-H(I-1))/(DX*H(I)**3.0)
        IF(P1(I).LT.0.0)503,504
  504   CONTINUE
```

```
      PF(I)=U*(Y(I+1)-Y(I-1))
      PL(I)=(UP-3.0*U*(Y(I)/H(I)))*(H(I+1)-H(I-1))
      P2(I)=-3.0*(PF(I)+PL(I))/(DX*H(I)**3.0)
      A3(I)=COS(X(I))
      B3(I)=SIN(X(I))
      PP3(I)=(1.0/H(I)**4.0)*(H(I+1)-H(I-1))/(2.0*DX)
      F2(I)=(A3(I)-3.0/H(I)*B3(I)*(H(I+1)-H(I-1))/(2.0*DX))/H(I)**3.0
      G2(I)=(B3(I)+3.0/H(I)*A3(I)*(H(I+1)-H(I-1))/(2.0*DX))/H(I)**3.0
      GO TO 32
  503 CONTINUE
      P1(I)=0.0
      P2(I)=0.0
      A3(I)=0.0
      B3(I)=0.0
      PP3(I)=0.0
      F2(I)=0.0
      G2(I)=0.0
   32 CONTINUE
   30 CONTINUE
C
C       BEGIN CALCULATING TILTING MOMENT, HHAT, AND TILT
C
      DO 701 I=1,51
      PP1(I)=PP3(I)*B3(I)
      PP2(I)=PP3(I)*A3(I)
      P3(I)=P2(I)*B3(I)
      P4(I)=P2(I)*A3(I)
      A2(I)=F2(I)*B3(I)
      B2(I)=G2(I)*B3(I)
      C2(I)=F2(I)*A3(I)
      D2(I)=G2(I)*A3(I)
  701 CONTINUE
      HAV1=0.5*(PP1(1)+PP1(51))
      HAV2=0.0
      HAV3=0.5*(PP2(1)+PP2(51))
      HAV4=0.0
      HAV7=0.5*(PP3(1)+PP3(51))
      HAV8=0.0
      P3INT1=0.5*(P3(1)+P3(51))
      P3INT2=0.0
      P4INT1=0.5*(P4(1)+P4(51))
      P4INT2=0.0
      HINTA1=0.5*(A2(1)+A2(51))
      HINTA2=0.0
      HINTB1=0.5*(B2(1)+B2(51))
      HINTB2=0.0
      HINTC1=0.5*(C2(1)+C2(51))
      HINTC2=0.0
      HINTD1=0.5*(D2(1)+D2(51))
      HINTD2=0.0
      HINTF1=0.5*(F2(1)+F2(51))
      HINTF2=0.0
      HINTG1=0.5*(G2(1)+G2(51))
      HINTG2=0.0
```

BEST AVAILABLE COPY

```
      DO 401 I=2,50
      HAV2=HAV2+PP1(I)
      HAV4=HAV4+PP2(I)
      HAV8=HAV8+PP3(I)
      P3INT2=P3INT2+P3(I)
      P4INT2=P4INT2+P4(I)
      HINTA2=HINTA2+A2(I)
      HINTB2=HINTB2+B2(I)
      HINTC2=HINTC2+C2(I)
      HINTD2=HINTD2+D2(I)
      HINTF2=HINTF2+F2(I)
      HINTG2=HINTG2+G2(I)
401   CONTINUE
      HAV5=(HAV1+HAV2)*3.0*DX
      HAV6=(HAV3+HAV4)*3.0*DX
      HAV9=(HAV7+HAV8)*3.0*DX
      P3INT=(P3INT1+P3INT2)*DX
      P4INT=(P4INT1+P4INT2)*DX
      HINT1=(HINTA1+HINTA2)*DX
      HINT2=(HINTB1+HINTB2)*DX
      HINT3=(HINTC1+HINTC2)*DX
      HINT4=(HINTD1+HINTD2)*DX
      HINT5=(HINTF1+HINTF2)*DX
      HINT6=(HINTG1+HINTG2)*DX
420   CONTINUE
      PAV1=0.0
      DO 101 I=2,50
      PAV1=PAV1+P2(I)
101   CONTINUE
      PAV=(0.5*(P2(1)+P2(51))+PAV1)/50.0
      PSUM=PAV*50.0*DX
      PRINT 918,PAV
918   FORMAT(10X,*AVERAGE PRESSURE=*,E12.5)
      IF(MNUM.GT.1)GO TO 513
400   CONTINUE
      SIGH1=P4INT-(HINT4*P3INT)/HINT2
      SIGH2=HINT3-(HINT4*HINT1)/HINT2
      SIGH3=HAV6-(HAV5*HINT4/HINT2)
      SIGH4=(HINT6*HAV5)/(HINT2*SIGH3)
      SIGH5=HAV9/SIGH3
      SIGH6=HINT6/HINT2
      SIGH7=SIGH2*SIGH5-HINT5+HINT1*SIGH6-SIGH4*SIGH2
      SIGH8=SIGH1*SIGH5-PSUM+P3INT*SIGH6-SIGH4*SIGH1
      HAHAT=SIGH8/(6.0*U*SIGH7)
      HHAT=(HAHAT*SIGH2)/SIGH3-SIGH1/(6.0*U*SIGH3)
      HBHAT=((HAHAT*HINT1)-P3INT/(6.0*U)-(HHAT*HAV5))/HINT2
      DO 509 I=1,51
      HAWAVE(I)=HAHAT*SIN(X(I))
      HBWAVE(I)=HBHAT*COS(X(I))
      HMWAVE(I)=HAWAVE(I)+HBWAVE(I)
```

```
  509  CONTINUE
C
C          HHAT AND TILT HAVE NOW BEEN OBTAINED
C
       DO 511 I=1,51
       P5(I)=-6.0*U*(HAHAT*F2(I)-HBHAT*G2(I)-HHAT*3.0*PP3(I))
  511  CONTINUE
       DO 512 I=1,51
       P2(I)=P2(I)+P5(I)
  512  CONTINUE
       DO 516 I=1,51
       TA(I)=P2(I)*B3(I)
       TB(I)=P2(I)*A3(I)
  516  CONTINUE
       TAINT=0.5*(TA(1)+TA(51))
       TBINT=0.5*(TB(1)+TB(51))
       DO 514 I=2,50
       TAINT=TAINT+TA(I)
       TBINT=TBINT+TB(I)
  514  CONTINUE
       TORKA=DX*TAINT
       TORKB=DX*TBINT
       MNUM=MNUM+1
       GO TO 420
  513  CONTINUE
       DO 402 I=1,51
       H(I)=H(I)*HBAR-HBAR
       Y(I)=Y(I)*HBAR
       HMWAVE(I)=HMWAVE(I)*HBAR
  402  CONTINUE
       HS=HS*HBAR**2.0
       HHATDIM=HHAT*HBAR
       HBAR=HBAR+HHATDIM
       HS=HS/HBAR**2.0
       PRINT 403,(HHAT,HAHAT,HBHAT,HBAR,TORKA,TORKB)
  403  FORMAT(10X,*HHAT=*,E12.4,2X,*HAHAT=*,E12.4,2X,*HBHAT=*,E12.4,2X,
     1 *HBAR=*,E12.4,2X,*TORKA=*,E12.4,2X,*TORKB=*,E12.4)
       DO 404 I=1,51
       HMWAVE(I)=HMWAVE(I)/HBAR
       H(I)=(H(I)+HBAR)/HBAR+HMWAVE(I)
       HT(I)=H(I)*HBAR-HBAR
       Y(I)=Y(I)/HBAR
  404  CONTINUE
  103  CONTINUE
       DO 201 I=1,51
       BB2=0.0
       DO 202 J=1,51
       IF(J.EQ.1)203,204
  203  BB1(J)=-P2(J)*4.0/ DX
       GO TO 205
```

```
  204   BB1(J)=P2(J)/(ABS(X(I)-XI(J))**2.0)
  205   CONTINUE
        BB2=BB2+BB1(J)
  202   CONTINUE
        BB2=BB2-0.5*(BB1(1)+BB1(51))
        BB(I)=BB2*HS*DX**3.0
  201   CONTINUE
        BB(1)=0.0
        BB(51)=0.0
C
C          COMPUTATION OF ELASTIC DEFLECTION
C
        CALL MVS(A,51,51,BB,1,XX,DET,IDET,G,IR,IER)
        PRINT 601, IER
  601   FORMAT(10X,*IER=*,I2)
        IF(IER.EQ.1)GO TO 9999
  405   CONTINUE
        B1=0.5*(Y(1)/(H(1)**2.0)+Y(51)/(H(51)**2.0))
        B2=0.0
        DO 06 I=2,50
        B2=B2+(Y(I)/H(I)**2.0)
   06   CONTINUE
        DO 10 I=1,51
        B(I)=((U*U*DX)/(2.0*3.141592654)*(B1+B2)-U*U*Y(I)/H(I)**2.0)
        B(I)=B(I)*DX**2.0
   10   CONTINUE
        B(1)=0.0
        B(51)=0.0
C
C          COMPUTATION OF THERMAL DEFLECTION
C
        CALL MVS(A,51,51,B,1,XS,DET,IDET,G,IR,IER)
        PRINT 500,IER
  500   FORMAT(10X,*IER=*,I2)
        IF(IER.EQ.1)GO TO 9999
        DO 206 I=1,51
  206   YY(I)=XS(I)+XX(I)
        PRINT 800,(P2(I),XX(I),XS(I),YY(I),Y(I),H(I),HT(I),I=1,51)
  800   FORMAT(/,51(/,10X,7E15.5))
        HH=Y(13)*HBAR
        HHO=YY(13)*HBAR
        IF(ABS(HH).GT.ABS(HHO))4444,3333
 4444   CONTINUE
        PRINT 917
  917   FORMAT(/,10X,*PERTURBATION IS BEING SUPPRESSED*)
        GO TO 2222
```

```
 3333  CONTINUE
       HMIN=AMIN1(H(1),H(2),H(3),H(4),H(5),H(6),H(7),H(8),H(9),H(10),
      1 H(11),H(12),H(13),H(14),H(15),H(16),H(17),H(18),H(19),H(20),
      2 H(21),H(22),H(23),H(24),H(25),H(26),H(27),H(28),H(29),H(30),
      3 H(31),H(32),H(33),H(34),H(35),H(36),H(37),H(38),H(39),H(40),
      4 H(41),H(42),H(43),H(44),H(45),H(46),H(47),H(48),H(49),H(50),
      5 H(51))
       PRINT 702,HMIN
  702  FORMAT(10X,*HMIN=*,E15.5)
       YPR=HMIN/25.0
       DO 03 I=1,51
       Y(I)=-YPR*SIN(X(I))
       YY(I)=YY(I)-Y(I)
       H(I)=H(I)+YY(I)
   03  CONTINUE
       YTEST=HMIN
       IF(YTEST.LT.0.0 )GO TO 8888
       NUM=NUM+1
       IF(NUM.GT.100)9999,6666
 8888  CONTINUE
       PRINT 316
  316  FORMAT(/,10X,*THE SURFACES HAVE TOUCHED*)
 9999  CONTINUE
 2222  CONTINUE
       PRINT 314,(H(I),Y(I),I=1,51)
  314  FORMAT(1H1,51(/,10X,2E15.5))
       STOP
       END
000000000000000000000  END OF RECORD
C
C         EXPERIMENTALLY MEASURED SURFACE PROFILE
C
0.           +1.63501E-06+1.38347E-06+2.76694E-07-2.71663E-06-2.76694E-06
-4.90503E-06-7.54602E-06-1.04389E-05-1.28914E-05-1.37089E-05-1.63501E-05
-1.73059E-05-1.63501E-05-1.42372E-05-1.22877E-05-1.22870E-05-1.22860E-05
-1.23000E-05-1.24000E-05-1.25770E-05-1.34699E-05-1.38347E-05-1.50924E-05
-1.53062E-05-1.30298E-05-1.15331E-05-1.00616E-05-8.65298E-06-7.20662E-06
-7.20602E-06-5.96148E-06-4.03719E-06-2.96800E-06-1.03129E-06+1.60494E-11
-1.25770E-07-1.38347E-06+8.80390E-07+8.30082E-06+9.68429E-06+1.18224E-05
+1.14451E-05+1.02503E-05+9.14348E-06+8.46432E-06+7.70970E-06+6.56519E-06
+5.34523E-06+3.52156E-06+0.00000E+00
```

APPENDIX F

PROGRAM FOR COMPUTING FACE LOAD AND INITIAL FACE PROFILE
CORRESPONDING TO GIVEN OPERATING CONDITIONS

```
      PROGRAM SUPORT(INPUT,OUTPUT)
C
C
C       COMPUTATION OF LOADS SUPPORTED FOR VARIOUS AMPLITUDES OF NON-
C     DIMENSIONAL SURFACE WAVE AND A RANGE OF SLIDING SPEEDS.  LOAD
C     IS GIVEN BY THE NET PRESSURE IN THE FLUID FILM.  FOR GIVEN QUASI-
C     STATIC SOLUTIONS (OPERATING CONDITIONS), THEINITIAL SURFACE
C     PROFILES ARE ALSO CALCULATED.  SINGLE-LOBED SURFACE PROFILES ARE
C     CONSIDERED, WHERE BOTH SURFACES ARE RESTRAINED FROM TILTING
C
C
      DIMENSION X(51),HC(51),P1(51),H(51),Y(51)
      DIMENSION A(51,51),G(51,51),IR(51),B0(51,1),XL(51,1)
      HBAR=1.0E-05
      DX=2.0*3.141592654/50.0
      HS=3.12782E-04
      DO 13 I=1,51
      DO 13 J=1,51
   13 A(I,J)=0.0
      DO 16 I=2,50
      A(I,I)=-2.0
      A(I,I+1)=1.0
      A(I,I-1)=1.0
   16 CONTINUE
      A(1,1)=1.0
      A(51,51)=-1.0
      A(51,1)=1.0
      DO 01 I=1,51
      X(I)=+0X*(I-1)
   01 CONTINUE
C
C       U IS THE SLIDING SPEED, NONDIMENSIONALISED WITH RESPECT TO THE
C     THEORETICAL CRITICAL SPEED FOR INITIALLY FLAT SURFACES.
C
      U=0.10
      IND=1
      YO=HBAR*0.10
      HAMP=YO/HBAR
 5555 CONTINUE
C
C       H(I) IS THE NONDIMENSIONAL FILM THICKNESS
C
      DO 02 I=1,51
      HC(I)=-YO*SIN(X(I))
      H(I)=(HC(I)+HBAR)/HBAR
   02 CONTINUE
      NUM=1
 6666 CONTINUE
      PRINT 111,NUM,U,HAMP
  111 FORMAT(1H0,10X,*NUM=*,I2,5X,*U=*,F5.2,5X,*HAMP=*,F6.3)
 7777 CONTINUE
C
C
C       P1(I) REFERS TO THE PRESSURE IN THE FILM.  WHEREVER P1(I) IS
C     NEGATIVE, THE FILM IS CONSIDERED BROKEN AND P1(I) IS SET TO ZERO.
C     P1 IS NONDIMENSIONAL.  TO  OBTAIN DIMENSIONAL PRESSURE, IT HAS TO
C     BE DIVIDED BY HBAR/W*SQRT(ALPHA/(MU*K).
```

BEST AVAILABLE COPY

```
C
C
      P1(1)=-3.0*U*(H(2)-H(50))/(DX*H(1)**3.0)
      IF(P1(1).LT.0.0)501,50
  501 P1(1)=0.0
   50 CONTINUE
      P1(51)=P1(1)
      DO 30 I=2,50
      P1(I)=-3.0*U*(H(I+1)-H(I-1))/(DX*H(I)**3.0)
      IF(P1(I).LT.0.0)503,32
  503 CONTINUE
      P1(I)=0.0
   32 CONTINUE
   30 CONTINUE
  420 CONTINUE
      PAV1=0.0
      DO 101 I=2,50
      PAV1=PAV1+P1(I)
  101 CONTINUE
      PAV=(0.5*(P1(1)+P1(51))+PAV1)/50.0
C
C
C       PSUM REPRESENTS THE NONDIMENSIONAL LOAD.  TO OBTAIN LOAD IN
C     POUNDS, PSUM HAS TO BE DIVIDED BY (HBAR*KAPPA)/(W*L)*
C     SQRT(ALPHA/(MU*K))
C
C
      PSUM=PAV*50.0*DX
      PLOG=ALOG10(PSUM)
      PRINT 818,PAV,PSUM,PLOG
  818 FORMAT(10X,*AVERAGE PRESSURE=*,E12.5,5X,*LOAD SUPPORTED=*,E12.5,
     1 5X,*LOG(LOAD)=*,F6.3)
      B01=0.5*(1.0/H(1)+1.0/H(51))
      B02=0.0
      DO 701 I=2,50
      B02=B02+(1.0/H(I))
  701 CONTINUE
C
C       WHEREVER THE FILM CAVITATES, HEATING IS ASSUMED TO BE ZERO
C
      DO 702 I=1,51
      IF(P1(I).EQ.0.0)703,704
  704 CONTINUE
      B0(I)=(U*U)/H(I)-(U*U*DX)/(2.0*3.14159265)*(B01+B02)
      B0(I)=B0(I)*DX**2.0
      GO TO 707
  703 B0(I)=0.0
  707 CONTINUE
  702 CONTINUE
      B0(1)=0.0
      B0(51)=0.0
      CALL MVS(A,51,51,B0,1,XL,DET,IDET,G,IR,IER)
C
C
C       XL(I) REPRESENTS THE THERMALLY GENERATED PART OF H(I), AND Y(I)
C     THE INITIAL, MACHINED SURFACE PROFILE
C
C
```

BEST AVAILABLE COPY

```
      DO 705 I=1,51
      Y(I)=H(I)-1.0-XL(I)
  705 CONTINUE
      YMAX=AMAX1(Y(1),Y(2),Y(3),Y(4),Y(5),Y(6),Y(7),Y(8),Y(9),Y(10),
     1 Y(11),Y(12),Y(13),Y(14),Y(15),Y(16),Y(17),Y(18),Y(19),Y(20),
     2 Y(21),Y(22),Y(23),Y(24),Y(25),Y(26),Y(27),Y(28),Y(29),Y(30),
     3 Y(31),Y(32),Y(33),Y(34),Y(35),Y(36),Y(37),Y(38),Y(39),Y(40),
     4 Y(41),Y(42),Y(43),Y(44),Y(45),Y(46),Y(47),Y(48),Y(49),Y(50),
     5 Y(51))
      YMIN=AMIN1(Y(1),Y(2),Y(3),Y(4),Y(5),Y(6),Y(7),Y(8),Y(9),Y(10),
     1 Y(11),Y(12),Y(13),Y(14),Y(15),Y(16),Y(17),Y(18),Y(19),Y(20),
     2 Y(21),Y(22),Y(23),Y(24),Y(25),Y(26),Y(27),Y(28),Y(29),Y(30),
     3 Y(31),Y(32),Y(33),Y(34),Y(35),Y(36),Y(37),Y(38),Y(39),Y(40),
     4 Y(41),Y(42),Y(43),Y(44),Y(45),Y(46),Y(47),Y(48),Y(49),Y(50),
     5 Y(51))
      YAMP=ABS(YMAX-YMIN)/2.0
      YINVERS=1.0/YAMP
      PRINT 706,YMAX,YMIN,YAMP,YINVERS
  706 FORMAT(10X,*YMAX=*,E12.5,5X,*YMIN=*,E12.5,5X,*YAMP=*,E12.5,5X,
     1 *HBAR/HINITIAL=*,F6.3)
      NUM=NUM+1
      U=U+0.4
     IF(U.GT.4.0)9999,6666
 8888 CONTINUE
 9999 CONTINUE
      U=0.10
      IND=IND+1
      YO=YO+HBAR*0.10
      HAMP=YO/HBAR
      IF(IND.GT.9)2222,5555
 2222 CONTINUE
      STOP
      END
```

REFERENCES

1. Sibley, L. B., and Allen, C. M., "Friction and Wear Behavior of Refractory Materials at High Sliding Velocities and Temperatures," ASME 61-Lubs 15.

2. Barber, J. R., "Thermoelastic Instabilities in the Sliding of Conforming Solids," Proc. Roy. Soc. A., 312 (1969), pp. 381-391.

3. Dow, T. A., "Thermoelastic Instabilities in Sliding Contact, Dissertation, Northwestern University," (1972).

4. Dow, T. A., and Burton, R. A., "Investigation of Thermoelastic Instabilities of Sliding Contact in the Absence of Wear," Wear, Vol. 19, (1972), pp. 315-328.

5. Dow, T. A., and Burton, R. A., "The Role of Wear in the Initiation of Thermoelastic Instabilities of Rubbing Contact," ASME Trans., JOLT, (January 1973), pp. 71-75.

6. Heckmann, S. R., and Burton, R. A., "Effects of Shear and Wear on Instabilities Caused by Frictional Heating in a Seal-Like Configuration," ASLE, Preprint No. 75-LC-1B-2.

7. Burton, R. A., Nerlikar, V., and Kilaparti, S. R., "Thermoelastic Instability in a Seal-like Configuration," Wear, Vol. 24, No. 2, (1973), pp. 177-188.

8. Burton, R. A., "The Role of Insulating Surface Films on Frictionally Excited Thermoelastic Instability," Wear, Vol. 24, No. 2, pp. 189-198.

9. Burton, R. A., Kilaparti, S. R., and Nerlikar, V., "A Limiting Stationary Configuration with Partially Contacting Surfaces," Wear, Vol. 24, No. 2, (1973), pp. 199-206.

10. Burton, R. A., and Nerlikar, V., "Clearance, Leakage, and Contact Temperature in a Thermoelastically Deformed Seal-Like Configuration," ASME Trans., JOLT, (July 1975), pp. 546-551.

11. Burton, R. A., and Nerlikar, V., "Effect of Initial Surface Curvature on Frictionally Excited Thermoelastic Phenomena," Wear, Vol. 27, No. 2, (1974), pp. 195-207.

12. Kilaparti, S. R., "Thermoelastic Instability in a Seal-Like Configuration," Dissertation, Northwestern University (1977).

13. Burton, R. A., Kilaparti, S. R., and Heckmann, S. R., "Modeling of Turbine Blade Tip Contact," ASME Trans., Journal of Engineering for Power, (October 1976), pp. 435-440.

14. Taniguchi, S., and Ettles, C., "A Thermoelastic Analysis of the Parallel Surface Thrust Washer," ASLE Trans., Vol. 18, No. 4, (1975), pp. 299-305.

15. Blok, H., "Thermal Instability of Flow in Elastohydrodynamic Films as a Cause for Cavitation, Collapse and Scuffing," Paper presented at the First Leeds - Lyon Symposium, University of Leeds, England, (September 12-13, 1974).

16. Cameron, A., "The Principles of Lubrication," Longmans Green and Co., Ltd., (1966).

17. Dow, T. A., and Stockwell, R. D., "Experimental Verification of Thermoelastic Instabilities in Sliding Contact," ASME Preprint Number 76-LUB-21.

18. Banerjee, B. N., and Burton, R. A., "Thermoelastic Instability in Lubricated Sliding between Solid Surfaces," Nature, Vol. 261, No. 5559, (June 3, 1976), pp. 399-400.

19. Lane, T. B., and Hughes, J. R., "A Study of the Oil-Film Formation in Gears by Electrical Resistance Measurements," British Journal of Applied Physics, Vol. 3, (1952), pp. 315-318.

20. El-Sisi, S. I., and Shawki, G. S. A., "Measurement of Oil-Film Thickness Between Disks by Electrical Conductivity," ASME Trans., J. Basic Engineering, (March 1960), pp. 12-17.

21. MacConochie, I. O., and Cameron, A., "The Measurement of Oil-Film Thickness in Gear Teeth," ASME Trans., J. Basic Engineering, (March 1960), pp. 29-34.

22. Denny, D. F., "Some Measurements of Fluid Pressures between Plane Parallel Thrust Surfaces with Special Reference to the Balancing of Radial Face Seals," Wear, Vol. 4, No. 1, (1961), pp. 64-83.

23. Stanghan-Batch, B. A., and Iny, E. H., "Pressure Generation in Radial Face Seals," Proc. 2nd Int. Conf. on Fluid Sealing, British Hydromechanics Research Association, Paper F4 (1964).

24. Winney, P. E., "The Thickness Measurement of Thin Fluid Films by a Magnetic Reluctance Technique," J. of Scientific Instruments (J. of Physics E), Sr. 2, Vol. 1 (1968), pp. 767-769.

25. Stanghan-Batch, B., and Iny, E. H., "A Hydrodynamic Theory of Radial-Face Mechanical Seals," J. of Mech. Engg. Sc., Vol. 15, No. 1 (1973), pp. 20-24.

26. Nau, B. S., "Hydrodynamic Lubrication in Face Seals," Proc. 3rd Int. Conf. on Fluid Sealing, British Hydromechanics Research Assoc., Paper E5 (1967).

27. Hamilton, D. B., Walowit, J. A., and Allen, C. M., "A Theory of Lubrication by Micro-Irregularities," ASME Paper 65-LUB-11 (1965).

28. Reiner, M., "Cross-Stresses in the Laminar Flow of Liquids," Phys. Fluids, Vol. 3, No. 3, (May/June 1960), pp. 427-432.

29. Tanner, R. I., "The Reiner Centripetal Effect in Face Seals," Proc. 1st Int. Conf. on Fluid Sealing, British Hydromechanics Research Assoc., Paper E1, (1961).

30. Nau, B. S., "Hydrodynamics of Face Seal Films," Proc. 2nd Int. Conf. on Fluid Sealing, British Hydromechanics Research Assoc., Paper F5 (1964).

31. Nahavandi, A., and Osterle, F., "The Effect of Vibration on the Load-Carrying Capacity of Parallel Surface Thrust Bearings," ASME Paper 60-LUB-3 (March 1960).

32. Stanghan-Batch, B. A., "Face Lubrication in Mechanical Seals," Instn. Mech. Engrs., C 59/71 (1971), pp. 54-59.

33. Ocvirk, F. W., "Short-Bearing Approximation for Full Journal Bearings," Tech. Note, NACA, 2808 (1952).

34. Georgopoulos, E., M.S. Thesis, Northwestern University (1976).

35. Burton, R. A., Letter to the Editor, Wear, Vol. 26 (1973), pp. 428-430.

36. Timoshenko, S. P., and Goodier, J. N., "Theory of Elasticity," McGraw-Hill Book Co. (1970).

37. Booker, J. F., "A Table of the Journal Bearing Integral," ASME Trans., J. Basic Engg., (June 1965), pp. 533-535.